

CRANFIELD UNIVERSITY

SONIA RUTH RINCON URBINA

MECHANICAL DEGRADATION OF COMPOSITE STRUCTURES
SUBJECTED TO ENVIRONMENTAL EFFECTS

SCHOOL OF AEROSPACE, TRANSPORT AND
MANUFACTURING

Master of Philosophy
Academic Year: 2015-2017

Supervisor: Doctor David Ayre/Doctor Hamed Yazdani
April 2018

CRANFIELD UNIVERSITY

SCHOOL OF AEROSPACE, TRANSPORT AND
MANUFACTURING

MPhil

Academic Year 2015-2017

SONIA RUTH RINCON URBINA

MECHANICAL DEGRADATION OF COMPOSITE STRUCTURES
SUBJECTED TO ENVIRONMENTAL EFFECTS

Supervisor: Doctor David Ayre
Doctor Hamed Yazdani
April 2018

© Cranfield University 2018. All rights reserved. No part of this
publication may be reproduced without the written permission of the
copyright owner.

ABSTRACT

Polymeric materials have inherent advantages thanks to the mechanical properties that they lend to a structure enhancing its useful life in factors of safety, reliability and aesthetics. Nevertheless, the durability may be affected by other considerations including environmental attack resulting in unexpected failures and maintenance costs, making it therefore essential to accurately predict the overall performance of these structures.

This study was designed to evaluate the joint strength of an adhesively bonded composite Single Lap Joint (SLJ), exposed to a hostile environment i.e. cycles of temperature and moisture, mechanical damage and fatigue.

The aged joints under hygrothermal cycles were tested under static and dynamic loads. A combined experimental-numerical Cohesive Zone Model (CZM) was calibrated to predict the joint strength degradation, and damage propagation. The composite SLJ of T800/M21 bonded with FM94 was subjected to hygrothermal cycles in an environmental chamber (maximum 70 °C and minimum - 20 °C), at maximum 85 % Relative Humidity (RH).

The results showed that the strength degraded consequent to the increasing number of cycles. The strength reduced by 42 % under static load after 714 cycles in comparison to unaged joints. The fatigue life was evaluated at 30%, 40% and 45% ultimate static load to a maximum of one million cycles, resulting in a continuous fatigue life reduction with the increase in the number of aging cycles.

A characterisation of the moisture diffusion parameters was performed on adhesive (FM94) and composite laminate (T800/M21) subjected to hygrothermal cycles. A displacement-diffusion analysis was conducted to determine the effect of moisture on the elasticity of the adhesive. The displacement-diffusion model results and shear lap test results were employed to establish the degradation parameters of the CZM, thus predicting the degradation of the joint with an accuracy of 13 % at 714 hygrothermal cycles.

Keywords: Hygrothermal cyclic ageing, adhesive joints, mechanical testing, finite element analysis.

ACKNOWLEDGEMENTS

My profoundest gratitude to my supervisors Doctor David Ayre and Doctor Hamed Yazdani for their constant support, patience, advice and consideration during this research. I would also like to thank Prof. Peter Foote for his recommendations and moral support through some difficult times.

I would particularly like to acknowledge the sponsorship for this research project provided by the Colombian Air Force and Colfuturo.

I would further like to express my appreciation to the academic staff as well as the technicians, special thanks to Prof. Phil Irving, Mr. Andrew Mills, Mr. Jim Hurley and Mr Ben Hopper.

I am very thankful to my friends and all my colleagues, Paul, Lesli Ann, Aurele, Diego, Giacomo, Luca, Paola, Thomas, Hernan, Wilson and Najat, without them this journey would not have been quite so awesome.

I don't have words great enough to express all my gratitude and infinite love for my family for being my inspiration throughout my life. This is for you Matilde, Nubia, and Sael. Thanks to my family and friends in Colombia, for the constant support and the encouragement to complete this life experience successfully.

I would also like to express my deepest gratitude to Doctor Cesar Rodriguez who supported me through good and bad times, thanks for your expert advice and encouraging words.

TABLE OF CONTENTS

ABSTRACT	i
ACKNOWLEDGEMENTS.....	iii
LIST OF FIGURES	vii
LIST OF TABLES	xi
LIST OF EQUATIONS.....	xiii
LIST OF ABBREVIATIONS	xv
GLOSSARY OF TERMS	xvii
1 INTRODUCTION	1
2 LITERATURE REVIEW.....	3
2.1 Adhesive Joints.....	3
2.2 Design Aspects	4
2.2.1 Type of Joint.....	4
2.2.2 Laminate Lay-Up and Stacking Sequence	8
2.3 Manufacturing Processes	9
2.3.1 Surface Preparation	10
2.4 Durability.....	12
2.4.1 Environmental Effects	12
2.4.2 Hygrothermal Cycles Effects	16
2.4.3 Fatigue Durability	18
2.5 Non-destructive Testing	20
2.5.1 Types of Defects	21
2.5.2 Non-Destructive Inspection Methods.....	21
2.6 Damage Prediction	23
2.6.1 Models to predict durability.....	23
2.6.2 Modelling Moisture Diffusion	23
2.6.3 Cohesive Zone Modelling.....	26
2.6.4 Environmental Degradation Models	31
2.7 Overview.....	37
3 METHODOLOGY, MATERIALS AND METHODS	41
3.1 Research methodology	41
3.2 Composites manufacturing	42
3.3 Single Lap Joint manufacturing.....	44
3.4 Hygrothermal cycles	47
3.5 Bulk adhesive specimens manufacturing.....	47
3.5.1 Preliminary test	48
3.5.2 Bulk adhesive sheet manufacturing	49
3.6 Materials characterisation	50
3.6.1 Gravimetric test	50

3.6.2 Diffusion coefficient	53
3.7 Mechanical properties	56
3.7.1 Composite CFRP	56
3.7.2 Adhesive FM94	56
3.7.3 Adhesively bonded single lap joint tests	57
3.7.4 Non-Destructive Inspection -NDI	59
3.7.5 Microscopy evaluation	59
3.7.6 Ultrasonic Inspection	60
4 EXPERIMENTAL RESULTS	63
4.1 Introduction	63
4.2 Moisture Characterisation	63
4.2.1 FM94	63
4.2.2 Composite laminate T800/M21	71
4.2.3 Swelling	73
4.2.4 Desorption following absorption FM94 and CFRP T800/M21 UD	74
4.2.5 Mechanical properties Adhesive FM94	75
4.3 Adhesive bonded single lap joint test	77
4.3.1 Mechanical testing	78
4.3.2 Non-Destructive Inspection-NDI	85
5 DEGRADATION MODELLING OF ADHESIVELY BONDED SINGLE LAP JOINT	91
5.1 Finite Element Analysis	91
5.1.1 Bulk adhesive	92
5.1.2 Single Lap Joint model	98
6 DISCUSSION	113
6.1 Introduction	113
6.2 Moisture absorption	113
6.3 Moisture effect adhesive mechanical properties	117
6.4 Mechanical test results	119
6.4.1 Lap Shear Test	119
6.4.2 Fatigue test	121
6.5 Non-destructive Inspection of adhesive bonded joints	123
6.6 Degradation Modelling	123
7 CONCLUSIONS AND CONTRIBUTION	127
FURTHER WORK	129
REFERENCES	131

LIST OF FIGURES

Figure 2-1 Stress distribution in SLJ [16].....	5
Figure 2-2 Peak failure load and lap shear of SLJ with different adherend thickness[2].....	6
Figure 2-3 strength of Secondary bonding joints with different overlap lengths (source:Song et al. 2010)	7
Figure 2-4 Failure SLJ with composite adherend modified [15].....	8
Figure 2-5 schematic surface appearance for different treatments a. peel ply, b. mechanical, c. laser [31].....	10
Figure 2-6 Moisture effects on Tg [48].....	13
Figure 2-7 Environmental effects in joints [50].....	14
Figure 2-8 Moisture absorption in polymeric composites [46].....	15
Figure 2-9 Hygrothermal ageing flight-cycles and maintenance operation for supersonic aircraft structures [57].....	17
Figure 2-10 Thermal ageing cycle [64]	20
Figure 2-11 Defects on adhesive joint [69]	21
Figure 2-12 Crack growth in cohesive zone [80]	26
Figure 2-13 Cohesive Interface [82]	27
Figure 2-14 Typical Traction Separation displacement curve taken from Abaqus	28
Figure 2-15 Three different fracture modes	29
Figure 2-16 Four classes of cohesive zone laws. (a) Polynomial, (b) Multilinear, (c). Exponential, (d) Rigid linear	30
Figure 2-17 Fatigue model prediction framework	31
Figure 2-18 Modelling moisture degradation on static and fatigue load[50]	34
Figure 2-19 General framework of the FE modelling (DF being degradation factor) [96]	35
Figure 3-1 Methodology flow chart	41
Figure 3-2 T800/M21 UD CFRP sheets before bonding.....	43
Figure 3-3 Joint bonded process: a) PTFE tips and film adhesive set up, b) before bonding, c) Final assembly bonded joint.....	44
Figure 3-4 Vacuum bag for joints bonding.....	45

Figure 3-5 CFRP end tabs bonded (a) bonded plates schematic (b) bonded plates	45
Figure 3-6 Geometry of the single lap joint specimen and final specimen.....	46
Figure 3-7 Upper photo shows clamping before curing. Bottom photo shows final specimen	46
Figure 3-8 Cycle of temperature and humidity.....	47
Figure 3-9 Mould made to cure the adhesive [70]	48
Figure 3-10 Left adhesive starting to degas. Right adhesive during the degassing process.	49
Figure 3-11 Left Adhesive cured in opened mould, Right side view adhesive cured in open mould	50
Figure 3-12 Gravimetric test samples.....	51
Figure 3-13 Fick's Diffusion Graph [46].....	55
Figure 3-14 Specimen type II Geometry [109], above the specimen.....	57
Figure 3-15 Single lap shear test configuration (a) General view, (b) laser extensometer, (c) SLJ schematic position in front of laser extensometer ..	58
Figure 3-16 Fatigue test configuration.....	58
Figure 3-17 Ultrasonic C-scan through immersion (a) scanning set up (b) probe and joint arrangement (c) scheme of scan direction and area	60
Figure 4-1 Moisture absorption for FM94 bulk adhesive (1mm thick), samples removed at hot-wet condition.....	64
Figure 4-2 Moisture absorption average FM94 bulk (1mm thick), at hot-wet condition	65
Figure 4-3 Predicted moisture absorption (1 mm thick) at hot-wet condition compared with experimental moisture uptake	66
Figure 4-4 Moisture absorption for FM94 bulk adhesive (1mm thick), at cold-dry condition	67
Figure 4-5 Moisture absorption average FM94 bulk (1mm thick), at cold-dry condition	68
Figure 4-6 Predicted moisture absorption (1 mm thick) at cold-dry condition compared with experimental data.....	68
Figure 4-7 Moisture Diffusion FM94 bulk, samples were taken out at hot-wet and cold-dry conditions.....	69
Figure 4-8 Schematic cyclic diffusion FM94	70

Figure 4-9 CFRP Moisture Absorption samples (2 mm thick)	71
Figure 4-10 CRFP Moisture Absorption average (2 mm thick).....	72
Figure 4-11 CFRP Predicted moisture absorption (2 mm thick) at hot-wet condition compared with experimental moisture uptake	73
Figure 4-12 Desorption FM94 bulk and T800/M21 laminate	74
Figure 4-13 Moisture absorption FM94 and T800/M21	75
Figure 4-14 Effect of Hygrothermal cycles on mechanical properties FM94	76
Figure 4-15 Variation ultimate tensile stress vs. moisture content wt (%)	76
Figure 4-16 Elastic modulus as function moisture content	77
Figure 4-17 Load-displacement curve unaged and aged SLJ	79
Figure 4-18 Shear strength as function of hygrothermal cycles.....	80
Figure 4-19 Displacement at failure of unaged and aged single lap joints	81
Figure 4-20 Typical surface failure	82
Figure 4-21 Photograph of failure surface unaged and aged (a) fracture failure, (b) adhesive contours	82
Figure 4-22 Fracture failure after 84 cycles	82
Figure 4-23 L-N normalised curves of SLJ unaged and aged (R= 0.1, f=5Hz). 84	
Figure 4-24 Failure surface SLJ tested under fatigue (a) mode failure typical pattern, (b) failure pattern aged SLJ at 336 cycles	85
Figure 4-25 Photographs of side view of unaged SLJ (a) 5X,(b)10X,(c)20X,(d) 40X	86
Figure 4-26 Photographs of side view of aged bondline (252 cycles) bondline (a) 5X, (b)10X, (c) 20X, (d) 40X	87
Figure 4-27 C-scan images of the bond region obtained at different ageing states	88
Figure 5-1 Configuration of Bulk adhesive	94
Figure 5-2 Von Misses stresses for different mesh densities	95
Figure 5-3 Mesh Bulk adhesive	96
Figure 5-4 FM94 Elastic modulus experimental and numerical data, the value of 3000 MPa was set	97
Figure 5-5SLJ Configuration and boundary conditions.....	98
Figure 5-6 Meshing of the SLJ	99

Figure 5-7 Comparative load-displacement SLJ behaviour using experimental and numerical data	103
Figure 5-8 Load-displacement behaviour of unconditioned SLJ.....	104
Figure 5-9 Failure process in SLJ (a) before damage,(b)crack initiation,(c) crack propagation, (d)Full damage.....	105
Figure 5-10 schematic degradation process for bilinear traction-separation curve	106
Figure 5-11 Variation Strength of SLJ	109
Figure 5-12 Numerical and experimental load-displacement curves FM94.....	110
Figure 6-1 Moisture absorption CFRP G814 (4 mm thickness) exposed to water at different temperatures reported by [45] and T800/M21 (2mm thickness) exposed to hygrothermal cycles	117
Figure 6-2 Influence of water and Temperature on fatigue life for a fixed stress range of 4.7 MPa [139]	122

LIST OF TABLES

Table 1. Factors affect the bond's durability modified [11]	4
Table 2 Examples of stacking sequence used for bonded and bolted joints	9
Table 3 Autoclave Curing Process [102]	43
Table 4 Curing Adhesive process [103].....	44
Table 5 Characterisation moisture samples description	51
Table 6 268 gsm ⁻¹ T800/M21 UD properties	56
Table 7 Fatigue test matrix.....	59
Table 8 FM94 moisture absorption comparison between hot-wet and cold-dry	70
Table 9 Summary of test data unaged and aged SLJ	79
Table 10 FM94 properties	93
Table 11 Details of different meshes employed in the mesh convergence analysis	95
Table 12 Finite Elements results	96
Table 13 Composite Laminate Properties T800/M21 [UD 0°/45°/90°/-45°] _s	99
Table 14 CZM Calibration.....	102
Table 15 Load-displacement results validation unaged SLJ	104
Table 16 Properties of aged adhesive and cohesive used in the CZM of SLJ	107
Table 17 Comparison static response SLJ under hygrothermal ageing conditions	109
Table 18 Comparison of moisture diffusion properties found for FM94 with other results reported.....	114
Table 19 Comparison of moisture diffusion properties found for CFRP T800/M21, together with other results reported	115

LIST OF EQUATIONS

(2-1).....	5
(2-2).....	5
(2-3).....	5
(2-4).....	24
(2-5).....	32
(2-6).....	32
(2-7).....	33
(2-8).....	33
(2-9).....	33
(2-10).....	33
(2-11).....	36
(2-12).....	36
(2-13).....	36
(2-14).....	36
(3-1).....	52
(3-2).....	53
(3-3).....	53
(3-4).....	54
(3-5).....	54
(5-1).....	92
(5-2).....	92
(5-3).....	100
(5-4).....	100
(5-5).....	101
(5-6).....	102
(5-7).....	102
(5-8).....	107
(5-9).....	107

LIST OF ABBREVIATIONS

C	Moisture concentration
CCA	co-curing with adhesive
CCN	Co-curing without adhesive
CFRP	Carbon fibre reinforced polymer
CME	Coefficient of moisture expansion
COB	Co-bonding
CZM	Cohesive Zone Model
D	Diffusion Coefficient
Dh	Diffusion Coefficient
Dh (T)	Diffusion coefficient at temperature specific
E	Elastic modulus
FAA	Federal Aviation Administrator
FCP	Fatigue Crack Propagation
FCP	Fatigue crack propagation
FE	Finite Elements
FRP	Fibre Reinforced Polymer
FT	Tear Failure
G(T,t)	Moisture absorption function
h	thickness
kN	Kilo Newton
LASAT	Laser shock adhesion
LBI	Laser Bond Inspection
LSS	Laminate stacking sequence
M (T,t)	Moisture content function Temperature and time
Mb	Moisture at start of experiments
MCL	Modified crack layer
Mm	Moisture saturation
NDE	Non- Destructive Evaluation
NDI	Non-destructive inspection
NDT	Non-destructive techniques
NPL	National Physical Laboratory Materials Centre
PCMs	Polymer composites materials

PTFE	Polytetrafluoroethylene
R	Stress ratio
RH	Relative Humidity
SDF	Sequential Dual Fick model
SEB	Secondary bonding
SLJ	Single lap joint
T	Temperature
t	time
Tg	Glass transition temperature
UD	Unidirectional
UT	Ultrasonic Technique
Wc	Mass specimen post exposure
Wo	Mass specimen initial drying
wt	Weight

GLOSSARY OF TERMS

Adhesive: epoxy resin (FM94) capable of holding of an adhesive joint in a composite laminar system of CFRP, by a surface bond that can transmitting important structural loads.

Aging: answer of adhesive joint in a composite laminar system of CFRP, after to exposure to hygrothermal conditions using as model a flight of an aircraft for an interval of time.

Adherend: composite laminar system of CFRP joint to another similar through an adhesive.

Hygrothermal effect: result in the properties of a material CFRP due absorption of humidity and the change of temperature.

Fatigue life: Number of cycles necessary to bring an adhesive bond to the point of failure when the bond is subjected to repeat cyclic stressing under specified conditions.

Fatigue strength: Force that a joint will withstand when the force is applied repeatedly for an infinite number of cycles.

1 INTRODUCTION

The main goal of this research is to evaluate the structural strength of an adhesive joint in a composite laminar system of Carbon Fibre Reinforced Polymer (CFRP), which is exposed to a harsh environmental condition. The degradation plan includes mechanical and chemical effects including temperature, moisture and stress (fatigue) to identify the behaviour of the joints.

The Aircraft Industry continuously faces repair issues of composite structures; engineers have to decide what type of joint is able to maintain the integrity for a given time, encouraging the necessity to know about bonded joint characteristics over the long term. Adhesive joints have shown a significant advantage in comparison to traditional mechanical fastening [1] because of the lower weight, reduced stress concentration, high specific stiffness and strength that improve the structural performance [2].

However, the use of bonded joints in primary structures and repairs have been restricted, because of some Airworthiness Authority's concerns about aviation-safety issues related to a lack of knowledge about long-term durability, difficulty with quality assurance, limited standardization of the manufacturing process and repair techniques [3]. For that reason, a study for joint strength prediction in terms of life/strength will provide confidence when using adhesively bonded-joints, instead of the mechanically fastened joints because these induce weakening in two properties: tension, 40 to 60 %; and compression, 15 % [4].

The development of new failure criteria and propagation models is complicated by the difficulty of obtaining repetitive experimental data, more so because composite joint analysis started from models adapted from the typical experiments of metals. There was evidence that failure mechanisms and damage propagation of composites are more complex and have different behaviour than metals [5].

RESEARCH QUESTION

Based on the degradation induced by hygrothermal cycles and load in a CFRP bonded joint; what variables does a numerical model employ to predict the joint strength?

HYPOTHESIS

An experimental degradation programme (hygrothermal cycles and load) will demonstrate behavioural trends and mechanical properties of an adhesive joint (joint strength and failure mechanisms). The experimental data will be used to validate a numerical model designed to predict joint behaviour.

The aim of this research is to evaluate structural strength of an adhesive joint in a CFRP system under a hostile environment (temperature, humidity and load), and develop a numerical model to predict joint behaviour.

This must be done because the joint behaviour has not fully been determined under these conditions and therefore brings into question overall structural integrity.

The scope of this investigation is limited by time constraints and the mechanical behaviour of the laminar system CFRP in the degradation environment. It means that durability issues such as fatigue, temperature and moisture resistance are covered by the scope. However, optimization of the materials, execution and production, as well as economic issues, are outside the scope of this research.

OBJECTIVES

- To measure the performance of bulk adhesive and of joints under mechanical and chemical effects including temperature and moisture cycles and stress (fatigue).
- To identify a numerical model (joint degradation) to predict the behaviour of the joint for long-term use.
- To evaluate the bonded joints with Non-Destructive Inspection to verify the structural performance and to characterise the damage.

2 LITERATURE REVIEW

This literature review provides important information about the more relevant factors that affect the strength and durability in bonded joints and which must be identified and controlled during design, manufacture and service life. This review has therefore been focused principally on: (1) design aspects, (2) environmental impact, (3) studies of the durability of adhesive joints, and (4) damage predictions.

2.1 Adhesive Joints

The bonding of two materials is due to adhesion by the molecular attraction between two parties and is used for the purpose of transferring loads. These materials can be epoxies, polyesters, polyurethanes, methacrylate, etc., [4]. The most common types employed are epoxies [6]. Adhesive bonding is structurally more efficient than conventional joining due to its weight reduction, elevated stiffness and strength, and better stress distribution under cyclic loading [7] [2]. However, disadvantages of bonded joints are (a) the absence of a Non-Destructive Technique (NDT) that can assure the quality of the manufacturing process [8] and (b) adhesive joints cannot easily be disassembled to replace damaged parts [9]. Additionally, joining of thick sections can be susceptible to high peeling stresses [10].

The durability of bonded joints can be affected by many parameters as listed by Bardis and Kedward [11] , and who also described the variables of each one, Table 1. These factors can be classified into two main groups; the first being related to materials and manufacturing procedures, such as materials substrate, adherend lay-up, type of adhesive, surface preparation, manufacturing process, and type of joint, which can be controlled at the design stage; and a second group dependent on the service life conditions, such as load and environmental conditions (i.e. temperature, moisture, chemicals) [12].

Table 1. Factors affect the bond's durability modified [11]

		FACTOR	VARIABLES
Controlled in the design: Materials and manufacturing procedures	Materials	Adherend Material	Fibre, composite, matrix, metal
		Adherend Lay-Up	0° _[n] , quasi-isotropic, other lay-up ; orientation of ply on bonding surface
		Adhesive type	Film adhesive, type of carrier cloths, type of filler, percentage of filler
		Adhesive Preparation	Hand-mixed, machine-mixed, apply vacuum to remove trapped air
	Manufacturing	Type joint	Single lap, double lap, tapered lap, scarf, butt and double strap, stepped lap.
		Bonding process	Secondary bonding, co-cured, co-bonding.
		Bondline Thickness Control	Glass microbeads/silane treatment, wires, tabs/tape, applied pressure
		Compressed "Shop Air" Blowing	Pressure, exposure time
	Surface preparation	Grit Blast	Pressure, grit size, number of passes, speed of passes
		Hand Sanding	Grit size, number of passes, pressure applied
		Peel Ply or Release Film	Nylon, polyester, none
		Solvent wiping	Acetone, isopropyl alcohol, number of wipes, applicator type
		Temperature Exposure	Temperature, exposure time, pre-bond, post-bond, under load
Humidity Exposure		Humidity %, exposure time, prebond, postbond.	
Controlled by the service life	Environmental Degradation	Humidity, temperature, pressure, hygothermal cycles, solar radiation, water.	
	Corrosion	Acids, hydraulic fluid, jet fuel, anti-icing additives, pollution	
	Load	Fatigue, bending.	

2.2 Design Aspects

2.2.1 Type of Joint

The single lap joint is the most common type of joint used to measure the behaviour of adhesive joints; as it is economic and easily repeatable. However, the single lap is the weakest joint as a result of eccentricity of loading. The misalignment causes bending moments (through thickness direction), resulting in high peeling stress of adherend and non-uniform shear stress in the adhesive layer [13] [14] [15]. Figure 2-1 shows the shear and peel stress distribution along the overlap.

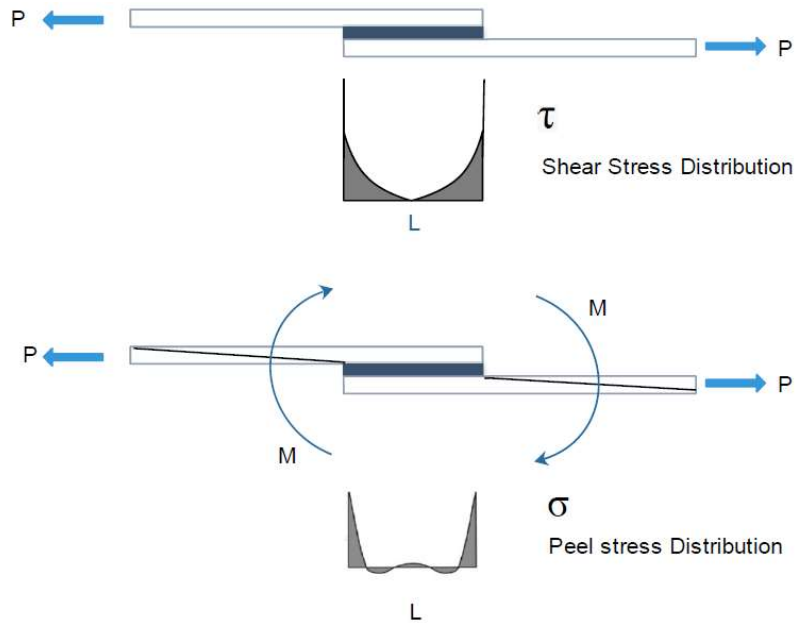


Figure 2-1 Stress distribution in SLJ [16]

The Linear-Elastic Volkersen's Analysis described the shear stress (τ) distribution with the equation (2-1). This analysis assumes that the adhesive is deforming only in shear and the adherends deform elastically only in tension. A_1 and A_2 are arbitrary constants, defined by the boundary conditions [17].

$$\tau_x = A_1 \cosh wx + A_2 \sinh wx \quad (2-1)$$

$$w = \sqrt{\frac{G}{Et_s t_a} \left(1 + \frac{t_{s \text{ top}}}{t_{s \text{ bottom}}}\right)} \quad (2-2)$$

Where G is the adhesive shear modulus, E the adherend modulus, and t_s and t_a the adherend and adhesive thickness. Then the maximum shear stress (τ_{max}) is presented in equation (2-3) with (l) as overlap length.

$$\tau_{max} = \sqrt{\left(\frac{Gl^2}{2Et_s t_a}\right)} \quad (2-3)$$

Hence, based on (2-3) it is understood that the strength of the joint depends on both properties of the adherend and the bondline interface, as well the geometry parameters [18].

- **Effects of increasing either adherend thickness or adherend stiffness:**

The load-bearing capacity is increased because the peak stress levels are reduced and the stress distribution in the bondline becomes more uniform [13]. However, the adherend thickness increment is limited to an appropriate range in relation with the bondline thickness [19].

Li et al [2] found that the ultimate load and shear strength increased with the increment of the adherend thickness, as seen in Figure 2-2, but its relation is not directly proportional to an efficiency factor of approximately 0.25.

- **Increase in the adhesive thickness or reduction of shear modulus of the adhesive:**

The effect being that the peak adhesive stress is reduced and the shear strains are distributed along the whole dimension, resulting in lower strains per unit length [13]. Taib, A. et al [20] studied the effect of adhesive thickness on the strength, and they found a significant increment of the failure load and displacement with the reduction of the adhesive layer thickness.

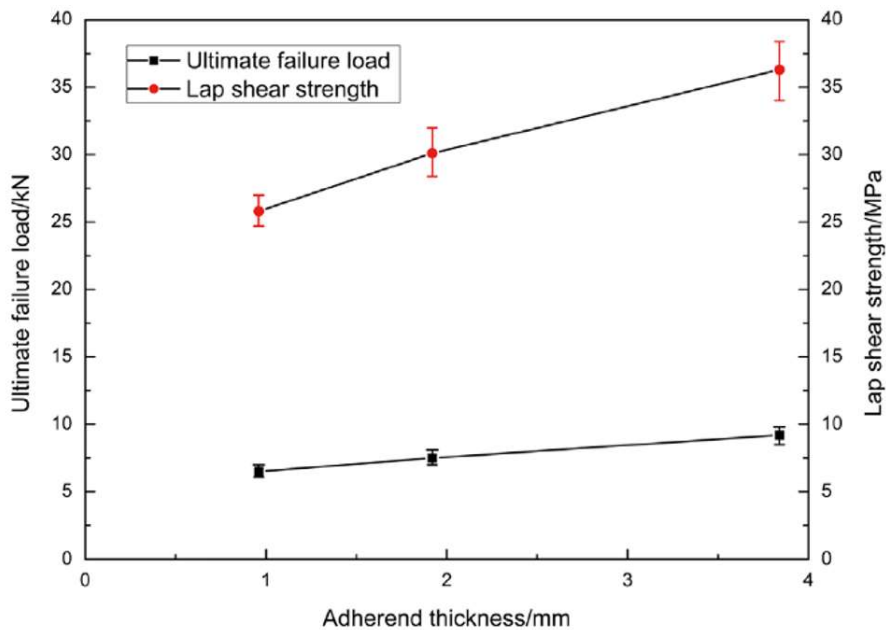


Figure 2-2 Peak failure load and lap shear of SLJ with different adherend thickness[2]

- **Effects of Overlap Length**

The overlap length must be enough to reduce the stress concentration caused by the eccentricity path load and ensure low stresses in the middle of the overlap. A low-stress region in the middle can avoid creep failure. An overlap length approximately ten times the minimum adherend thickness is recommended because an overlap excessively long does not substantially increase the static or fatigue strength, but it may produce a weight penalty [13].

The increasing of the overlap length increases the failure load and reduces the shear stress. The load increment is not linearly proportional with the overlap increase because the load transfer is governed by the edge of the bond area [13].

A comparison of strength for different overlap lengths of single lap joints is shown in Figure 2-3. It illustrates the reduction of the strength versus the overlap length increment. Song et al. [21] considered 25.4 mm overlap length as 100 % joint strength because this length represents the medium value of strength (failure load 11.7 kN). And length of 38.1 mm registered 24 % lower strength (failure load 12.4 kN) than the baseline (25.4 mm). Similar results were reported by Li et al. who tested CFRP single lap joint at different overlap lengths and reported that at longer overlaps, the peel stress increased causing delamination failure [2].

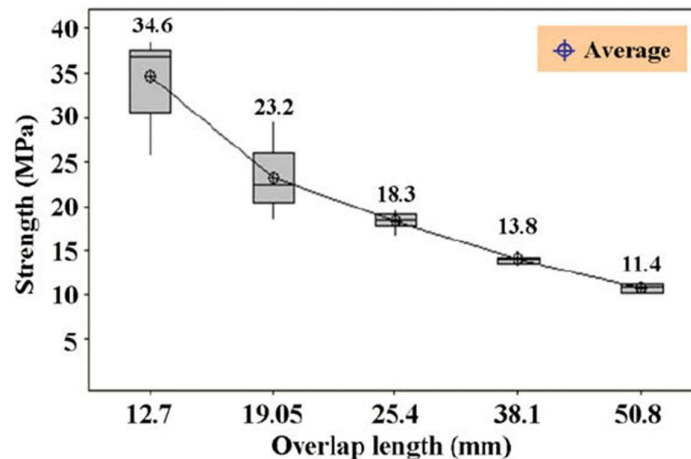


Figure 2-3 strength of Secondary bonding joints with different overlap lengths (source:Song et al. 2010)

However, Volkersen's theory does not take account of two important factors namely the eccentricity of the load path, and the adherend bending. Hence, in addition to the adhesive shear stress, the design analysis has to evaluate the effect of the peel stress and the secondary bending stress.

Specifically in composite adherends, the bending stress leads to inter-laminar failure mode. The composite adherend is weaker under inter-laminar tensile stress than the adhesive in peel stress [15]. As shown in Figure 2-4 the peel stress near the end of the adherends leads to delamination. For that reason, fillets and end tabs are used as measures to minimise the eccentricity in single lap joints and avoid adherends failure [13], [22].

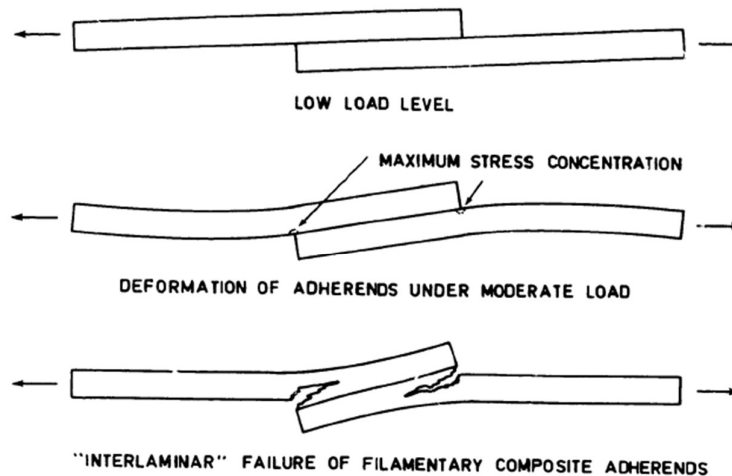


Figure 2-4 Failure SLJ with composite adherend modified [15]

2.2.2 Laminate Lay-Up and Stacking Sequence

Laminate Stacking Sequence (LSS) affects properties in things such as strength, stiffness, stability and damage tolerance. Thus in order to obtain an optimum strength the Military Handbook [19] recommends a homogeneous, balanced and symmetric LSS, allied to a minimum of four different ply angles to get a quasi-isotropic material. The National Physical Laboratory (NPL) Manual states that the distribution of plies should preferably be of 25 % plies in 0° , 25 % plies in 90° and 50 % plies in $\pm 45^\circ$ [13].

Additionally, this same NPL Manual suggests, for bolted joints, the quasi-isotropic lay-up ($0^\circ/90^\circ/\pm 45^\circ$) shows better performance. Moreover, if the laminate has a

highest percentage of 0° layers and a small percentage of transverse fibre layers, the failure will result in shear out. The European Space Agency (ESA) Structural Material Handbook states that the stress concentration is reduced with addition of ±45° layers [13].

Matthew and Tester [14] studied the impact on the strength of CFRP bonded joints, with different configurations of stacking sequence for 6, 8, 10 and 12 plies. And they found that for a configuration of 8 ply laminates, the best performance is obtained using 0° layers in the outside of each substrate.

Researchers commonly use a balanced and symmetric quasi-isotropic lay-up to develop their studies of both mechanical and bonded joints, as shown in Table 2. Authors used differently distributed orientation plies in order to reduce the stress concentration and cleavage. Some studies employed only 0° layers while other researchers such as [2], [23], [24], and [25] selected a stacking sequence used by the aircraft industry. Overall however, there is as yet not a unified stacking sequence to evaluate the strength.

Table 2 Examples of stacking sequence used for bonded and bolted joints

JOINT	AUTHOR/YEAR	LAMINATE STACKING SEQUENCE
Adhesive	Ashcroft et al., 2001 [1]	[0/-45/45/0] _{2S}
	Knight et al.,2012 [26]	[0] ₁₆
	Hu et al., 2014 [27]	[0/90/0/90/0/90/0/90/0]
	Hong, Hand and Chang, 2015[28]	[0] _{12T}
	Li et al.,2015 [2]	
Mechanical	Zhai et al.,2015 [24], Soutis, 2014 [25], Atas and Soutis, 2014 [25]	[45/0/-45/90]_{2S}
	Bodjona et al.,2015 [29]	[45/0/-45/90] _{4S}
	Atas and Soutis,2014[25]	[0/90/45/-45] _{2S}
	Saleem et al.,2015 [23]	[90/45/0/-45] _{2S}

2.3 Manufacturing Processes

There are five conditions for manufacturing a durable adhesive joint: correct surface preparation, proper mixing or applying of the adhesive, controlling bond

line thickness, uniform pressure during curing, proper time and temperature of curing [6].

2.3.1 Surface Preparation

The adhesive bond quality is significantly affected by the surface preparation; ideally the stress should be transmitted through adherend/adhesive interface. An adhesive joint has to satisfy three characteristics: (a) it must avoid wet surface, (b) allow bonding between adherend and adhesive and (c) it should be durable.

The durability of an adhesive bond depends on the chemical strength, and it is influenced by physical and chemical interfaces [30]. In order to improve durability, the surface roughness, surface chemical treatment and contaminants must be controlled.

There are several treatments to prepare the surface of composite adherends, mainly grit blasting, peel ply, atmospheric plasma and atmospheric laser and various chemical treatments.

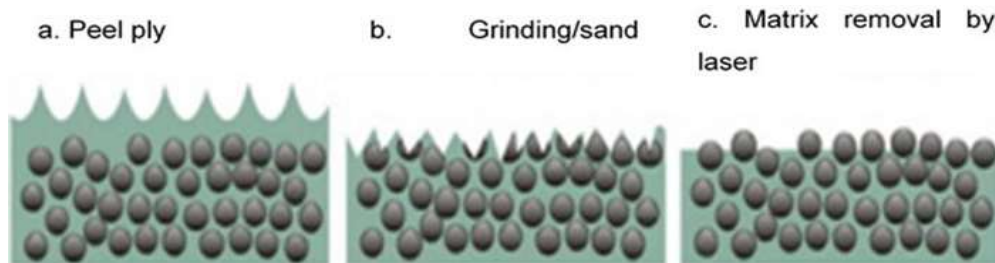


Figure 2-5 schematic surface appearance for different treatments a. peel ply, b. mechanical, c. laser [31]

Peel ply treatment consists of a layer of open-weave material (nylon, fiberglass) added on to the surface of the prepreg lay-up, and it is removed after curing immediately before bonding [32]. The resulting surface is clean and rough, but with low activated surface and high risk of contamination [31]. This technique is used in the aerospace industry for surface preparation of CFRP structures; however, the increment of use of complex manufactured components has caused this technique to be deemed unsuitable for CFRP repair areas [33].

Mechanical treatment by abrasive paper or blasting (aluminium or sand grit) causes the first resin layer to be removed with the potential contaminants. The grit blasting process is cheaper, but it can damage the carbon fibre [34], [35].

Atmospheric Pressure Plasma (APP) is a physical-chemical process that uses an ionized gas (Argon, Oxygen, Nitrogen, and Ammonia). The ionised gas molecules penetrate and activate the ions, electrons and radicals of the surface; as a result, the surface is modified without affecting the bulk properties [36]. Plasma treatment offers the best surface energy and joint strength [35]. However, it is not currently used in the aerospace industry [37].

Laser treatment may ablate a thin resin layer without damaging the fibre but removes all the contaminants [31]. It needs minimal previous preparation and is carried out dry. The advantage of this process is its suitability for large and complex areas [33]. Nevertheless, the final state of the surface has to be closely evaluated because of changes in the thickness of the resin layer.

Hart-Smith, Redmon and Davis studied the use of nylon peel ply and identified that a mechanical abrasion is required to remove nylon residue as the nylon is incompatible with epoxy materials [38]. On the other hand, Knight *et al.* later stated that using polyester peel ply in Carbon surface preparation may offer surface roughness and minimise the contamination, because the polyester ply does not require the use of an agent to remove it [26].

Madge *et al.* [39] and Kumar Singh [34] evaluated the strength of bonded composite joints and found that the peel ply surface preparation offers less strength behaviour than mechanical treatments, plasma and laser.

Gomatam and Sancaktar studied the effect of different surface treatments for bonded joints subjected to fatigue load after being exposed to environmental conditions. Substrates of aluminium and steel were treated with grit blasting, silane coupling and plasma. The authors found that the grit blasting retarded the absorption of moisture, preventing the joint degradation [40].

Gude *et al.* [35], studied the influence of different surface treatments on the strength of joints aged under hygrothermal conditions of 55 °C and 95 %RH. They

tested polyester ply, grit blasting and APP and found that surface preparation with plasma showed a better adhesive joint strength before the environmental attack. However, after hygrothermal-ageing, the joint treated by peel ply showed better strength properties as compared to APP treatment [35]. This because ageing is harsher on high energy surface materials, as is the case of plasma treatment. Encinas *et al.* [41] agree with the disadvantaged response of plasma treatment surface under humidity conditions[41]. This considered, the peel ply offers a better response after aging because of the low activated energy surface which results in a relaxation of stresses in the interface.

2.4 Durability

2.4.1 Environmental Effects

Despite the inherent advantages of the polymeric structures, there are concerns regarding performance under harsh and changing environmental conditions. For that reason, researchers have been evaluating the complex degradation mechanisms and testing configuration to identify: the durability of bonded joints; the effects of contaminated bonded surfaces; and non-destructive techniques to predict the failure and fatigue [42], [43].

Several researchers analyse resistance to environmental degradation of polymers and composites through the physical, chemical and mechanical variables by monitoring changes in area and weight, and analysing resistance by their loss and/or gain of humidity as a function of time.

Specifically in the case of the moisture, some authors have shown changes in the properties of adhesives and polymer composites materials (PCMs) such as variation of plasticization, swelling, micro-cracking and crazing, hydrolysis, strength loss or an increase of ductility, as a result of the effect of humidity absorption, some being reversible and some not. [44], [45].

All thermal, mechanical and chemical changes are related to the moisture transport in the polymer and are directly connected with the molecular-sized free volume in the polymer, and the water affinity of the polymer. The amount of free holes is influenced by the curing degree, chain stiffness, stoichiometry and

cohesive energy density of the polymer. The water affinity depends on the polymer network's sensitivity to create hydrogen bonds with the water molecules, the hydrogen chain may also occur through a chemical reaction known as hydrolysis [46], [47].

One mechanism of the moisture diffusion, occurs through the free volume, not by interaction with the polymer molecules nor by affecting the dimension. Another mechanism which occurs at the hydrolysis reaction phase results in molecular structure changes because the moisture interrupts the Van Der Waals bonds between the polymer chains [46]. In epoxies, change of the glass transition temperature (T_g), swelling and plasticization have been observed because of the interrupted interchange of hydrogen bonding with the polymer [47]. *Figure 2-6* shows the effect of the moisture content on the T_g of some structural adhesives.

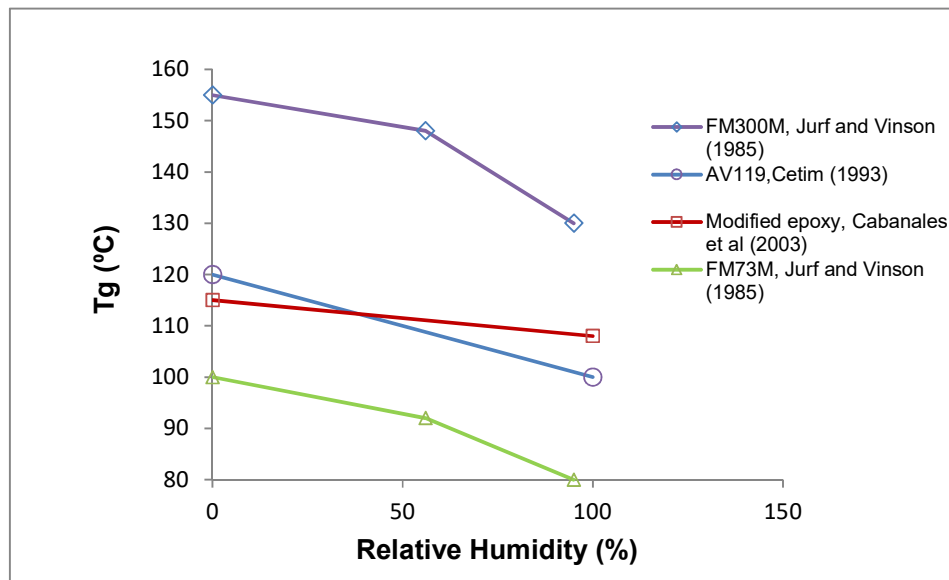


Figure 2-6 Moisture effects on T_g [48]

Changes in temperature may also affect the behaviour of polymers i.e at a higher T_g the properties suffer a continuous degradation, resulting in oxidation, chemical attack and mechanical creep [49], [44].

In humid conditions, an increment of the temperature causes reduction of the solubility of adhesive, increases the diffusivity and moisture content [46]. At sub-zero temperatures there is a change in water state, causing swelling,

hygrothermal stresses and polymer interlocking breaks. Those local fractures are known as cracking/crazing. In this case, the molecular structure may be affected thus modifying the Tg [45].

Several efforts have been made to study the environmental effects on joint durability. Adhesive bonding of aluminium- aluminium, aluminium-composite, steel-composite and composite-composite have been studied. Banea and da Silva [44] affirms that for the specific case of composite-composite bonded joint, the kinetics of water absorption is different compared to metal-bonded joints. The water is absorbed into the joint and causes degradation of the adhesive, the Fibre Reinforced Polymer (FRP) composite, and the interface as illustrated in Figure 2-7.

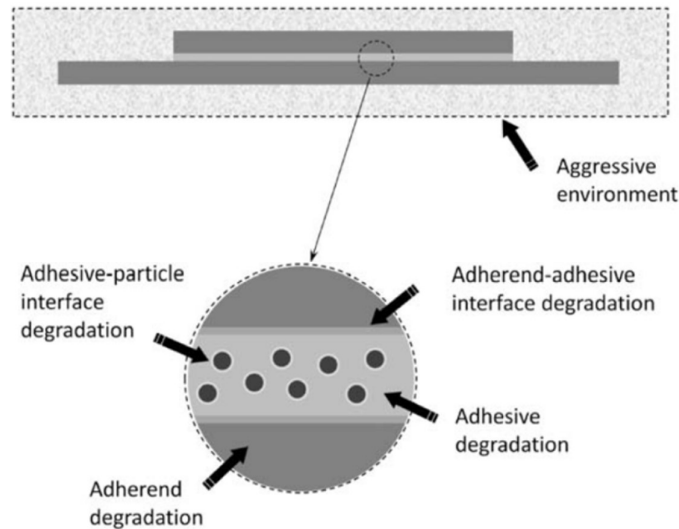


Figure 2-7 Environmental effects in joints [50]

The adhesive when affected by the mechanism of plasticization causes swelling, cracking and hydrolysis [51]. Three damage mechanisms caused by moisture have been identified for composite substrate: resin matrix modification, interface fibre/matrix debond, and fibre degradation. *Figure 2-8* illustrates the different diffusion mechanism discussed previously and the damages suffered by a fibre-reinforced polymer composite.

In bonded joints, the interface stability under humid conditions plays an important role in the joint strength. In the interface, the moisture diffusion occurs more

quickly than in the bulk adhesive. The moisture enters into the bulk adhesive travels speedily through the interface and is absorbed into the composite adherend by diffusion and capillary phenomenon [51][52]. Those mechanisms may reduce the bond strength adhesion between the adherend and the adhesive. However, according to Banea and da Silva [44] in epoxy/FRP composite interface, the thermodynamic work of adhesion remains positive after ageing in water, which can reduce the probability of interfacial failure.

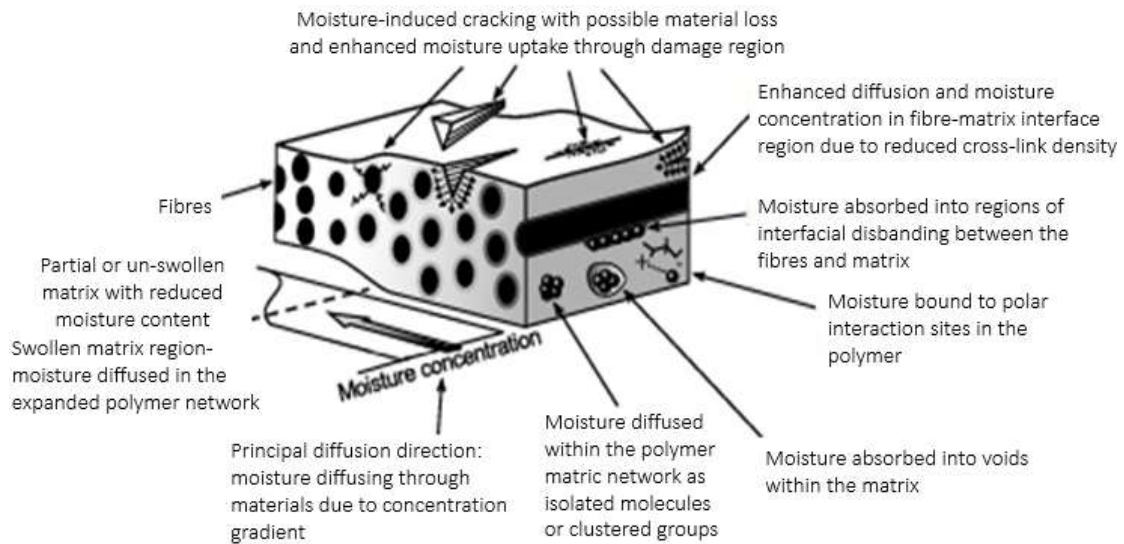


Figure 2-8 Moisture absorption in polymeric composites [46]

Knight et al. [26] investigated the impact of the ageing of a single lap joint under environmental conditions of 82°C and 85 % RH for 772 days. They used CFRP adherend of Toray T800H/3900-2 and secondary bonding of AF555M adhesive. They found a reduction in the shear strength and modifications of failure modes. Although they did not find indications of interfacial failure in the adhesive after a drying process, there was evidence of a reduction in the strength which shows that some irreversible changes took place. They attributed the effect on the strength, after the water desorption, to new bonds between water molecules and adhesive networks. Parker [53] studied the strength of CFRP-epoxy bonded joints, the joints were ageing at 50°C and 96 % RH (over saturated K₂SO₄) for 375 days and tested at 20 °C, 60 °C and 80 °C. They found evidence of interfacial failure after a long exposure time at hot humid conditions, and joint strength reduction caused by moisture content and temperature increment.

2.4.2 Hygrothermal Cycles Effects

The moisture and temperature effects have been extensively studied simulating static environmental conditions, as discussed in the previous section. However, the strength degradation of adhesively bonded joints is heightened when the joints experience cyclic humidity and temperature [54], [55].

Composites have to resist stress while being exposed to an aggressive environment in aerospace applications. These extreme conditions include humidity, pressure, high and low temperatures, hygrothermal stockings as well as harsh solutions such as solvents, paint strippers, aviation fuel or lubricants, salt water, hydraulic and de-icing fluids [56], [35].

The operating temperatures in an aircraft have several changes due to the conditions of use; normally low temperatures occur during high altitude flight, or when the plane flies in cold climate it may decrease to around $-54\text{ }^{\circ}\text{C}$. High temperatures can be present depending on the area in the structure and type of aircraft. In flight, the components near to the engines can reach $130\text{ }^{\circ}\text{C}$, also during take-off, some parts are exposed to temperatures of up to $92\text{ }^{\circ}\text{C}$. On the ground, the skin of the frame in tropical and hot climates can reach $71\text{ }^{\circ}\text{C}$ [56].

Jedidi et al. designed an accelerated hygrothermal cycle to evaluate polymer matrix composites used under conditions of supersonic aircraft. The cycles modelled the time on the ground, take off, flight at subsonic and supersonic mode, and landing. The study was focused on the drying effect, at high temperatures ($130\text{ }^{\circ}\text{C}$), in the durability of the composites used in primary structures. The study showed a novel procedure to design an accelerated hygrothermal cycle to represent supersonic environmental conditions. They performed the flight-cycle conditions and the maintenance time. *Figure 2-9* shows the moisture and temperature realistic changes along the flight operations. They used Fick's Law to characterize the moisture state in conditions of absorption (during maintenance operation in ground) and desorption after flying 300 flight-cycles [57].

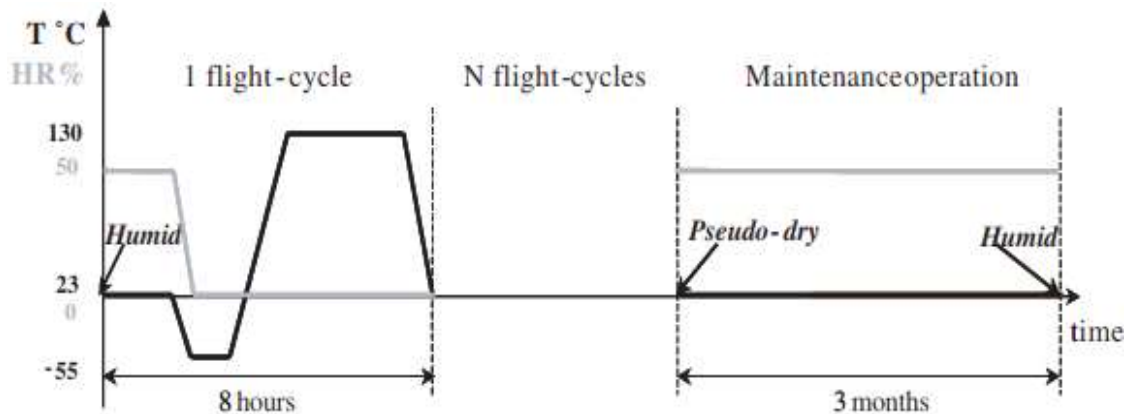


Figure 2-9 Hygrothermal ageing flight-cycles and maintenance operation for supersonic aircraft structures [57]

Hu et al. performed a mixed experimental-analytical study to characterise the effect of cycle-temperature on an adhesive bonded joint of CRFP-steel with adhesive Araldite AV138. They used a cohesive model to predict the strength degradation and validated with the experimental data. Single lap joints were conditioned under cycles of two hours of heating up +80 °C and cooling to -30 °C. Samples were taken every 84 hours for up to a total of 672 hours. Additionally, samples without degradation were tested in order to compare against those with a level of degradation. They found that the tensile strength was reduced with relation to the number of cycles and that the mode of failure changed from cohesive failure to adhesive failure after the cycles [27].

Korta et al. [55] developed an experimental and numerical study to determine the effect of the humidity-temperature cycle of ageing on shear and tensile strength of multi-material bonded joints. They employed two different adhesives to bond single lap samples of CFRP to steel and CFRP to aluminium. The testing was performed according to SAE standards for the automotive industry, considering two different cycle types. The first was at accelerated heating up to 85 °C and 95 %RH and holding for 5 hours. This was followed by a heating up to 180 °C and holding 1.40 hours and cooling to -40 °C. The second cycle was a heating up to 85 °C and 95 %RH and holding for 8 hours to finalise with cooling to -40 °C. To

predict the behaviour some finite element analysis was carried out using Altair Radios solver. They found with this ageing that an important number of samples showed premature failure. The cycle of temperature led to the debonding of joints. The reduction of strength properties was more severe in the case of samples subjected to the first type of ageing. Also, samples of cylindrical joints of CFRP-CFRP were tested under tensile load, after the ageing, the tensile performance of CFRP-CFRP joints was increased [55].

Agarwal et al. [58] performed freeze-thaw cycles to Steel-CFRP lap joints; they found strength reductions of 28 % after 40 cycles and change in the type of failure mode. The reduction can be attributed to microcracks caused by the expansion of the water molecules at low temperature [59].

Additionally, some researchers have demonstrated that cooling an epoxy resin at sub-zero temperature after saturation at high temperature (below the T_g) results in higher water absorption [60]

2.4.3 Fatigue Durability

Predicting fatigue is a difficult task due to the complex modes of crack initiation, propagation, variable behaviour of adhesive, substrate and interface faced with moisture and temperature environments, the geometry of joint and complex performance of composite under loading cycles. However, fatigue durability can be evaluated from the loss of strength, and fatigue resistance when the element is subjected to diverse environmental conditions [61] and [62].

The influence of the humidity and the temperature on fatigue have been extensively studied, especially joints of metal adherends.

Broughton and Mera [62] studied the fatigue behaviour of a double lap joint subjected to environmental conditions of 70 °C and 95 %RH for 750 hours and testing at -55 °C, 20 °C and 130 °C. They used two different adhesives F6552/T650-35 and HP655 with substrates of CFRP. Fatigue life was reduced after ageing conditions, at the elevated temperature test (130 °C) the impact was significantly higher.

Ashcroft and Shaw [8] studied the effect of temperature on Fatigue Crack Propagation (FCP), they tested double lap and strap lap joints of CFRP at -50°C , 22°C and 90°C and found that temperature has an important effect on the fatigue crack growth rate. Also, the induced failure shifted from adherend layer to adhesive layer as the temperature increased. Furthermore, they used a mechanical failure model in order to predict the threshold failure with a good approximation.

Despite the fact that humidity and temperature diminish the joint strength, the temperature has a high toll on the joint durability [63].

Abdo and Aglan, (1997) [64] worked in determining the influence of aerospace cyclic thermal ageing on the static and fatigue behaviour of the adhesive SLJ of Aluminium 7075-T6 and Adhesive 3M AF-163-2K. The thermal cycle was in accordance with ASTM D1183 test procedure C and consists of increasing the temperature up to 74.5°C with less than 10 %RH for 48 hours, followed by a decrease of temperature down to 23.5°C and 100 %RH for 48 hours. This was then followed by a reduction in temperature to -58°C and 100 %RH for 8 hours and then finally increasing the temperature up to 39°C and 100 %RH for 64 hours, as shown in Figure 2-10. Samples were tested at 2 weeks, 4 weeks and 6 weeks thermal cyclic duration. Under a static condition, the joint strain increased with the number of cycles, and the displacement increased to 2.5 mm for the 6 thermal cycles, but the load strength joint was not significantly affected by the cycling. For fatigue testing, the fatigue strength was reduced by 47 % at 6 thermal cycles. The failure mode was a cohesive failure. The degradation by moisture was presented at the first cycles and caused an increase in the fatigue crack propagation. Moreover, a Modified Crack Layer (MCL) model was employed to predict the failure with successful results.

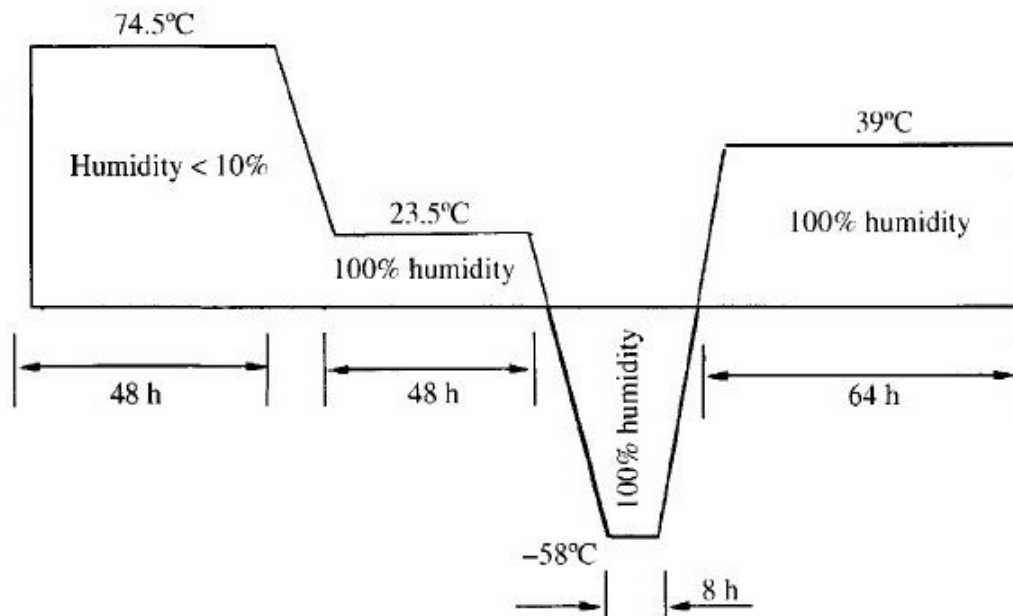


Figure 2-10 Thermal ageing cycle [64]

2.5 Non-destructive Testing

According to the Federal Aviation Administration (FAA), the continued airworthiness of both bonded structures and composite repairs need to be assured with an inspection to detect and to quantitatively estimate any defect size [65]. Also, the assurance of the bond is an important part of the qualification of the joint in civil and automotive industries.

There is an apparent lack of means to non-destructively measure the bond strength in primary structures of aircraft. Structural engineers don't have actual bond strength values so they can't predict the life. In manufacturing, the bonding process is more controlled than in repair. It is because the variability process can lead to degradation of strength. For this reason, developing the NDT is a priority to determine the joint strength [6].

The composite inspections have been performed with techniques such as ultrasonic, X-ray radiography, visual inspection, leak test, bond test, acoustic emission, low-frequency vibration, thermography, shearography, and holographic [66]. They have successfully detected defects; nevertheless, they have not been able to detect weak bonds (kissing bond). So, the actual NDT is

not effective to assure the quality in terms of bond strength, physical and chemical properties of adhesion, or prediction of crack growth [67].

2.5.1 Types of Defects

The NDI studies have been focusing on the characteristic of failure of the adherend/adhesive interface. The main designers' concern focuses on the joint structures working at nearly full strength because the degradation causes reduction or loss of bond strength [6].

Examples of effects found in the adhesively bonded joint are delamination, debond, porosity, voids (high volume porosity), incorrect matrix cure and cracks, weak and kissing bonds [67]. Disbonds are related to moisture content, lack of surface preparation, impact damage or local over-heating, see *Figure 2-11*. These disbonds can be detected by ultrasonic or acoustic inspection.

Weak bonds are associated with a design issue. The adherends are in intimate contact but the interface doesn't ensure a mechanical load transfer capacity, and this kind of defect is not detectable presently by non-destructive inspection [68] [6].

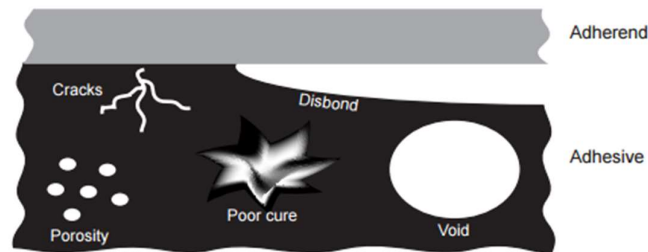


Figure 2-11 Defects on adhesive joint [69]

2.5.2 Non-Destructive Inspection Methods

The testing methodology used to define the properties of materials is known as Non-Destructive Evaluation (NDE). The NDE studies to measure the bond strength have been addressed to determine the chemical bonding in the interface [6].

The developments to inspect bonds have been using physical waves for the evaluation of the bond strength. The material response of front wave is seen as

a mechanical property. The parameters such as, frequency, signal shape and amplitude of the wave are used as criterion for qualification of the adhesive joint [67]. Ultrasonic and laser are the most common methods used in the industry for bonded joint inspections. Recently, studies also have tested shearography, computational tomography and holographic techniques to evaluate bonded structures.

Ultrasonic applies to composite using frequency of 5 MHz, this technique includes methods such as pulse-echo, through-transmission, ultrasonic spectroscopy, harmonic imaging, oblique incidence, guided waves, ultrasonic acoustic and shear wave resonance. Although for the NDE technology, the ultrasonic methods have not allowed detecting changes of bond strength, they can provide information about the morphological and elastic characteristics of the interface of bonded joints [67] .

Active Thermography, this technique induces an external temperature gradient; the thermal flow in the structure is monitored to detect temperature resulting over the surface. It is unable to detect weak bonds due to the anisotropy of the composite materials and the small heat diffusion. However, thermography combined with the proper tool of excitation is a potential NDE method to measure the bond strength [67].

The Laser Shock Adhesion (LASAT) developed by CNRS and Laser Bond Inspection (LBI) created by Boeing and LSP Technologies, are the most efficient tool. Laser shock wave generated by plasma propagates through the joint structure in compression with a reflection signal on the back surface that induces a tensile load that can rupture a weak bond, attenuating the signal read [67].

Although some limitations of thickness arise because of the attenuation, laser adhesion tests have been used to describe different levels of adhesion of weak composite bonds and correlated with the mechanical strength values and validated with post-failure tests such as interferometric confocal microscopy, ultrasonic and visual inspection [6].

2.6 Damage Prediction

2.6.1 Models to predict durability

In order to predict the service life of adhesive joints exposed to a hostile environment, the moisture diffusion behaviour in the adhesive joints has to be known. Diffusion models have been developed to understand the phenomenon; those can be grouped based on the mechanism of diffusion moisture in the adhesive.

The first diffusion assumes that the water molecules diffuse into the epoxy and reside in free volume of the material. The second model assumes a chemical interaction between water molecules and the polymer matrix. A third mechanism, known as anomalous diffusion, combines physical and chemical interactions. Furthermore, a phenomenon of capillary diffusion affects some variables as temperature, surface effects and swelling [12], [70].

There are three main approaches to predict the durability of adhesive joints; one is the stress- life approach, which is based on the stress and strain of the adhesive joint. The main advantage of this approach is that it is simpler than others, but it needs care with the refinement and converging of the mesh. The second approach is fatigue crack initiation/propagation approach. This method supposes that materials have defects and the cracks and crack growth follow a fracture criterion. The fatigue crack initiation method has been less studied because of the difficulty to link a model of nucleation of crack, and to find the initiation phase. Additionally, a fracture mechanics method can be limited to the pre-existence of crack to establish the strain energy release rate.

Finally, the Cohesive Zone Model (CZM) based on a traction-separation constitutive law, can model multiple cracks; without a need to know the directions of propagation, in order to predict the initiation and failure [61], [70].

2.6.2 Modelling Moisture Diffusion

To determine moisture concentration there are two methods of testing currently in use. First, there is no uniform moisture distribution so the specimens

are exposed to moisture for a fixed time. This method is used as a form of quality control and also to compare batches of materials with similar geometry and manufacture conditions. The second method involves specimens been subjected to moisture until they reach the equilibrium condition and this is then used to determine properties of the material associated with the diffusion process. Its condition depends on the thickness of the bond layer [71], [72].

The moisture diffusion in polymers is governed by mechanisms and physical phenomena, which are taken as factors in the mathematical model. Fick's Law has been presented as the simplest mathematical equation to describe the diffusion in polymers. Fick's Law assumes that molar flux caused by diffusion of a substance through a unit area is proportional to the concentration gradient as shown in (2-4). Fick's Law assumes that the water molecules don't interact with polymer molecules [12].

$$F = -D \frac{\partial C}{\partial x} \quad (2-4)$$

However, some polymers have not shown Fick's moisture diffusion behaviour [70], [73], [12]. Hence, based on different findings, the concentration models have been grouped as follows [46]:

Concentration Independent of Fick's Law:

- Water molecules move freely.
- Mobility is smaller than stress relaxation rate of the polymer structure.
- No interaction between molecules.
- The diffusion becomes zero at saturation level.

Concentration Dependent of Fick's Law:

- At temperatures above the glass transition temperature (T_g).
- Free volume, void size and mobility are increased.
- Internal stress relaxation is not instantaneous.
- Diffusion is dependent on moisture (history), boundary conditions and time.

Non-Fick's Law or Anomalous:

- At temperatures below T_g .
- Hydrolysis of polymer molecules.
- Mobility and stress relaxation rate are similar.
- A dual-mode absorption, Fick's diffusion and polymer relaxation phenomena.

The diffusion of moisture in polymers is usually studied with Fick's Second Law, which describes the concentration in non-permanent state for three dimensional spaces.

Liljedahl [48] who studied the diffusion through FM73 adhesive, got a good agreement with Fick's diffusion model. Gude, Prolongo and Ureña, (2013) employed the solution for Fick's Law proposed by Crank [74] to find the concentration of moisture in a carbon fibre/epoxy bonded joint.

On the other hand, Mubashar [70] reported the non-Fick diffusion behaviour of FM73 adhesive, it was immersed in water until saturation at 50°C and 70°C and then subjected to cycles of desorption. The moisture diffusion for absorption was not predicted by Fick's model, while for desorption the model presented a good correlation with the experimental data.

Wahab *et al.*, (2001) worked to develop an accurate transient diffusion model based on the diffusion stress analysis model. They studied experimentally, numerically and analytically the diffusion of moisture in adhesive joints of CFRP, a sample of composite and adhesive were conditioned at 45°C/85 %RH and 90°C and 97 %RH. The moisture absorption of adhesive showed Fick's behaviour while the absorption in composite at 90°C and 97 % RH presented non-Fick's behaviour.

Models have been developed to predict non-Fick's diffusion behaviour. One of these is a modification to Fick's Law known as Dual Fick's Model, which considers two mechanisms in parallel with different diffusion properties. Ameli *et al.* [75] proposed that a Sequential Dual Fick's (SDF) model may be used to predict the

moisture concentration in adhesive joints subjected to fluctuating temperature and humidity.

A second uptake stage has been noted in epoxy adhesives, at low temperatures [76]. In these cases of the second stage of rapid diffusion, Amelia et al. [12] have affirmed that a SDF model can predict the diffusion behaviour and maximum moisture content.

2.6.3 Cohesive Zone Modelling

The Cohesive Zone Modelling (CZM) has been used widely to predict the failure load of bonded joints and more recently employed to predict the degradation caused by moisture and temperature cycles [77],[78].

The mechanical fracture is described by a phenomenological model, which uses a material model represented by a traction- separation law or cohesive law. The cohesive model is used to predict the damage initiation, propagation, and ultimate failure. Before the initiation, the material remains bonded by traction as cohesive zone elements. Then, two new surfaces are initiated while the crack is growing, see Figure 2-12; the crack propagates and finally the material fails and separate originating two new surfaces. The traction changes in relation to the displacement of the surfaces [79].

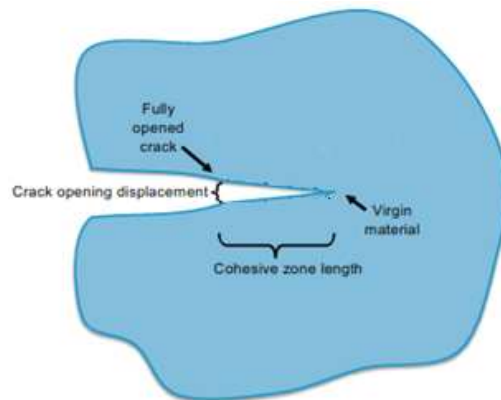


Figure 2-12 Crack growth in cohesive zone [80]

To model composite failure, micro mechanical concepts or cohesive laws can be used. As shown Figure 2-13, the interface between two materials is modelled as a cohesive layer of elements [81].

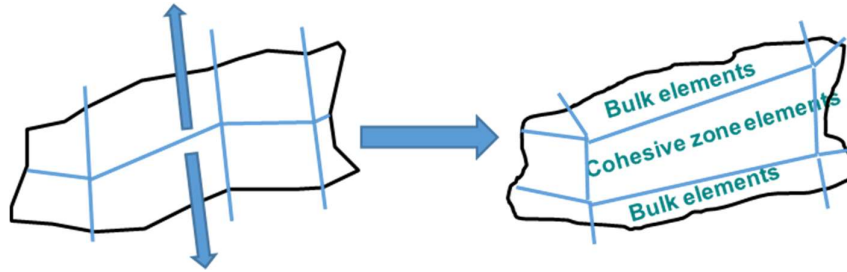


Figure 2-13 Cohesive Interface [82]

In numerical applications there are three methods to formulate the cohesive layer [83]:

1. Modelling as an interface between two bonded bodies where the thickness of the layer is overlooked. The material law model considers that the fracture energy is intrinsic because of traction.
2. Modelling as an elastoplastic continuum with fracture parameter where the adhesive layer is considered by volume. The material properties are degraded progressively by the evolving damage parameters using traction separation law.
3. Modelling as a bi-material interface consistent with layer thickness where the macroscopic response of the interface is described under the cohesive law.

The first approach is commonly used to model interface in composite laminates, interface in bonded joints, or interface between solid phases of materials [84]. The second method uses a continuum mechanical method and it presents the highest degree of accuracy; however, it requires elastic properties as well as fracture adhesive parameters. It is also numerically more complex to implement. The continuum approach is used to model the cohesive fracture of the adhesive bond [84]. The balance is reached using modelling method 3, achieving greater accuracy than modelling method 1, and offers greater simplicity than modelling method 2 [83].

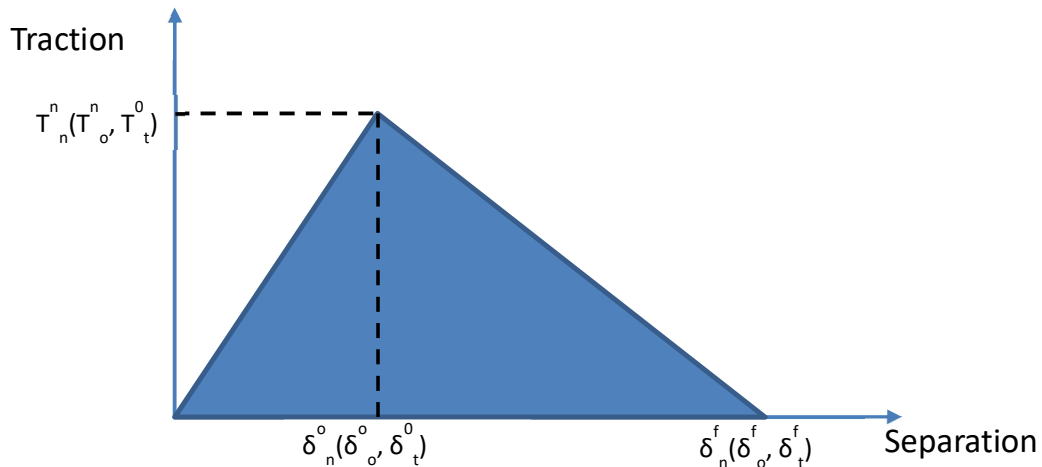


Figure 2-14 Typical Traction Separation displacement curve taken from Abaqus

The cohesive law constitutes a relationship between the traction acting in the interface and the interfacial separation between two bonded materials. There are mainly three parameters in cohesive law; cohesive energy (G_c), cohesive traction (T) and displacement (δ), as seen in Figure 2-14. There is displacement in the normal direction (δn) to the surface interface and tangential direction (δt) to the surface interface, which depends on the traction acting on the normal direction (T_n) and tangential direction (T_t) respectively. The area under the curve is the energy (G_c) needed for separation.

Cohesive damage occurs when the maximum stress (T_n^0, T_t^0) is exceeded. After the peak traction, a linear softening stage continues, until the separation reaches the maximum value (δ_n^0) (δ_t^0). At this critical point, the stress is zero, as shown in Figure 2-14.

There are three fracture modes, when separation occurs as a result of normal loading to the crack plane the failure mode is known as mode I or opening. When failure occurs as a result of traction tangential to the crack plane, it is known as mode II or mode III. In mode II the load is in-plane shear and mode III is out of plane shear, as shown in Figure 2-15. The combination of any separation mode is known as mixed failure mode [81], [85].

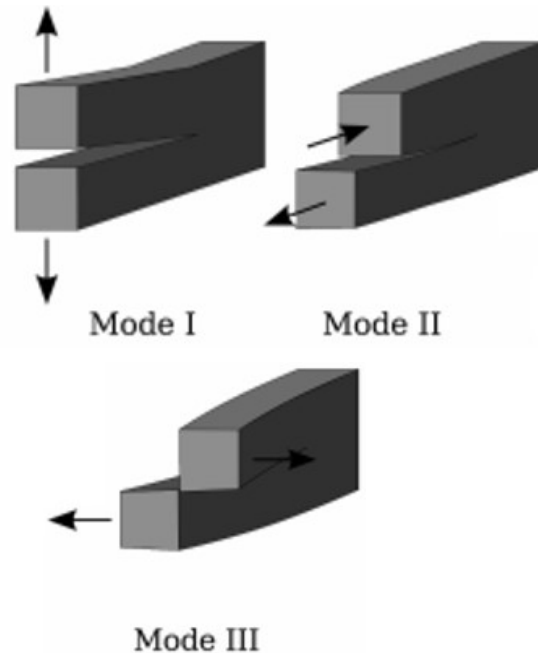


Figure 2-15 Three different fracture modes

There are several cohesive zone law configurations described in the literature. They can be categorised in the following ways [86]:

- Polynomial cohesive zone law[87]. This has been used to model ductile materials failing at mode I and for mixed failure mode [88], as shown by *Figure 2-16 (a)*.
- Piece-wise linear cohesive zone law, multilinear, trapezoidal [89], for modelling adhesively bonded sandwich structure and polymer matrix composites. This is widely applied for different materials. *Figure 2-16 (b)*.
- Exponential cohesive zone law [90], used for brittle materials and Scheider and Brocks [91] employed this configuration for modelling ductile materials. See *Figure 2-16 (c)*.
- Rigid-linear cohesive zone law, either known as bilinear or linear decreasing, Camacho and Ortiz (1996) [92] applied this law for brittle materials. See *Figure 2-16 (d)*.

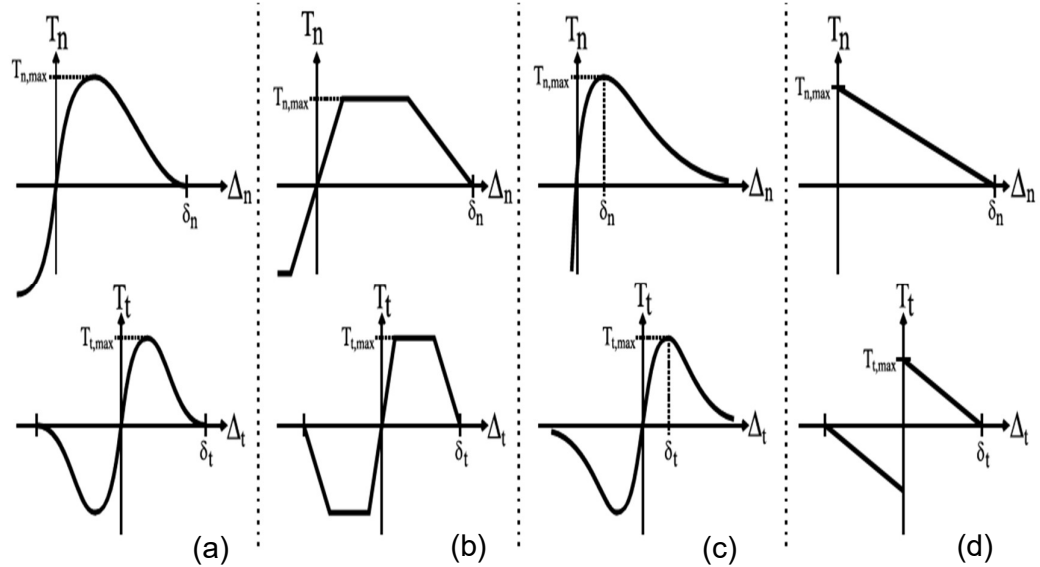


Figure 2-16 Four classes of cohesive zone laws. (a) Polynomial, (b) Multilinear, (c). Exponential, (d) Rigid linear

The CZM law configurations can be adapted to the behaviour of the thin material or interface to be simulated. In recent times, an accurate CZM can be selected through the advanced techniques. However, the experimental tests are still challenging. Hence, the CZM is simplified and defined based on the knowledge of the materials to be modelled [84].

The CZM law effect depends on the geometry and mechanical behaviour of material and interface. Pinto *et al.*, (2009) found for single lap joint with stiffer adherends, that the CZM shape used has a significant effect on the accuracy of the results [93]. In this way, bonded joints of ductile adhesives have often been simulated with the trapezoidal law, and to simulate brittle materials a bi-linear CZM (known as triangular shape) is frequently used [84].

Sugiman, Crocombe and Aschroft [54] studied the effects of ageing in fatigue of an adhesive SLJ. The joints were immersed in deionised water at 50°C for 2 years. They found that the fatigue strength is reduced with the increase of moisture; although there is a saturation level in which the trend of fatigue reduction stabilises. In order to determine the fatigue, they used a CZM, and

suggested non-linear fatigue degradation parameters to predict failure load and the failure process of the SLJ.

2.6.4 Environmental Degradation Models

Several degradation models have been developed to predict the damage of adhesive joint subjected to environmental degradation.

Ashcroft, Wahab and Crocombe, (2003) used a combination model of a diffusion moisture analysis and mechanical stress analysis to predict the fatigue resistance of a CFRP joint subjected to environmental ageing. The lap- strap joints were tested under fatigue load at -50°C, 25°C and 90°C, being exposed to conditions of high humidity at 25 °C (95 %RH) and 90 °C (97 %RH) [94].

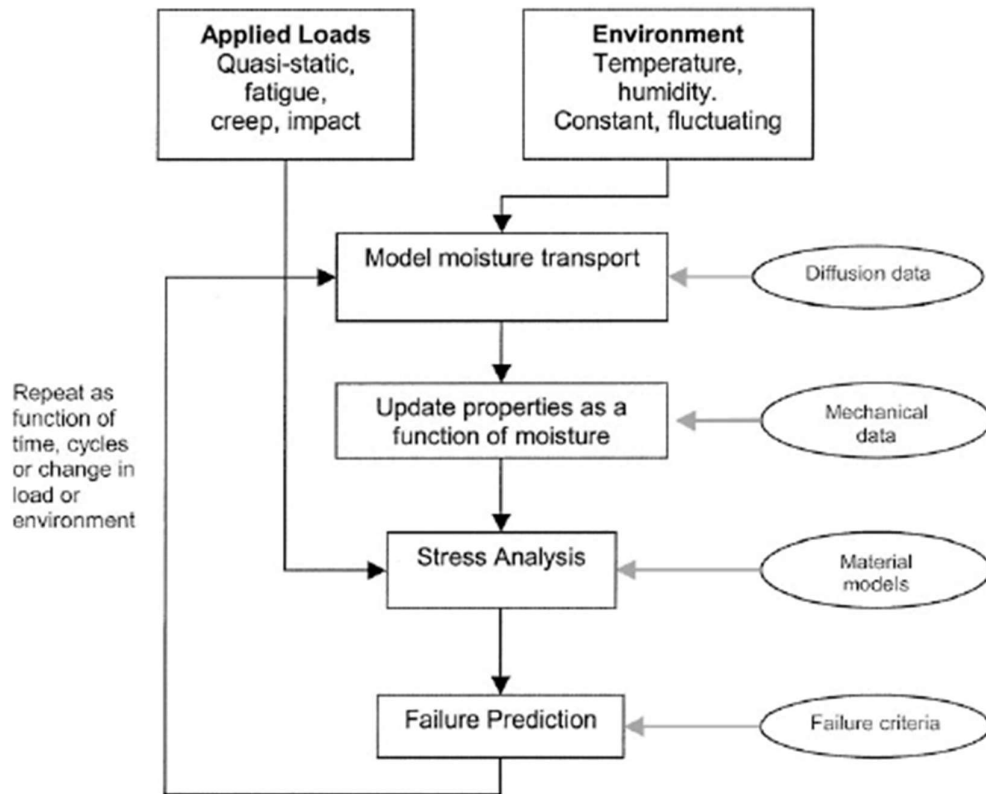


Figure 2-17 Fatigue model prediction framework

Firstly, the moisture concentration distribution was achieved through a mass diffusion modelling; the analysis needed the diffusion coefficient of the materials. Then, the diffusion elements were changed to solid elements for the stress

analysis. The stress-strain of each adhesive element is determined, based on the moisture concentration. The analysis assumed for the CFRP that the properties weren't affected by the moisture. Finally, a failure criterion was employed to determine the damage in the joint, elastic fracture and nonlinear elastoplastic fracture conditions were used to predict the trend fatigue failure. This coupled model was validated with the experimental results. Figure 2-17 shows a diagram summary of the model steps.

Katnam et al. [50], used a combination of mechanical diffusion and cohesive zone approach to predict moisture effect in the static and fatigue failure of adhesive bond of 2024-T3 with FM73 adhesive. Single lap and double lap joints were immersed in de-ionized water at 50°C for 360 and 720 days and tested under static and fatigue load. The frame of the mixed model used is shown see *Figure 2-18*. Their assumptions for the numerical model were:

- A bilinear traction separation response represents the failure in the adhesive bond line.
- Moisture degradation can be represented by the moisture-dependent traction-separation response.
- The bondline fatigue damage has degraded the bilinear traction-separation response
- Moisture degradation and stress damage can be accumulative.
- The moisture diffusion (D) doesn't depend on moisture concentration
- The moisture gained by the adhesive obeys Fick's Law.

Using a FE model in Abaqus and the analogy between heat transfer analysis and diffusion analysis, the moisture concentration in the adhesive bondline was calculated for 320 and 720 days. The concentrations were exported into the static and fatigue failure step to degrade the cohesive parameters. The parameters were degraded as shown in equation (2-5) of the static model.

$$\sigma_m = \sigma_m^d(1 - c) + c\sigma_m^s \quad (2-5)$$

$$\Gamma_m = \Gamma_m^d(1 - c) + c\Gamma_m^s \quad (2-6)$$

$$E = E^d (1 - c) + cE^s \quad (2-7)$$

Where, (c) is assumed as the normalized moisture concentration and $(\sigma_m^d, \Gamma_m^d, E^d)$ the dry conditions and $(\sigma_m^s, \Gamma_m^s, E^s)$ moisture condition.

For the fatigue conditions, a strain-based model was assumed:

$$\frac{dD}{dN} = \alpha (\varepsilon_p - \varepsilon_t)^\beta \quad (2-8)$$

$$\hat{\sigma}_m = \sigma_m(1 - D) + b^2 = c^2 \quad (2-9)$$

$$\hat{\Gamma}_m = \Gamma_m(1 - D) \quad (2-10)$$

Where, D is damage variable, N number cycles, ε_p is maximum principal strain in the adhesive bondline, ε_t is the threshold strain, α and β are constants.

The static strength reduction and the fatigue life were successfully predicted by the cohesive zone model and the strain-based fatigue damage model respectively.

Han, A. D. Crocombe, et al. (2014) proposed an experimental work followed by a numerical simulation study, to investigate the residual strength of degraded adhesively bonded joints. Their study focused on aluminium joints bonded with FM73 subjected to a combined mechanical-hygrothermal ageing (immersion in water at 50 °C). Fick's model was used to calculate the diffusion coefficient and moisture concentration. The fully coupled approach consisted of two steps; (1) to model the long-term ageing process of the joint, combined thermal-hygro-mechanical loading, and (2) to simulate the quasi-static tensile testing of the adhesive joints, aged in step 1, using CZM. The schematic description of the general work is shown in *Figure 2-19* [95].

The first step, a fully-coupled degradation process was used to simulate the joint under creep and hot-wet conditions. The model contains four field variables (moisture diffusion, elasticity, creep and thermal, and swelling expansion). The adhesive layer was modelled with 3D coupled thermal-displacement elements. The experimental results of bulk adhesive tests were the material input of model

and the aged single lap test results of the validated numerical study. Finally, the results of the first step were transferred to step 2 (Han, a. D. Crocombe, et al. 2014).

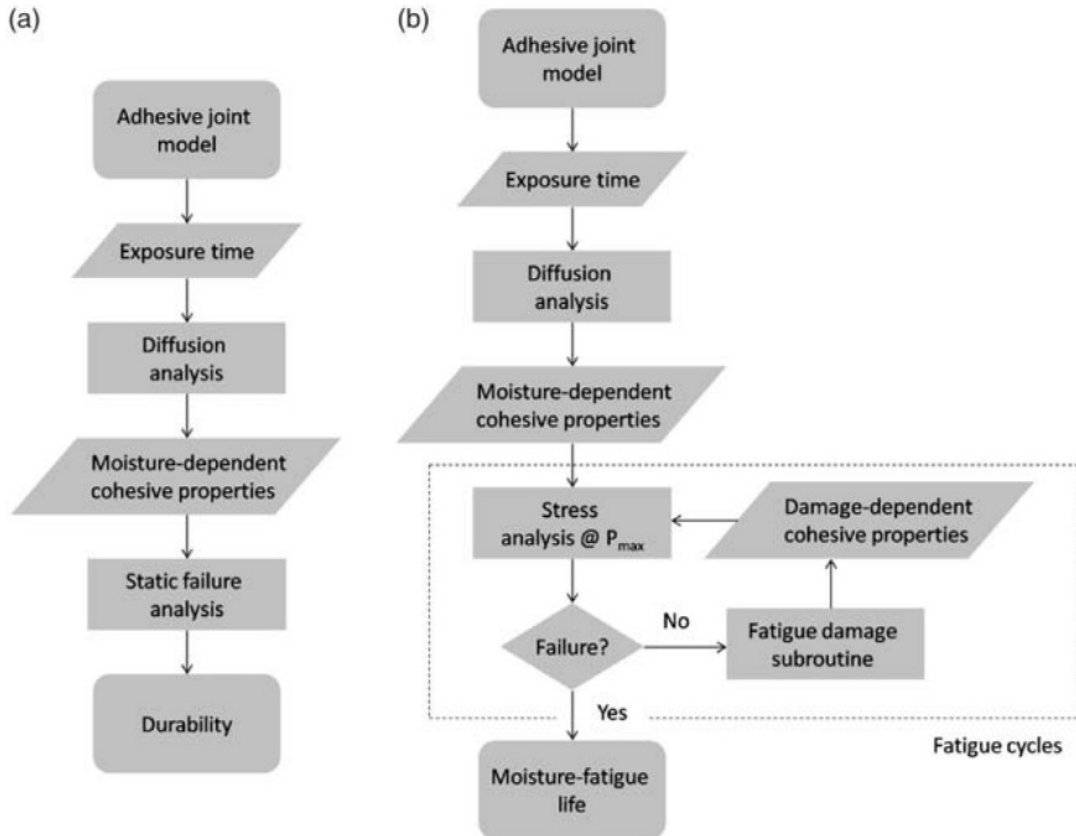


Figure 2-18 Modelling moisture degradation on static and fatigue load[50]

The second step, a bilinear CZM was implemented to simulate the quasi-static tensile test. A quadratic stress criterion was introduced as initiation damage criteria. The adhesive layer was modelled with 3D cohesive elements. The unaged calibration parameters were taken from the experimental data, on the adhesive bulk tensile test and double cantilever beam test. The aged bulk adhesive tests were performed to determine the degraded Young's modulus (E) and degraded Shear modulus (G). The degraded normal stiffness and shear stiffness were calculated by dividing the E and G modulus by the adhesive layer thickness. Also, a linear relationship was undertaken between the drop of the tripping traction and fracture energies and the reduction of the strength of the aged bulk adhesive.

The simulation of moisture distribution, stress and damage prediction showed a good correlation with the experimental results. The author proposed that this method can be used to model interfacial failure for bonded joints.

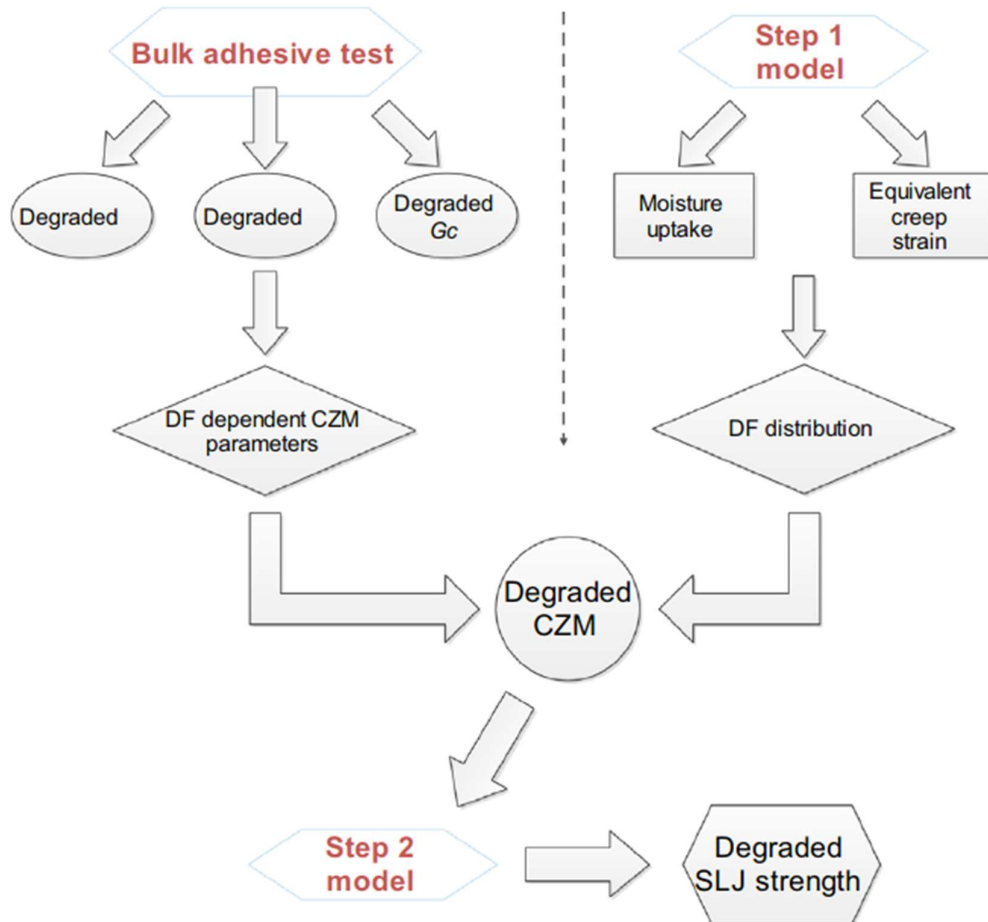


Figure 2-19 General framework of the FE modelling (DF being degradation factor)
[96]

A similar approach was implemented by Liu *et al.* [97] to simulate the hygrothermal effects on composite double lap shear joints (immersed in water at 90 °C for 60 hours). The moisture diffusion was simulated according to Fick's Second Law and two diffusivities were calculated for laminated composite. The diffusion perpendicular to the fibre direction was used in the equation (2-11). The diffusion along the fibre direction was assumed as 1.85 times the diffusivity perpendicular to the fibre direction.

The moisture diffusion of the joint was modelled in Abaqus through the mass diffusion model. Thus with results of the diffusion analysis, the moisture concentration was transferred as a field variable and output for the hygrothermal stress analysis.

$$D = 0.57^{(-4993/T)} \quad (2-11)$$

Where,

T: Temperature (K)

The hygrothermal analysis was performed to determine the strain induced by the thermal expansion and swelling using (2-12).

$$\{\varepsilon\} = [S]\{\sigma\} + \{\beta\}\Delta C + \{\alpha\}\Delta T \quad (2-12)$$

$$\{\sigma\} = [Q]\{\varepsilon\} - \{\beta\}\Delta C - \{\alpha\}\Delta T \quad (2-13)$$

A cohesive zone model was implemented to evaluate the interface degradation. The unaged and aged adhesive properties were taken from the tensile adhesive experimental data, and the degraded parameters for the cohesive layer were estimated by multiplying a factor.

$$T^h = T_0 \sqrt{\frac{\sigma^h}{\sigma}} f \quad (2-14)$$

Where,

T^h : Critical traction with moisture

T_0 : Critical traction without degradation

σ^h : Ultimate strength of adhesive with moisture

σ : Ultimate strength of adhesive without degradation

f: Degrading factor

The numerical model was validated with the experimental data, the failure load and the failure mode were predicted in good agreement with the experimental results.

2.7 Overview

The durability of adhesive bonded joints depends on factors of design and service conditions; such as materials, dimensions, bonding process and environmental conditions, and type of load. The effects of these factors are the parameters within which this research was developed.

Single Lap Joints (SLJ) are frequently implemented due to their simplicity and repeatability, thanks to this SLJ testing was chosen to measure its performance under environmental effects.

Elastic properties of adherend and adhesive, length overlap and surface preparation, are crucial factors when designing joints under shear and bending adhesive stresses. Taking this into consideration, a quasi-isotropic and balanced laminated composite was defined as adherend, with a surface prepared peel ply and with a geometry as suggested by ASTM [98] standard and NPL[99] and enhanced with end tabs to minimise the eccentricity load effect.

In a bonded joint, it is important to know and to evaluate the behaviour of adhesive, adherends and interface. They work as a unique system with respect to any environmental degradation, each individual behaviour (be it laminate, adhesive, bondline interface) can affect the performance and the degradation mechanism of the joint.

Particularly with moisture, some authors have showed changes of the properties of epoxy adhesive such as variation of plasticity, strength loss or increase of ductility as a result of the effect of humidity absorption. In the same way the composite adherents absorb moisture and this can affect the kinetics of water absorption in the adhesive [44]. Moreover, at temperatures above glass transition temperature T_g , the composite matrix properties suffer a continuous degradation [44]. Additionally the moisture diffusion is affected by the temperature in the degradation process [7]; for example, at high temperature the diffusion increases, while at sub zero temperature the diffusion decreases and the swelling causes polymer interlocking breaks.

Aeronautical structures encounter hygrothermal cycles (changes of humidity and

temperature) during their operating conditions. In normal conditions on the ground the moisture is high, and in tropical areas the temperature can rise to 70 °C. In order to evaluate the joint behaviour faced with a combined degradation effect caused by temperature and moisture cycles, a hygrothermal cycle (heating up to 70 °C and 85 %RH and cooling to -20 °C) followed by loading (including fatigue) was performed.

In order to identify an appropriate model to evaluate the damage cause by the hygrothermal cycles, the factor of moisture diffusion and temperature effects on bonded joints were reviewed. The conclusion therefore being that:

The environmental effects on the bonded joints durability is a major concern for the aviation authorities and industry as a whole. Joint behaviour over time is still unknown and without reliable NDT methods to determine joint strength as such it is difficult to predict failure.

The materials based on epoxies are affected by temperature and humidity due to the process of moisture diffusion. Moisture diffusion in laminated composites and adhesives are generally described by Fick's second law. Even in absorption and desorption cycles, this law is still applied due to the simple solutions and acceptable accuracy. During the diffusion process, water molecules may form some strong bonds with the molecules of the adhesive. Then, despite a desorption process in the joint, the degradation and reduction of strength may be irreversible.

The moisture causes changes of the properties, plasticization, swelling, micro cracks, hydrolysis, debonding, and loss of strength. Moisture transport mechanism first occurs through the free volume and then through reactions between the polymer chain and the water molecules. In summary, those new bonds induce a reduction in the glass transition temperature by interruption of interpolymer chain (Van der Waals bonds).

In composite bonded joints, the bondline interface is the area that is most sensitive to the transportation of moisture. The diffusion through the interface can cause degradation of the bond adhesion between the adherend and adhesive. In

contrast with the metal bonded joints, the thermodynamic work of adhesion in composite joints remains positive under humid conditions.

The environmental degradation models have shown a similar approach methodology, consistent in determining the moisture effect, thermal effects and mechanical analysis, and together with CZM to predict the damage based on the degradation of the traction-separation parameters.

In conclusion, to develop the degradation model, the moisture diffusion characteristics (diffusivity, thermal expansion coefficient and moisture content in saturation) need to be identified and be experimentally achievable. As such the CZM was identified to model the bondline interface of SLJ.

Current NDT techniques such as ultrasonic, thermography, sherography, laser, radiography, acoustic emission, etc., are able to detect defects such as delamination, debond, porosity, void, and crack. However, due to anisotropic material performance, there still are no non-destructive techniques able to detect all kinds of defects in composite bonded joints.

Studies have shown the application of ultrasonic C-Scan testing to the evaluation of degradation of adhesively bonded joints with consistent results. This consideration therefore allows one to define the ultrasonic technique as a tool to evaluate the aged SLJ and characterise the damage after the hygrothermal cycles.

3 METHODOLOGY, MATERIALS AND METHODS

This chapter describes the methodology, materials, equipment and procedures used to develop the research. The research methodology designed is shown as a schematic diagram, which is highlighted in four phases linked together to meet the proposed objectives.

3.1 Research methodology

To investigate the strength and durability of an adhesive joint ageing under a hygrothermal cycle, the methodology consists of four phases as shown in Figure 3-1.

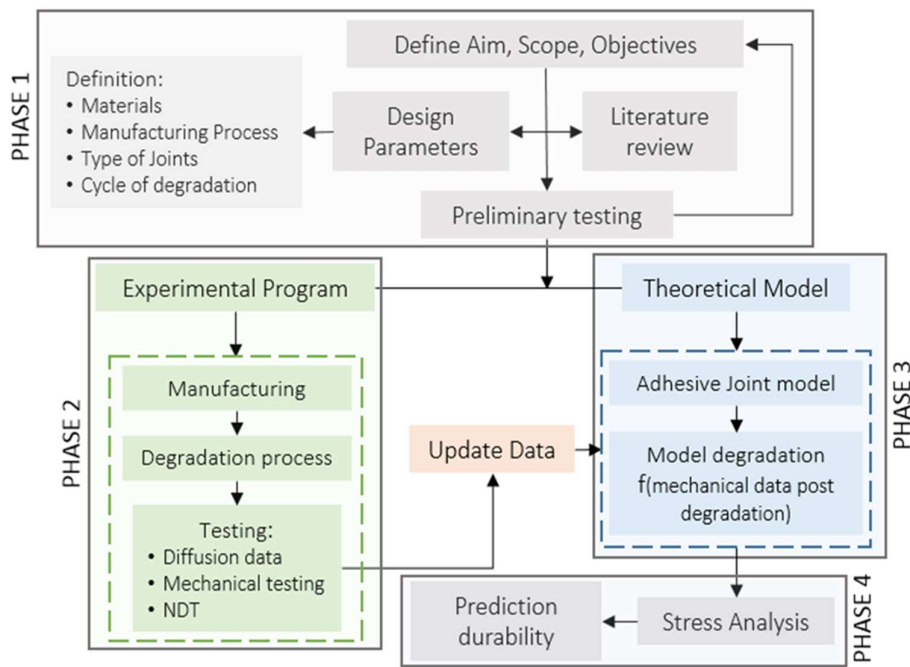


Figure 3-1 Methodology flow chart

Phase 1: The descriptive methodology was used in the preliminary part. The scope of the research is determined based on the literature review; previous studies and results were used to determine parameters for the experimental phase and to identify a numerical model. A campaign of preliminary testing and a familiarisation was developed to understand the methodology, to acquire training in the manufacturing procedures, tools and equipment of testing, and develop the experimental program (phase 2) based on learned lessons.

Phase 2: An experimental campaign was performed to acquire data which was subsequently used to validate the model and to study the behaviour of the joint under static and cyclic load after ageing. Absorption characterisation of the Carbon Fibre Reinforced Plastics (CFRP) and bulk adhesive, mechanical tests, visual and ultrasonic inspection were used to evaluate and explain the joints behaviour after the environmental attack.

The experimental program was divided in three principal parts and consists of: firstly, the manufacture of the single lap joints and the bulk adhesive samples; secondly, the performance of an environmental attack on the joints and specimens; and finally, a systematic series of test were conducted to characterise the absorption materials, the joint strength, material properties, non-destructive inspection of the joints and failure analysis.

Phase 3: Development of an analytical numerical model was undertaken as a parallel activity with phase 2. The model was updated with experimental results from mechanical testing and the cohesive parameters.

Phase 4: The validated model was used to predict the damage and failure of the single lap joint subjected to environmental cycles, and finally the discussion and analysis of the results.

3.2 Composites manufacturing

The material prepreg Hexcel T800/M21 was cut into layers of 600 mm x 600 mm, to manufacture two (02) panels of eight (8) plies. The stacking sequence selected was a quasi-isotropic of $[0^\circ/45^\circ/90^\circ/-45^\circ]_s$, according to the literature, a better performance is reached with a laminate quasi-isotropic lay-up, the optimal distribution contains a 25 % plies of 0° layers, a minimum of 10 % of 90° and a 50 % of plies in ± 45 $[100]$, $[25]$, $[101]$, $[21]$.

Before starting the vacuum bagging process, the laminate surface was covered with a nylon peel ply. Peel ply surface preparation was done to improve the mechanical and chemical adherence, and to avoid substrate damage or contamination.

Additionally, a study of different surface preparation treatment of carbon bonded joints, ageing at 55 °C and 95 % RH for about 33 days, has shown that the peel ply surface treatment provided the strongest bond possible for the joint. This was attributed to the lower surface energy of the substrates and the thicker polymer layer caused by peel ply compared with grit blasting and plasma treatments [35].

The curing cycle was in an autoclave in accordance with the manufacturer’s instructions [102]. An initial vacuum pressure of one bar was used to remove trapped air. Then the curing in the autoclave was performed at 180 °C for 2 hours. It is explained in Table 3.

Table 3 Autoclave Curing Process [102]

ITEM	VALUE
Vacuum (bar)	0.94
Autoclave Pressure	Apply 7 bar gauge Reduce vacuum to a safety value of -0.2 bar when the autoclave pressure reaches 1 bar gauge
Rate Heating (°C/min)	1 - 3.0
Holding (min)	120
Temperature T (°C)	180
Cooling (°C/min)	2 - 5
Venting pressure (°C)	60

Finally, the cured panels were cut into sheets of 300 mm x 100 mm as shown in Figure 3-2.

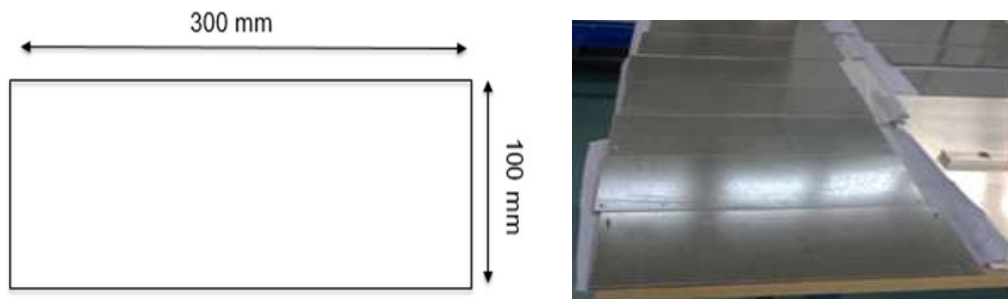


Figure 3-2 T800/M21 UD CFRP sheets before bonding

3.3 Single Lap Joint manufacturing

To manufacture the single lap joints, a secondary bonding procedure was used. A bonding fixture was used to ensure overlap dimensions and accurate alignment of the joint. See Figure 3-3. Two pins in each border of the substrate were used to fix the overlap area as shown Figure 3-3 (c).



Figure 3-3 Joint bonded process: a) PTFE tips and film adhesive set up, b) before bonding, c) Final assembly bonded joint

Before bonding, the panels were dried in the oven to remove trapped moisture in the surface. The peel ply was removed at the same time of the bonding process. A debonding strip of Polytetrafluoroethylene (PTFE) of 0.1 mm thickness and 2 mm width was laid in the free ends of bonded joints, see Figure 3-3a. These were used to avoid a fibre Tear Failure (FT) [61], and thus ensure consistent failure results.

The secondary bonding was made according to data-sheet Cytec FM 94 as described in Table 4. Although Cytec recommends the application of 0.28 MPa of pressure (a condition which would require autoclave), the process vacuum bag curing was chosen to simulate a repair scenario, as shown in Figure 3-4.

Table 4 Curing Adhesive process [103]

PROPERTIES	UNIT	VALUE
Pressure	MPa	0.1
Rate heating	°C/min	1.7 - 2.8
Holding	min	60
Temperature	T (°C)	121

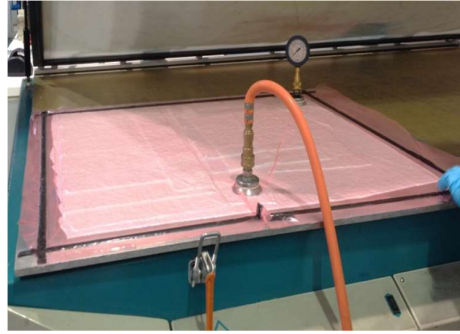


Figure 3-4 Vacuum bag for joints bonding

Balancing end tabs were bonded on opposite faces of the joint to minimise the eccentricity of load [13], as shown in Figure 3-5. Those CFRP tabs had dimensions of 50 mm x 150 mm. They were bonded with Huntsman Araldite 420 A/B, mixing 10 parts by weight resin with four parts hardener. Clips were used to get the pressure and fix the tabs. The cure was made in the oven at 60 °C for 4 hours.

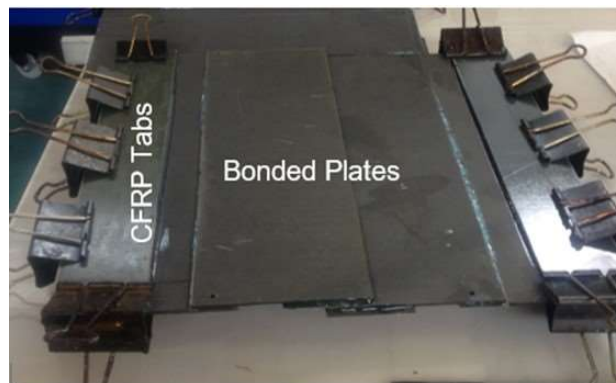
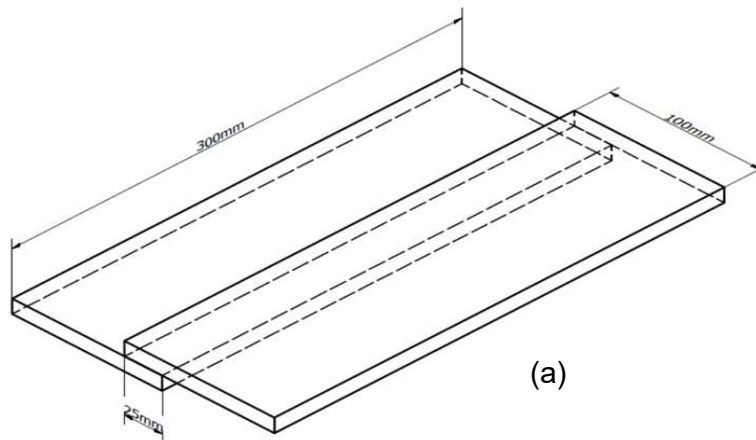


Figure 3-5 CFRP end tabs bonded (a) bonded plates schematic (b) bonded plates

Finally, the bonded plates were cut in single lap joints SLJ of 25 mm width, 175 lengths and 25 mm overlap. Figure 3-6 shows the geometry and the PTFE crack initiators can be identified. The SLJ geometry is according to ASTM D5868-01 (reapproved 2014) with a variation of adhesive thickness and substrate length.

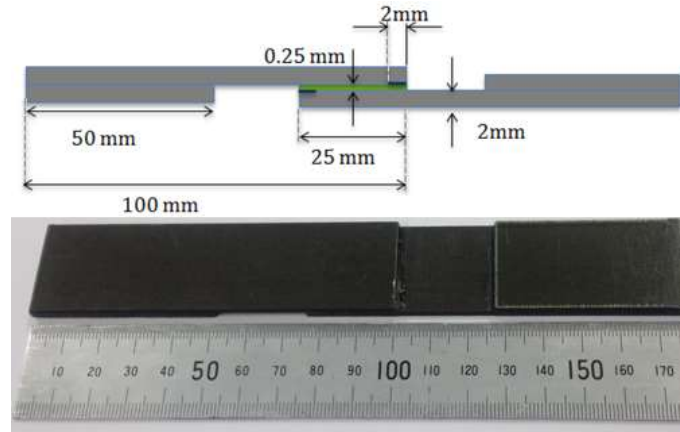


Figure 3-6 Geometry of the single lap joint specimen and final specimen

Furthermore, aluminium tabs were attached to the gripping zone, to prevent tear stress in the specimens in the grip area, during the mechanical testing.

All tabs were bonded with an aerospace adhesive, Araldite 420 A/B. The surface was mechanically abraded with sand paper and cleaned with acetone; to clamp the end tabs, clips were used as shown in Figure 3-7. The liquid adhesive was cured at 50 °C for 4 hours in the oven.

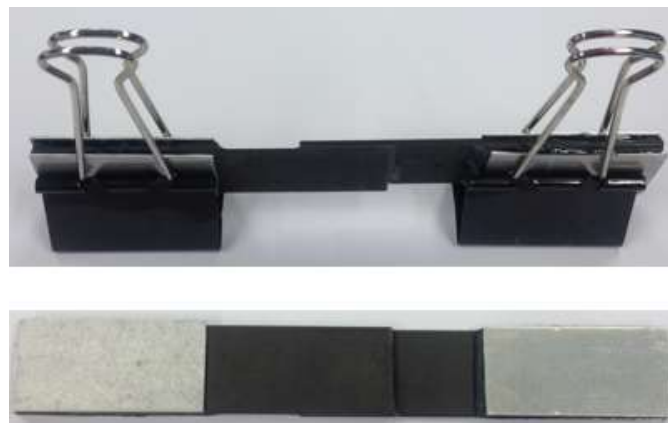


Figure 3-7 Upper photo shows clamping before curing. Bottom photo shows final specimen

3.4 Hygrothermal cycles

Flight operation conditions cause composite joint structures to be subjected to different environments, such as the combined effect of temperatures, dry and wet atmosphere, etc., [43]. Low temperatures occur at high altitude flight operation or ground storage during cold weather. According to MIL-Handbook 17, the majority of commercial aircraft components are designed to the maximum temperature of 71 °C and 85 % RH, without taking account of components close to engines or landing gear. [19].

An environmental chamber was used to simulate the conditions of temperature and humidity. Multiple cycles of heating to 70 °C, with 85 % Relative Humidity holding for four hours, then cooling to -20 °C holding for two hours then heating again were carried out continually. The cycles are presented in Figure 3-8.

Joint samples and bulk adhesive samples were conditioned for a specific number of cycles, then they were removed to be tested under static and fatigue load. Following the approach recommended by Abdo and Aglan [64], the time intervals defined to evaluate the behaviour were 42, 84, 168, 252 and 336 cycles.

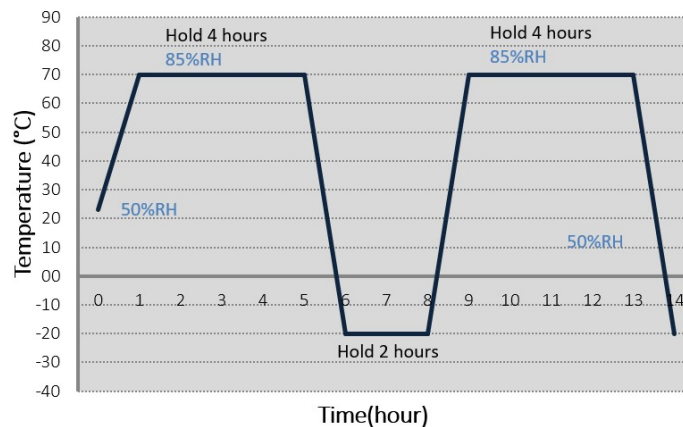


Figure 3-8 Cycle of temperature and humidity

3.5 Bulk adhesive specimens manufacturing

In order to perform tensile tests and moisture absorption tests, there was a need to manufacture sheets of bulk adhesive (1 mm thickness). Hence, a lay-up of four layers of FM94, each one of 0.25 mm thickness, were stacked together and cured.

3.5.1 Preliminary test

Studies with FM94 adhesive were not found in the literature, however there is widely available research about FM73 film adhesive, which is produced by the same manufacturer CYTEC. For this reason, the experiences of other researchers were used to identify the optimal process to achieve the bulk adhesive samples.

- **Closed mould technique:** To manufacture FM73 bulk adhesive specimens [70] a metallic closed mould was used with heat and pressure, as can be seen Figure 3-9. For that reason a closed mould technique was implemented with FM94 adhesive. Layers of 150mm x 150 mm were cut, stacked and pressed using a steel roller to reduce the voids between layers. The rectangular metal mould was used to keep the flow during the curing. To close the mould, two metallic plates were affixed above and below. Films of PTFE were used to avoid adhesive sticking to the mould, as seen in Figure 3-9 Mould made to cure the adhesive [70]

The adhesive was cured at 121 °C for 60 minutes. Curing was performed in a GE Moore hot press [103]. Finally, the cured bulk adhesive was of uniform thickness but had a high void content.

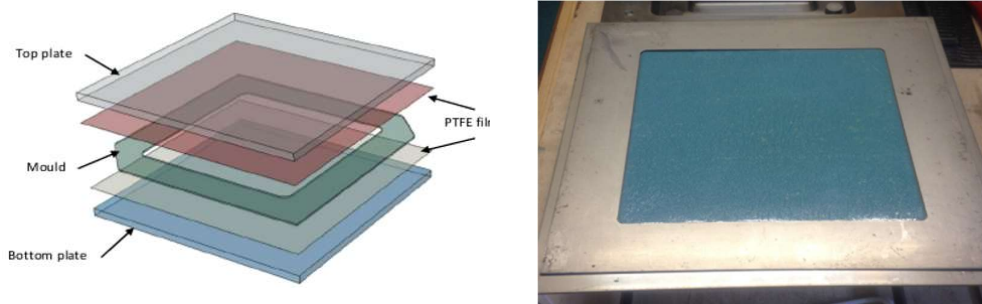


Figure 3-9 Mould made to cure the adhesive [70]

- **Degassed prior close mould technique:** Liljedahl [48] employed a degassing process to minimise the amount of voids of FM73 bulk adhesive specimen. This procedure was hence used to manufacture the FM94 bulk adhesive. The layers stacked were placed in a vacuum oven, the adhesive was heated and degassed at 80 °C - 90 °C for 10 minutes and the procedure was repeated three times. Figure 3-10 shows the process of degassing, and how the

trapped air comes up. During the degassing process, the adhesive under vacuum looks like a foam. Once the vacuum was removed, the air bubbles disappeared and the adhesive shape was recovered.

The degassed adhesive was set in the metallic mould. The mould was closed with the top plate. The adhesive was cured under hot pressure as described above. The specimen however was seen to contain bigger voids than that of the technique without degassing.



Figure 3-10 Left adhesive starting to degas. Right adhesive during the degassing process.

- **Open Mould technique:** Four adhesive layers of 50 mm x 160 mm were stacked (to get 1 thickness bulk adhesive) and placed in a glass plate. Spacers were used to control the flow during the curing. The adhesive was cured at 121 °C for 60 minutes. As a result, the amount of voids was reduced and the sheet remained at a thickness of 1 mm. Also, the process resulted in a flat surface across the entire specimen. The final adhesive sheets are shown in Figure 3-11.
- **Degassed prior to cure in an opened mould:** A degassed adhesive and opened mould curing process was tested. The adhesive was degassed in the vacuum oven for 10 minutes at 80 °C - 90 °C. Then, the adhesive was placed on a glass plate and cured at 121 °C for 60 minutes. The sheet showed several voids.

3.5.2 Bulk adhesive sheet manufacturing

Once defined the opened mould cured was the method to produce the bulk adhesive sheet, six bulk adhesive sheets (50 mm x 160 mm dimensions) were manufactured. As was mentioned above, four adhesive layers were stacked over a glass (cover with PTFE tape to avoid sticking). The adhesive sheets were cured and samples were cut with dimensions 150 mm x 10 mm.



Figure 3-11 Left Adhesive cured in opened mould, Right side view adhesive cured in open mould

Lastly, after cutting the specimens were polished to avoid sharp changes in the borders. However, it is an important to highlight that they presented a notable amount of voids.

3.6 Materials characterisation

In order to characterise the moisture diffusion and mechanical properties of materials, specimens of the composite adherend and bulk adhesive were prepared. The specimen dimensions were defined based on standards for plastics; determination of water absorption BS EN ISO 62:2008 and determination of tensile properties from the adhesive BS EN ISO 527:2012.

The laminated composite mechanical properties were taken from the literature as later described in this section.

To make the adhesive bulk sheets free of voids was a significant challenge during the process of manufacturing the specimens. Several techniques were investigated to obtain a specimen with a negligible number of voids.

Several of Fick's behaviours have been reported for both epoxies and carbon fibre composite with epoxy matrix at temperature below the T_g [48] [45][73]. Hence a Fick's Law solution has been implemented to determine the Diffusion coefficient and to predict the moisture concentration in the bulk materials.

3.6.1 Gravimetric test

In order to evaluate the moisture diffusion in the adhesive and CFRP substrates, gravimetric testing was done according to ASTM D5229/D5229M-14[104]. The moisture uptake during the cycles was determined to calculate the diffusion

coefficient “D” and the moisture concentration “Mm” at saturation. Hence, bulk adhesive and CFRP T800/M21 samples, with dimensions of 50 mm x 50 mm and 1 mm thickness, were conditioned in the environmental chamber with the same hygrothermal cycles used with the joints.

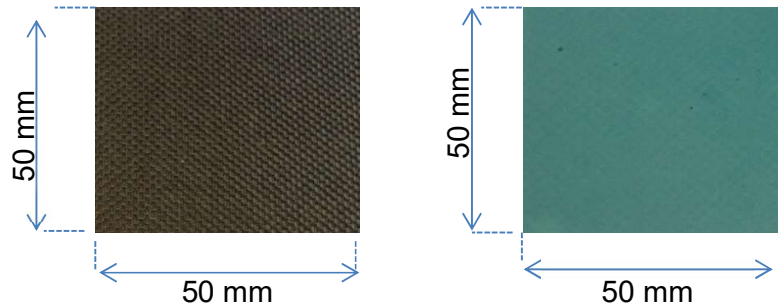


Figure 3-12 Gravimetric test samples

In the research, the moisture transport in the materials occurs under dynamic conditions of moisture and temperature. As described in section 2.4.1, the moisture diffusion is directly influenced by the temperature. For that reason, carrying out the moisture characterisation at two different conditions for the adhesive bulk was considered. One series of specimens were removed from the environmental chamber at dry low temperature. Another group of bulk adhesive specimens were removed at hot- wet conditions. In the case pf CFRP samples, these were removed only during hot-wet conditions. Procedures made for drying and weighing were the same for all of the samples.

Table 5 Characterisation moisture samples description

Material	Dimensions	# Sample	Conditioning		Samples Name
			Enviroment	Remotion for testing	
Adhesive FM94	50 mm X 50 mm, 1 mm thickness	7	Heating up 70 °C/85 % RH holding for 4 hours.	About 70 °C/85 % RH	A1-A4
			Cooling until -20 °C holding for 2 hours.	About - 10 °C	A5-A8
T800/M21 UD CFRP	50 mm X 50 mm, 2 mm thickness	4	Cycles 8 hours each.	About 70 °C/85 % RH	C1-C4

At the outset, to determine the initial weight, all the specimens were cleaned with acetone and stored in a desiccator for two hours before they were weighed. Following that, the samples were dried in an oven at 50 °C for 24 hours, then

specimens were removed and cooled in a desiccator before being weighed again. After weighing they were returned to the oven, and this procedure was repeated until the mass reached the constant value. This final constant value will thus be considered the initial weight condition [105], [71].

To measure the moisture gained, all pre-dried samples were conditioned in an environmental chamber under the hygrothermal cycle. Heating until 70 °C and 85 %RH and holding for 4 hours, follow by a temperature reduction to - 25 °C for 2 hours. Each cycle takes eight hours and runs continuously.

The samples were removed periodically from the environmental chamber and kept in a sealed bag as they were being moved to the balance area. Samples were wiped with cloth to remove the moisture from the surface, and then they were weighed immediately on a balance with an accuracy of 0.01g. After weighing, the samples were enclosed within the bag again and moved to the environmental chamber.

The frequency of the gravimetric testing decreased gradually as the rate of gain of moisture diminished. Hence, for the first day the samples were weighed three times. Then over the first week, two readings were taken per day, one reading was taken each day over the second week, followed by a reduction of the frequency as the rate of weight gain is smaller [71].

The percentage of mass change was calculated using equation (3-1) for each time interval. The measures were taken over a period until that the moisture percentage achieved the equilibrium. The equilibrium or saturation is reached when the average moisture content changes by less than 0.02 % over at least three consecutive time intervals [104].

$$\text{wt}(\%) = \frac{(W_t - W_0)}{W_0} \times 100 \quad (3-1)$$

Where, W_0 , is the mass of the test specimen (mg) after initial drying and before moisture exposition.

W_t , is the mass of the test specimen (mg), after moisture exposition

The moisture content percentage wt(%) of each sample is recorded and plotted versus $\sqrt{(t/l)}$, t being the time of exposure and l the thickness of the sample.

The diffusion coefficient “D” was calculated from the slope of curve. The methodology to determine the diffusion coefficient is described later in the section 3.4.2.

In addition, after weighing, the samples were removed periodically from the environmental chamber, length and thickness were measured with a calliper and micrometre respectively.

Lastly, desorption test was performed; preconditioned and saturated samples were weighed prior to starting the heating process to 75 °C in a controlled temperature oven. The samples were removed and cooled in a desiccator, wiped and weighed. Then, they were returned to the oven for 24 hours. The percent mass loss was calculated with equation (3-1), and the procedure was repeated until the percentage of change was less than 0.1 %. The moisture loss as a function of $\sqrt{\text{time drying}}$ is plotted and the results compared against the mass moisture gained.

3.6.2 Diffusion coefficient

Fick’s Law has been widely used to describe the moisture diffusion in composite and polymeric materials, as mentioned in section 2.6. Fick's second Law of diffusion has been developed to predict a non-steady-state diffusion and also for diffusion in three dimensions.

$$\frac{\partial C}{\partial t} = D_z \left(\frac{\partial^2 C}{\partial z^2} \right) \quad (3-2)$$

According to ASTM *D5229/D5229M-14*, the moisture content (percentage) in the material, as a function of time and temperature, can be predicted with the Equation (3-3) [104].

$$M(T, t) = M_b + G(T, t)(M_m - M_b) \quad (3-3)$$

Where,

T = temperature °C

M_b = moisture at start of experiment (sample after oven-dry), % (taken as zero).

M_m = moisture equilibrium content (%).

h = average specimen thickness (mm).

G (T,t) = moisture absorption function, see equation (3-4),

$$G(T, t) = 1 - \exp \left[-7,3 \left(\frac{D_h(T) * t}{h^2} \right)^{0,75} \right] \quad (3-4)$$

Where, including all terms identified above, but with the exception of the following:

t = time (h) or effective moisture content.

D_h(T) Diffusion coefficient at specific Temperature

The method to characterise the moisture absorption was described in section 3.6.1. The weight of every sample was recorded at different predetermined times.

Figure 3-13 illustrates a typical curve of moisture content fitted to Fick diffusion law. Initially, the curve shows a linear acceleration increase of moisture content. This initial moisture gained is highlighted with a discontinued red line in Figure 3-13. Gradually, the absorption rate decreases as long as while the moisture uptake approaches a maximum value. The maximum moisture content is known as the saturation level (M_m). In Figure 3-13, this level is highlighted as M_m horizontal line according to [106] (King Jye Wong, 2013).

The moisture diffusivity constant- D_h -is calculated by the slope of the initial straight line using Equation (3-5) [104] (ASTM Standard, 2014).

$$D_h = \pi \cdot \left(\frac{h}{4 \cdot M_m} \right)^2 \cdot \left(\frac{M_2 - M_1}{\sqrt{t_2} - \sqrt{t_1}} \right)^2 \quad (3-5)$$

Where:

D_h = diffusion coefficient in the thickness direction.

h = average specimen thickness (mm).

$\left(\frac{M_2 - M_1}{\sqrt{t_2} - \sqrt{t_1}} \right)$ = Slope of linear portion of moisture absorption vs time^{1/2}.

M_m = effective moisture equilibrium content.

M_1 = moisture value 1 at time 1 (%).
 M_2 = moisture value 2 at time 2 (%).
 t_1 = time value 1 (h).
 t_2 = time value 2 ($t_2 > t_1$) (h).

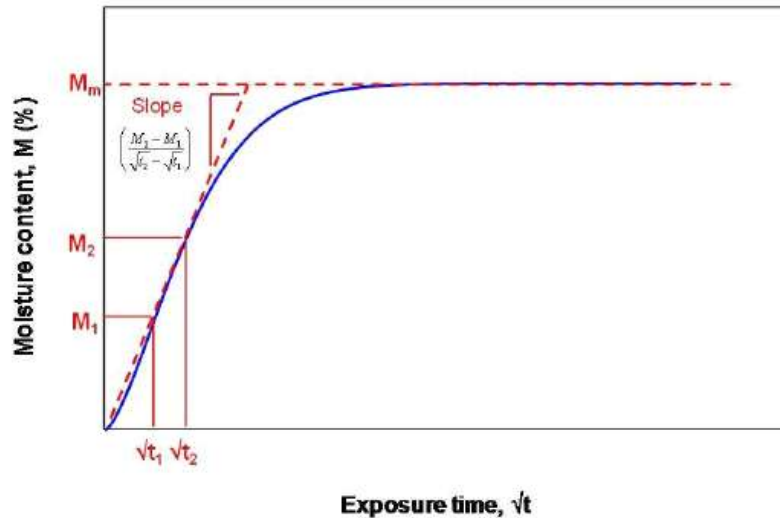


Figure 3-13 Fick's Diffusion Graph [46]

For determining the linear slope $\left(\frac{M_2 - M_1}{\sqrt{t_2} - \sqrt{t_1}}\right)$ two points were selected. For this study; M_1 is assumed as baseline moisture content ($M_1 = 0\%$) at t_1 equal zero. M_2 is considered equal to M_m , with the corresponding time (t_2). M_2 value is the point of interception between the straight line and the horizontal M_m line.

The equilibrium moisture content (M_m) was obtained calculating the average between the maximum and minimum moisture content value after reaching saturation.

Finally, Wong [46] states that a Fick's diffusion behaviour can be recognised, analysing predicted moisture uptake $M(T, t)$ against $t^{1/2}$. The graph should fulfil the next three rules:

- There is an initial linear stage of absorption, it has to achieve at least up to 60 % of M_m .
- After the straight line (initial linear slope), the absorption curve shows a concave zone, it extends to reach the equilibrium (M_m).
- Plots of moisture uptake against $t^{1/2}$ /thickness are superimposable at different thickness for the same material.

3.7 Mechanical properties

3.7.1 Composite CFRP

The T800/M21 UD ply properties have been taken from literature review [107].

Table 6 268 gsm⁻¹ T800/M21 UD properties

PROPERTIES		VALUE
Elastic Modulus (MPa)	E1	134700
	E2	7700
	E3	7700
Poisson's ratio	v23	0.5
	v12-v13	0.37
Shear modulus (MPa)	G12 =G13	4200
	G23	2500

3.7.2 Adhesive FM94

Adhesive samples type II (dimension of 10 mm x 150 mm) were cut from the sheet of cured bulk adhesive. The bulk tensile test followed the standards EN ISO 527-1:2012 and EN ISO527-3:1996 [108], [109]. The test was carried out to determine the materials tensile strength of unconditioned and conditioned bulk adhesive specimens. The tensile strength results were used to identify the effect of diffusion moisture on adhesive mechanical properties. Also, using stress-strain curves the elastic modulus (E) values were determined for the specimens and the effect of hygrothermal cycles on this values.

Before conditioning the samples to environmental attack, aluminium end tabs were bonded using Araldite 420 A/B liquid adhesive. The curing was carried out at room temperature for seven days. The geometry description and a sample can be seen in Figure 3-14.

Three tensile samples of each set were tested. Unaged specimens were tested to identify the initial condition. Aged specimens were conditioned at different periods in cycles (weeks): nought (0), 84 (four) and 168 (eight). Specimens were not tested at 42 and 252 cycles, because of the low rate of changes presented during the experiments.

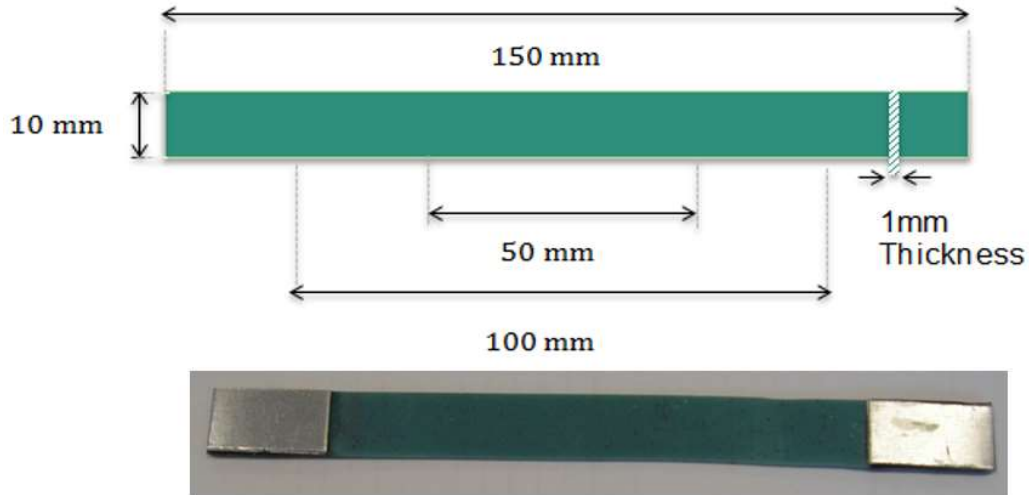


Figure 3-14 Specimen type II Geometry [109], above the specimen.

Immediately before the tensile test, the specimens were removed from the environmental chamber and dried with a wipe. The testing was done at once to avoid change of moisture in the specimen. The tensile test was carried out in the universal machine under a maximum load of 10 kN with a rate 0.5 mm/min. The displacement was measured using laser extensometer.

3.7.3 Adhesively bonded single lap joint tests

3.7.3.1 Lap Shear Test

Lap Shear Testing was conducted to determine the effect of degradation process in the strength of the joints. The tests were done according to standard test method ASTM D5868-01, 2001. The Electro-Mechanical Universal Machine, Instron 5500R with 30 kN load cell, was used for testing. A laser extensometer was employed to measure the deformation of the joint. The test ran until failure with a displacement rate of 1mm/min.

At least three samples were tested at each cycle. The maximum failure load was used to define the load levels of fatigue test.

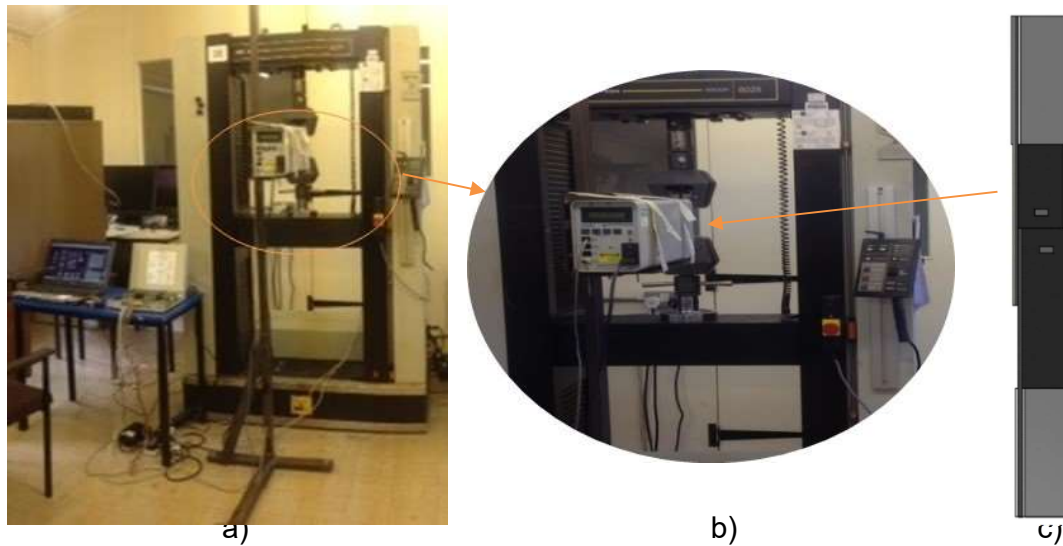


Figure 3-15 Single lap shear test configuration (a) General view, (b) laser extensometer, (c) SLJ schematic position in front of laser extensometer

3.7.3.2 Fatigue Test

The fatigue testing was performed according to the NPL Guide Fatigue and Creep testing of adhesives and thermoplastic joined systems [110], using a Denison Mayes-Group servo-hydraulic machine, as shown in Figure 3-16. Unaged and aged specimens were cycled up to 10^6 cycles under a sinusoidal wave with constant amplitude, stress ratio (R) equal to 0.1 and a frequency of 5 Hz. The frequency of 5 Hz was determined to reduce the hysteresis heating risk [110], a tension-tension fatigue regime was chosen in order to compare the results with other authors, who have evaluated fatigue of bonded SLJ [7], [50], [64], [111], [112].



Figure 3-16 Fatigue test configuration

The unaged and conditioned joints were tested at three different load levels (% of quasi-static strength). The number of hygrothermal ageing cycles and load levels tested are listed in Table 7.

Table 7 Fatigue test matrix

HYGROTHERMAL AGEING CYCLES	LOAD LEVEL	NUMBER OF SPECIMENS TESTED
0	40 %	10
	45 %	
	50 %	
	55 %	
84	30 %	10
	40 %	
	45 %	
336	30 %	10
	40 %	
	45 %	

Each set of specimens were removed from the environmental chamber upon reaching the time to be tested. Then, the joints were stored in a hermetic plastic box under moisture condition (50 %RH) and room temperature. The moisture condition was monitored with a thermos hygrometer DC 102.

3.7.4 Non-Destructive Inspection -NDI

In order to characterise the adhesive joint quality (pre and post ageing), two methods were employed. Firstly, visual inspection with optical microscope at low and high magnifications was used, as well as ultrasonic C-Scan technique.

3.7.5 Microscopy evaluation

To observe voids and changes caused by ageing, one control sample was observed pre and post-condition. The control sample was removed each two weeks and observed by optical microscopy using a NIKON Optiphot microscope, under reflected light mode at different magnification lens (2.5X, 5X, 10X).

The bonding edges were polished with an abrasive paper and they were inspected under microscope NIKON Eclipse and ME600 with different magnification lens. In addition, a fracture mechanical analysis was performed to evaluate and identify the failure mode of the joints.

3.7.6 Ultrasonic Inspection

As mentioned in the literature, ultrasonic technique (UT) is used to evaluate bonded joint and to detect bond defects such as debond, cracks or porosity [67], [113], [114], also recent studies have undertaken UT to evaluate degradation of adhesively bonded joints[113].

Based on these studies, an immersion technique was implemented with the Sonatest Ultrasonic C-Scan model VEO 16:64, and an arrangement consisting of a probe type Phased Array of 5 MHz, square pulse width 100 ns, 64 elements and a gain of 31 dB and gain reference of 23.9 dB.

A control sample was used as a representative specimen, which was periodically removed from the environmental chamber and inspected to characterise the ageing effect in the bond quality.

Ultrasonic C scans were taken of unaged joint and aged joints (at 84,168 and 252 cycles). The joint was removed from the environmental chamber each time interval, inspected by C-scan and returned to the chamber until the following evaluation. The arrangement of the ultrasonic through immersion of the SLJ is shown in Figure 3-17.

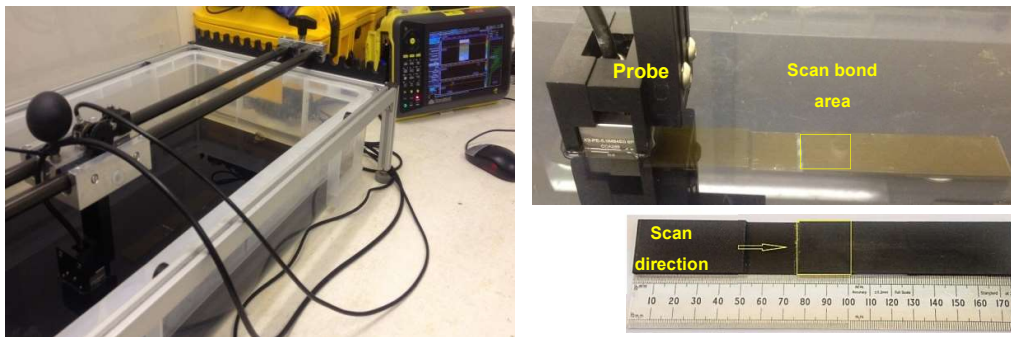


Figure 3-17 Ultrasonic C-scan through immersion (a) scanning set up (b) probe and joint arrangement (c) scheme of scan direction and area

The ultrasonic signal penetrates the adherend and reflects the first interface adherend/adhesive and even reached as far as the second interface and the back of the second adherend.

The C-scanned images from the bond region (yellow square, Figure 3-17) were reached by setting the gate on the reflections from the two interfaces and the back face of the second adherend. The C-scan image therefore is the mapping of the amplitude signal, the attenuation of amplitude signal is interpreted as the degree of bonding.

4 EXPERIMENTAL RESULTS

4.1 Introduction

The experimental programme to evaluate the behaviour of an adhesive composite joint exposed to environmental attack was described in Chapter 3. Moisture characterisation and mechanical tests were performed on bulk materials and composite single lap joints. The results of these tests are presented in this chapter.

4.2 Moisture Characterisation

In this work, three to four samples of each material, T800/M21 laminate and FM94 bulk adhesive were tested to determine the moisture diffusion under hygrothermal cyclic conditions (temperature and moisture). Diffusion coefficient results and the Fick's model analysis are described in this section, according to the procedures of section 3.6.1 and 3.6.2.

4.2.1 FM94

In order to know how the temperature and humidity cycles influence in the moisture diffusion, the gravimetric test was performed at two different conditions. The procedure was performed only for FM94 samples.

In the first series, four specimens were removed from the environmental chamber at hot wet condition stage (about 70 °C/85 %RH). In the second series, samples were removed from the environmental chamber at cold-dry condition stage (about -10 °C).

First series: The gravimetric test results of FM94 samples removed from the environmental chamber at hot-wet conditions (about 70 °C and 85 %RH) are illustrated in Figure 4-1. The graph shows the moisture uptake (wt %) versus the square root of time for 1 mm thickness, the moisture absorption of all specimens showed a similar trend. Initially, the moisture content rises linearly with time. The rate of absorption is faster during the first period, 24 h ($4.90 \text{ h}^{0.5}$), then the increment gradually goes down to reach a stable moisture content. The maximum moisture content was obtained after 120 h ($10.95 \text{ h}^{0.5}$) exposure time.

After reaching the equilibrium moisture content, there were some peaks in the value moisture absorption. The peaks were presented at 18.97 $h^{0.5}$, 22.45 $h^{0.5}$ and 25.92 $h^{0.5}$. The changes can be attributed to variants during the gravimetric measurement because although the samples were extracted from the chamber about 70 °C and 85 %RH, it is possible that they were taken at different times of the cycles (beginning of the hot-wet stage or after some hours under hot-wet condition). These variations could affect the amount of water adsorbed by the surface, slightly affecting the measurement of mass gained.

The gravimetric test was performed over a much longer period than that to achieve the saturation; the last measurement was greater than 40 $h^{0.5}$ (1600 h). The moisture uptake after this long period does not show drastic changes.

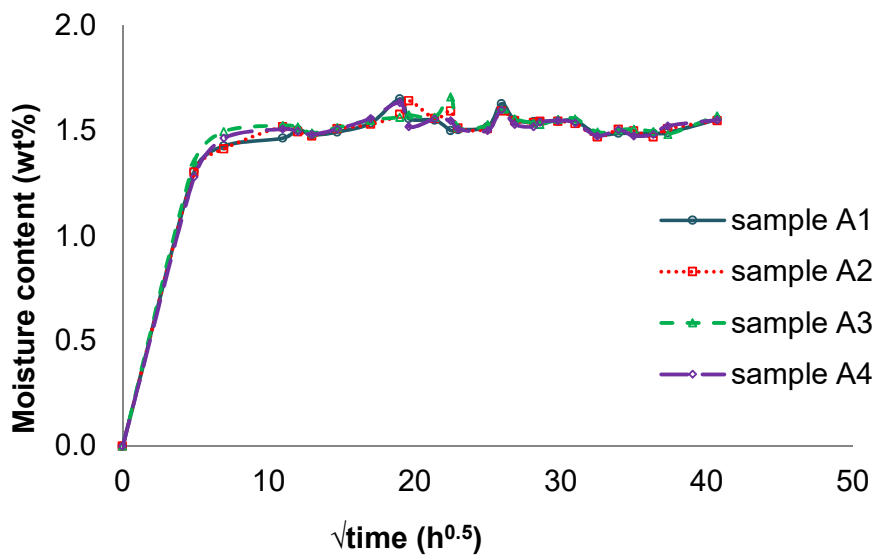


Figure 4-1 Moisture absorption for FM94 bulk adhesive (1mm thick), samples removed at hot-wet condition

To calculate the diffusion coefficient (D_h) and moisture concentration at saturation (M_m), the procedure of section 3.6.2 was followed. Figure 4-2 shows the moisture uptake average against the $\sqrt{\text{time}}$, for 1 mm thick. The standard deviation for each data point was calculated and represented by the error bars; the average value for the standard deviation was 0.02, which means a low disparity between the data.

The saturation average value (M_m) was determined between the minimum and the maximum moisture content. These limits (minimum and maximum) are illustrated with brown and green dashed lines respectively. The saturation content (M_m) obtained was 1.54 % and it is represented as a horizontal orange line.

The diffusion coefficient (D_h) calculated with the Equation (3-5) was 5.91×10^{-3} mm²/h and it is represented as the straight line slope (red line).

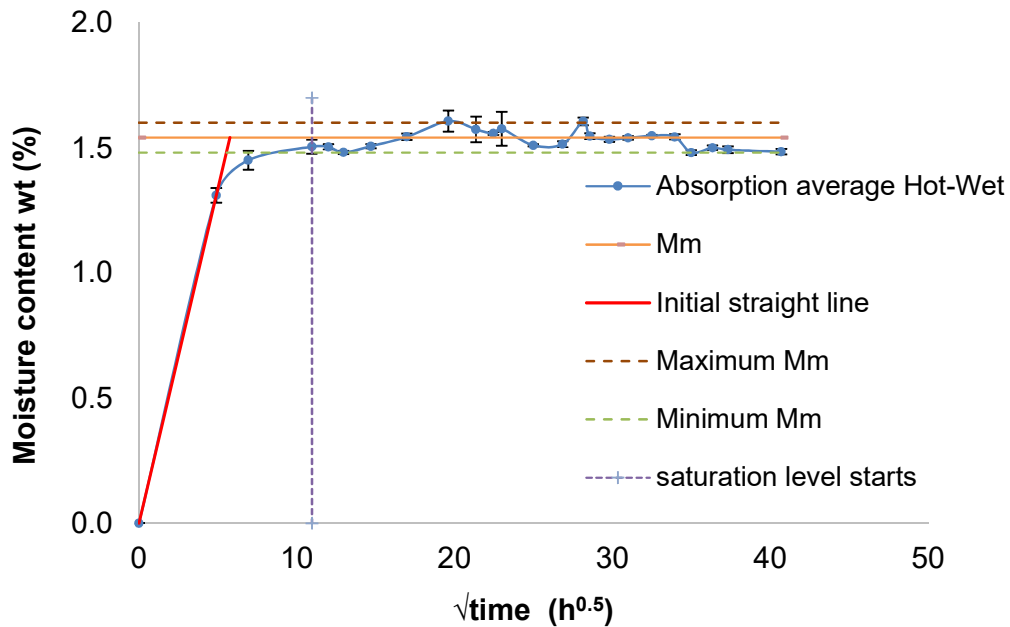


Figure 4-2 Moisture absorption average FM94 bulk (1mm thick), at hot-wet condition

The Fick's model was performed using the values D_h and M_m in the Equation (3-3) [104]. The $M(T, t)$ values were plotted against $\sqrt{\text{time}}$, as shown in Figure 4-3. The $M(T, t)$ curve obtained was compared to the experimental data, showing a good correlation of the experimental results. The prediction of moisture content was satisfactory.

Analysing $M(T, t)$ based on [46], it can be stated that: Firstly, the moisture absorption at the initial straight line achieved up to 1.31 % mass uptake equivalent to 85 % of M_m (moisture equilibrium). It was measured at 24 h ($4.9 \text{ h}^{0.5}$).

Secondly, the concave zone can be seen after the main increment of moisture absorbed. This portion of the curve has slow moisture content increment after 24 h and equilibrium at 120 h ($10.95 \text{ h}^{0.5}$).

Thirdly, the moisture absorption content was determined only at one thickness (1 mm). For that reason, a superimposable curve for different thickness cannot be confirmed.

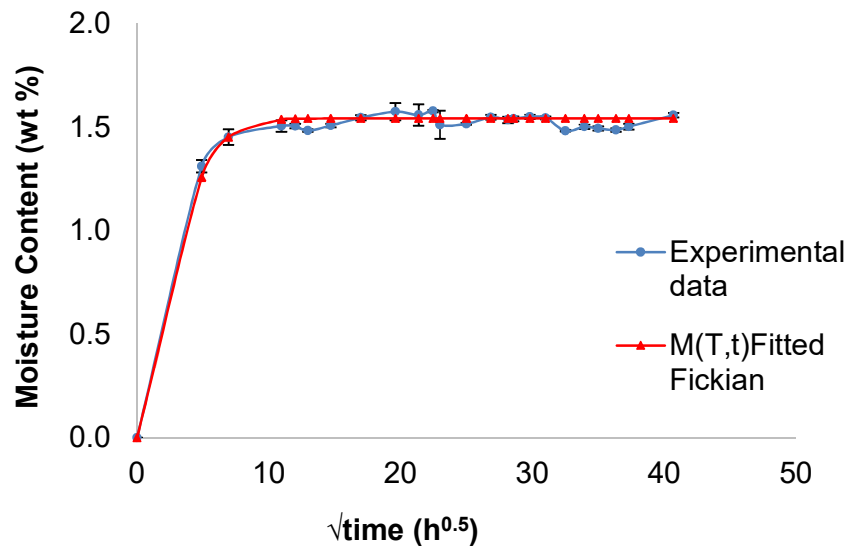


Figure 4-3 Predicted moisture absorption (1 mm thick) at hot-wet condition compared with experimental moisture uptake

In brief, two out of the three requirements were accomplished. It can be concluded that the absorption was governed by a Fick's diffusion law at hot-wet conditions.

Second series: Three bulk adhesive samples were gravimetric-tested to get the moisture diffusion at cold-dry. The samples were removed from the environmental chamber about $-10 \text{ }^\circ\text{C}$. This test was carried out in less time than specimens removed at hot-wet conditions.

Figure 4-4 shows the moisture uptake over the time exposure for bulk adhesive samples (1 mm thick). The three samples showed similar diffusion behaviour to each other and to samples removed at hot-wet conditions (first series). The major moisture absorption occurred in the first stage before 24 h ($4.9 \text{ h}^{0.5}$).

In contrast to the hot-wet condition, the concave zone was not clearly observed; after 36 h ($6 \text{ h}^{0.5}$) exposure, the absorption exhibited a very small increment with respect to the initial absorption and following a sharp increase at 60 h ($7.48 \text{ h}^{0.5}$). Those changes in the rate of absorption can be attributed to the short time interval between the first and the second reading. The moisture content tended to level off after 56 h ($7.48 \text{ h}^{0.5}$) – change of mass gained about 0.01 %-. According to ASTM D5229, the equilibrium state is reached when the moisture content changes less than 0.02 % [115].

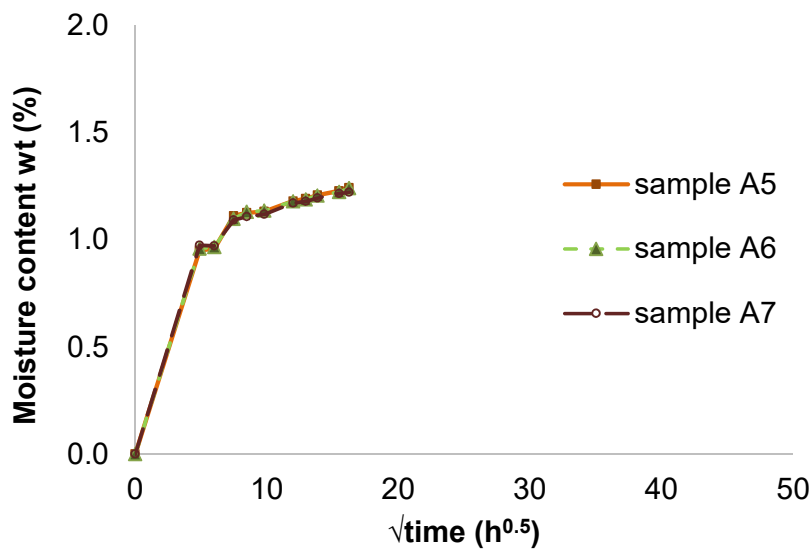


Figure 4-4 Moisture absorption for FM94 bulk adhesive (1mm thick), at cold-dry condition

Figure 4-5 illustrates the moisture average content for the samples removed at the cold-dry condition, the error bars refer to the standard deviation at each data point. The standard deviation was 0.02, meaning a good repeatability of the test with a good factor of control managed by the researcher. The maximum moisture concentration defined was 1.17 % and the diffusion coefficient (D_h) calculated was $5.60 \times 10^{-3} \text{ mm}^2/\text{h}$.

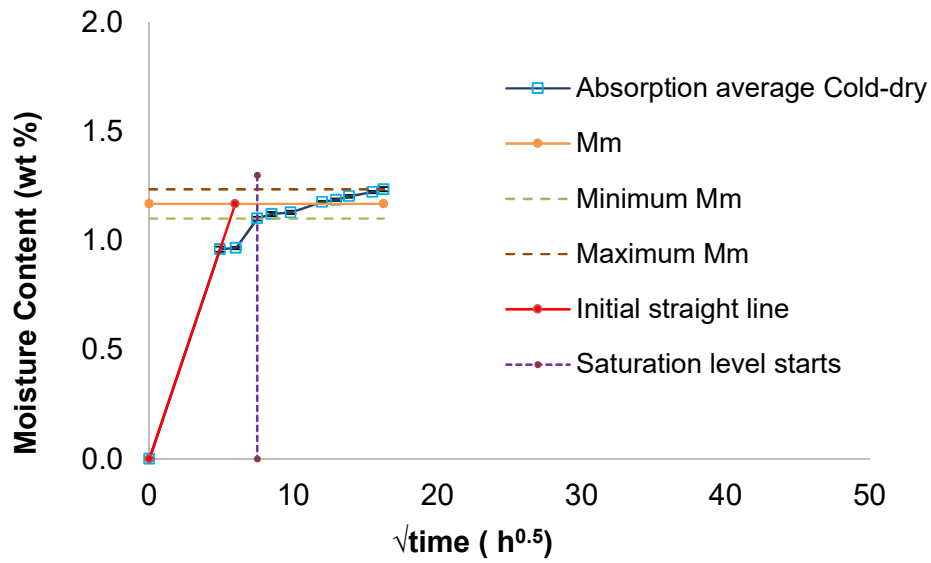


Figure 4-5 Moisture absorption average FM94 bulk (1mm thick), at cold-dry condition

Experimental data and the Fick's fitted curve are presented in Figure 4-6. Although this analysis shows good agreement with measured data, at higher exposure times the Fick's treatment gives an underestimation of moisture content.

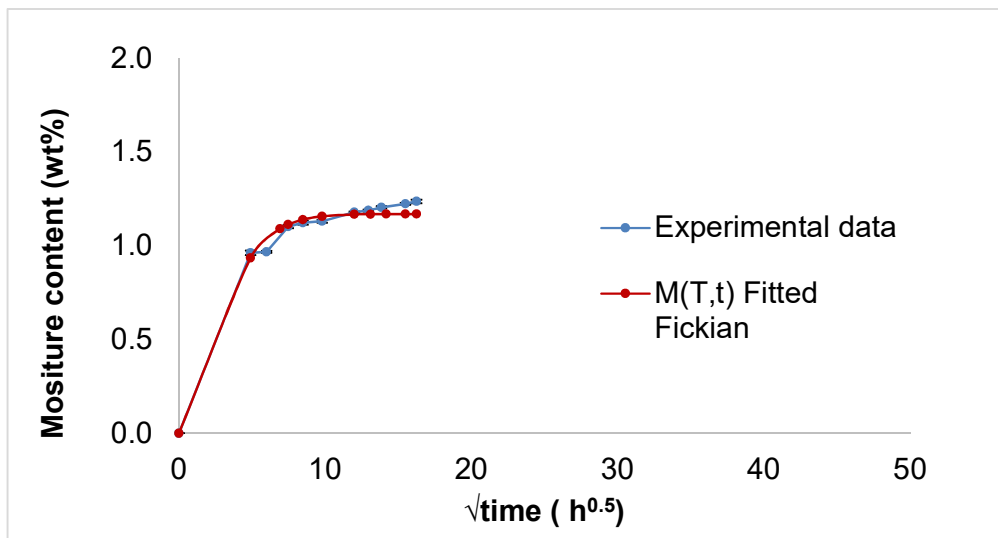


Figure 4-6 Predicted moisture absorption (1 mm thick) at cold-dry condition compared with experimental data

Analysing the Fick's characteristics: the initial absorption (linear stage) reached 0.97 % at $4.9 \text{ h}^{0.5}$ (24 h); this value equals 83 % of the maximum concentration M_m . Additionally, there is a concave portion before the saturation level. There is no experimental data for other thickness; hence the superimposable curve it cannot therefore be confirmed. In conclusion, similar to the diffusion under hot-wet conditions, moisture diffusion followed the second Fick's Law.

In fact, moisture diffusion of FM94 subjected to the hygrothermal cycles obeyed Fick diffusion behaviour. Here, changes in the diffusion rate can be observed between hot-wet and cold-dry conditions; these changes have evidenced diffusion dependence on the temperature. Temperature reductions caused a drop of diffusivity and the maximum moisture content. It can be seen in *Figure 4-7* where a comparison of moisture uptake at hot-wet and cold-dry is illustrated.

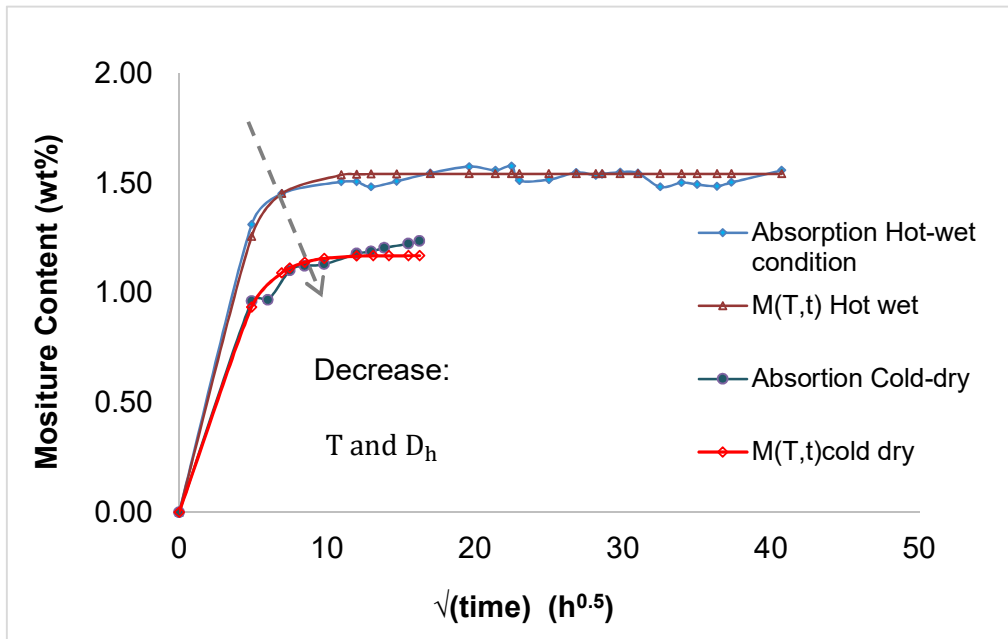


Figure 4-7 Moisture Diffusion FM94 bulk, samples were taken out at hot-wet and cold-dry conditions

Table 8 summarizes the results for bulk adhesive FM94, 1mm thickness. The diffusion rate at cold-dry was 5.3 % slower than the diffusion calculated for samples removed from the hygrothermal cycle at the hot-wet condition. This may be attributed to the increase of free volume, due to both molecular movements and thermal vibrations.

Table 8 FM94 moisture absorption comparison between hot-wet and cold-dry

CONDITION REMOVED FROM ENVIRONMENTAL CHAMBER	Mm %	Dh mm ² /h
70 °C/85 %RH	1.54	5.91E-03
About -10 °C	1.17	5.60E-03

The maximum concentration achieved at cold-dry was 5 % smaller than that at hot-wet condition, which may indicate that the maximum moisture content was driven by the relative humidity and the temperature.

Indeed, the diffusion regarding the hygrothermal cycle studied shows a dynamic behaviour. In other words, moisture diffusion content oscillates between an upper and lower value. A schematic description of the hygrothermal ageing cycles and the diffusion is shown in

Figure 4-8. It can be seen during the four hours at high-temperature and humidity (70 °C and 85 %RH), that the coefficient diffusion and the moisture uptake are higher whereas at freezing conditions (-10° and 0 %RH) the diffusion and the moisture content decrease.

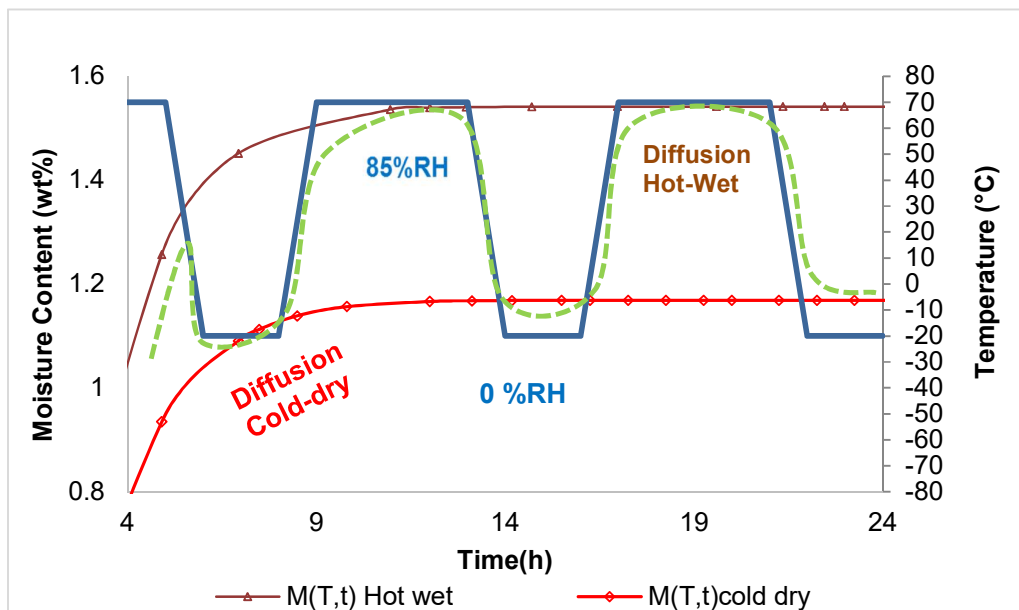


Figure 4-8 Schematic cyclic diffusion FM94

4.2.2 Composite laminate T800/M21

Four T800/M21 UD CFRP samples were gravimetric-tested to determine the moisture diffusion parameters. Tests were performed following the same procedure described in the Methodology Chapter, Section 3.6.1. In the case of composite specimens, the samples were only removed from the chamber at the hot-wet stage (about 70 °C/85 %RH).

The mass uptake, for all samples, as a function of the $\sqrt{\text{time}}$ is illustrated in Figure 4-9. The moisture absorption profile was similar for the four specimens. Initially, moisture rises in linear fashion with the square root of time, this rapid increment reached $10.95 \text{ h}^{0.5}$ (120 h). Follow by a steep drop where the moisture gained drop to 10 %. The absorption continued to rise slowly with some fluctuations and reached a state of apparent stabilisation.

The samples were exposed to temperature and moisture cycles, the changes in the moisture gained were not unexpected as the conditions were variable.

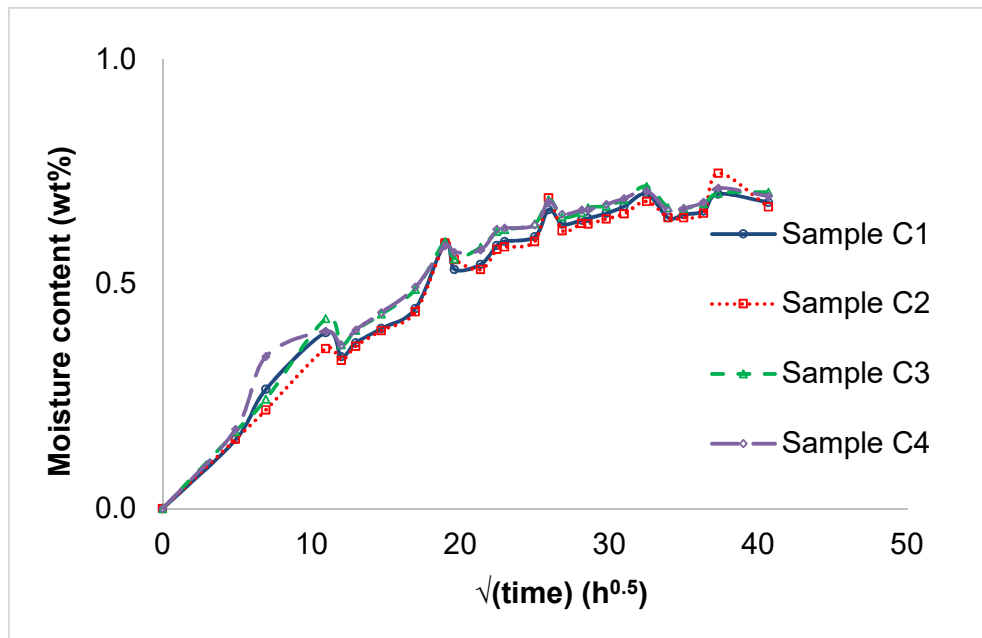


Figure 4-9 CFRP Moisture Absorption samples (2 mm thick)

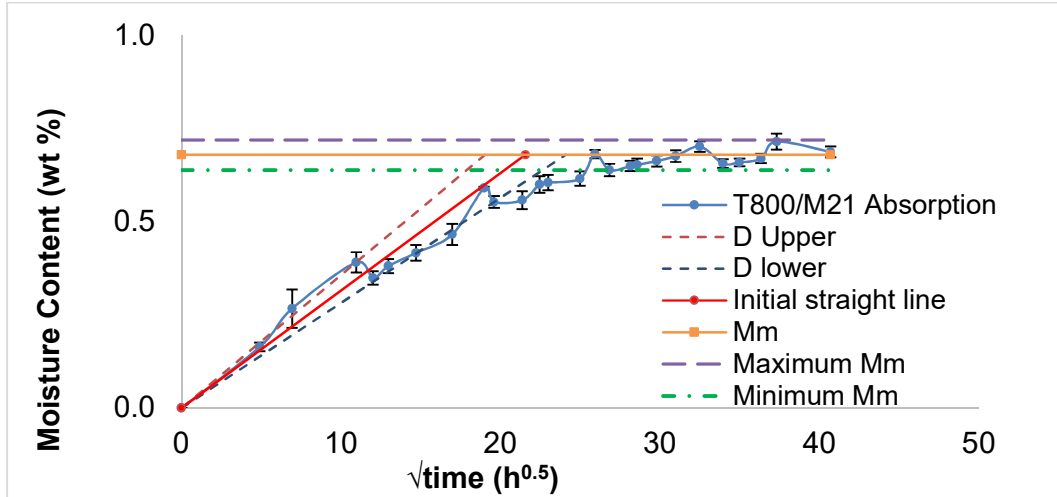


Figure 4-10 CRFP Moisture Absorption average (2 mm thick)

The moisture average is shown in Figure 4-10; error bars indicate the standard deviation for each data point. The standard deviation was 0.01 % that indicates low dispersion of data between samples. The spread of moisture absorption data over long time exposure can be attributed to another mode of interaction, that of the adsorption on the surface of CFRP.

Generally, the absorption was steady until it reached the apparent moisture equilibrium at $25.92 \text{ h}^{0.5}$ (672 h), after that point, the moisture uptake fluctuated between a maximum and minimum value. The T800/M21 saturation level average (Mm) was 0.68 % (samples removed from the chamber at hot-wet conditions). The maximum and minimum values are represented in Figure 4-10 with purple and green discontinuous line respectively.

Due to the drastic changes during the initial stage of absorption and to avoid overestimation of diffusion, two initial straight lines were drawn before defining the straight line diffusion. Two discontinuous lines were plotted; one –D upper- following the initial absorption until $10.95 \text{ h}^{0.5}$ and second –D lower- following the moisture uptake data after that time. Subsequently the ‘initial straight-line’ was drawn as an average between both discontinuous lines, red line in Figure 4-10. The diffusion coefficient (D_h) calculation for the trend slope was $1.7 \text{ E-3 mm}^2/\text{h}$.

Figure 4-11 shows the curve of the predicted moisture $M(T, t)$ as a function of the square root of time. It is compared with the experimental data results. The model

proposed based on ASTM showed good agreement [104]. Even though the absorption after $10 \text{ h}^{0.5}$ was overestimated, the moisture equilibrium content showed good correlation with the experiment results.

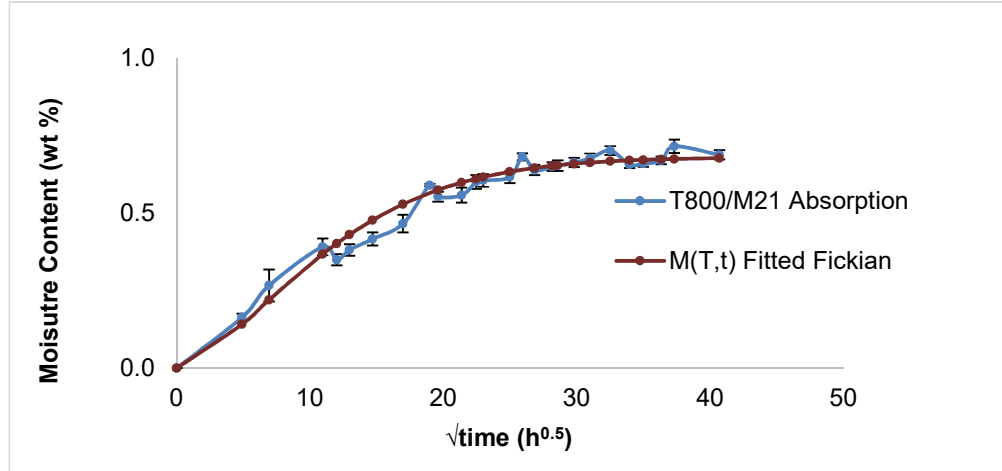


Figure 4-11 CFRP Predicted moisture absorption (2 mm thick) at hot-wet condition compared with experimental moisture uptake

Evaluating the predicted $M(T,t)$ curve, the initial moisture absorption (straight line) achieved up to 0.43 % absorption at $12.96 \text{ h}^{0.5}$. This absorption equals 63 % of maximum moisture content (M_m). The concave zone can be identified in *Figure 4-11*, the slow increment can be seen between $15 \text{ h}^{0.5}$ and $31 \text{ h}^{0.5}$ time. The moisture absorption was evaluated only for T800/M21 laminate 2 mm thickness; hence the superimposable curve for other thickness cannot be defined.

In conclusion, the moisture absorption of the T800/M21 laminate (2 mm thickness) exposed to the hygrothermal cycles obeys the Fick's Law behaviour.

Other authors have reported Fick's behaviour for composite fibre reinforcement, as in the case of carbon laminate IM7/977-2 exposed at 80C/80 %RH. [57]

4.2.3 Swelling

All samples after weighing were measured to identify dimensional changes. The tolerance on measurements was $\pm 0.01 \text{ mm}$. Neither swelling nor length modifications were detected in samples of adhesive FM94 and composite T800/M21.

4.2.4 Desorption following absorption FM94 and CFRP T800/M21 UD

Moisture desorption after the saturation test was performed to identify the materials desorption characteristics following the procedure described in the section 3.6.1. Figure 4-12 illustrates the change of mass during absorption and desorption as a function of time.

Both FM94 and T800/M21, showed an accelerated moisture loss in the first stage followed by a gradual reduction in mass change until it achieved the constant moisture content. Comparing the moisture desorption rate with the absorption rate, both materials presented a desorption rate faster than the moisture absorption.

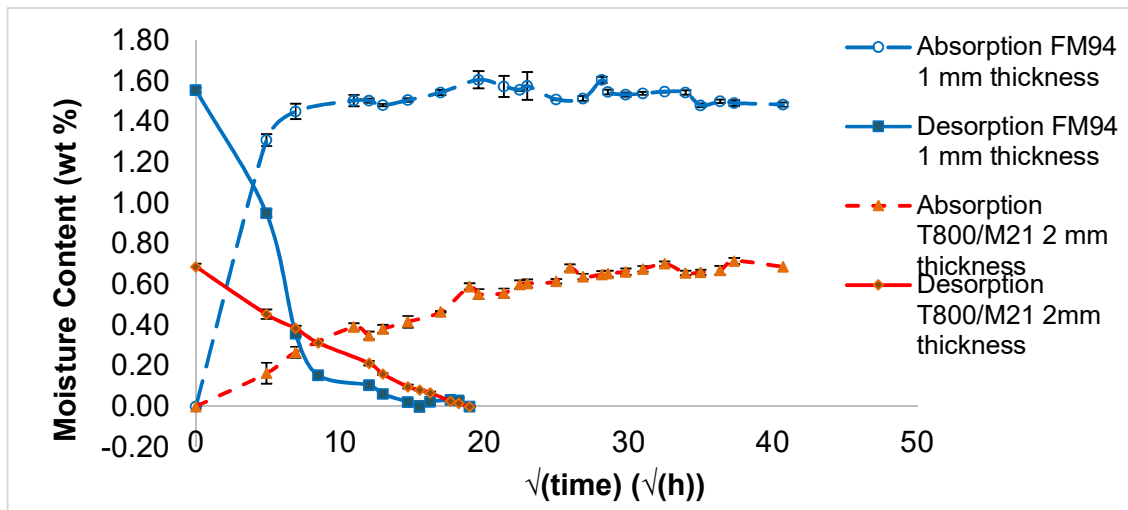


Figure 4-12 Desorption FM94 bulk and T800/M21 laminate

After the desorption test, any moisture absorption was found to be reversible indicating little or no chemical reaction (e.g. hydrolysis of the polymer chain).

The rate of diffusion for desorption was higher than the rate of absorption. Diffusion has been associated with the changes in the epoxy caused during the water absorption, interactions between water molecules and adhesive [70], [60].

The results from the work presented here show the diffusion rate in the composite laminate T800/M21 is 30 % slower than in the adhesive. This may suggest that the amount of moisture uptake by the joint is driven by the film adhesive. And as

a result the joint strength will be affected by the adhesive due to moisture absorption as well the stability of the interface, see Figure 4-13.

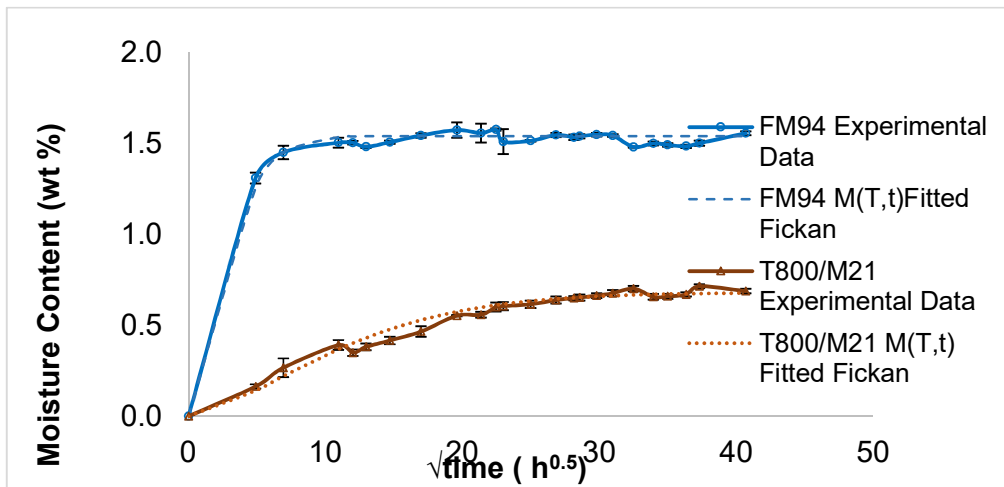


Figure 4-13 Moisture absorption FM94 and T800/M21

Although the diffusion and moisture content under the hygrothermal cycles showed dynamic behaviour, the difference between both conditions was about 0.9 %. It can be interpreted that the moisture diffusion profile was driven by the hot-wet conditions. Agreeing with this approach, commercial aircraft industries have affirmed that the moisture content depends mainly on the ground relative humidity during non-flight operations [116].

For that reason, the moisture properties used in the degradation model implemented in this study used the diffusion coefficient and moisture concentration measured at hot-wet conditions.

4.2.5 Mechanical properties Adhesive FM94

To determine the mechanical properties dependence to the hygrothermal cycles (i.e tensile strength and elastic modulus), bulk adhesive specimens were tested under static load, as described in Section 3.5 and 3.7.

Figure 4-14 shows the tensile stress against strain curves of unaged and aged bulk adhesive samples. Three specimens were plotted for each ageing condition (0, 84 and 168 cycles). It can be noted that neither tensile strength nor the strain showed changes with the increase in hygrothermal cycles.

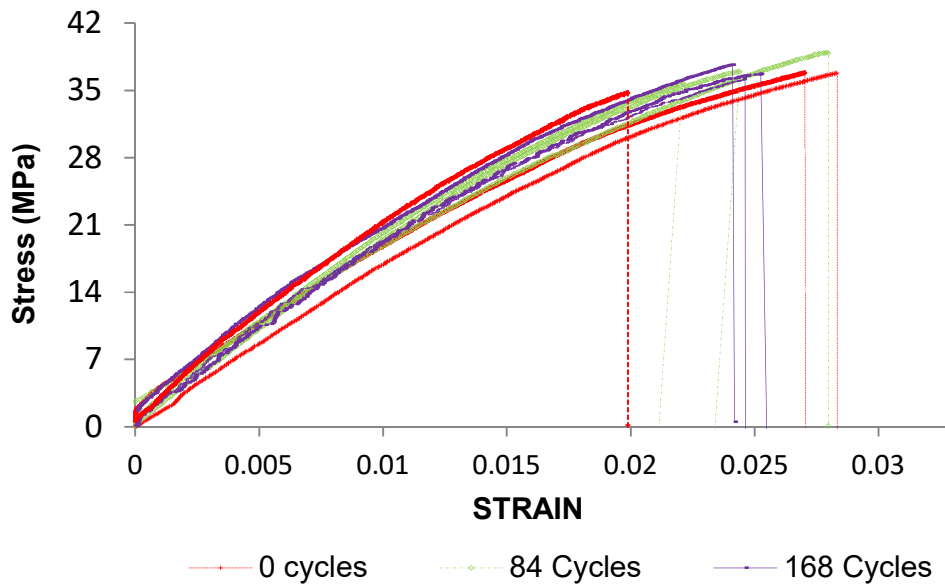


Figure 4-14 Effect of Hygrothermal cycles on mechanical properties FM94

The tensile strength average of all samples (unaged and aged) was 36 MPa with a standard deviation of ± 1.56 MPa, the results agree with Roh and Sun, who estimated a failure stress of 5 000 psi failure stress which is equivalent to 35MPa [117]. But, my resultant tensile strength was lower than the 50MPa reported by Zavatta [118].

Figure 4-15 shows the variation of the tensile stress average versus moisture content. The moisture content values of 0 %, 1.51 % and 1.54 % were taken from the experiments done (as seen in Section 4.2.1) and corresponded to 0, 84 and 168 cycles respectively. The error bars refer to the standard deviation for each set of samples tested.

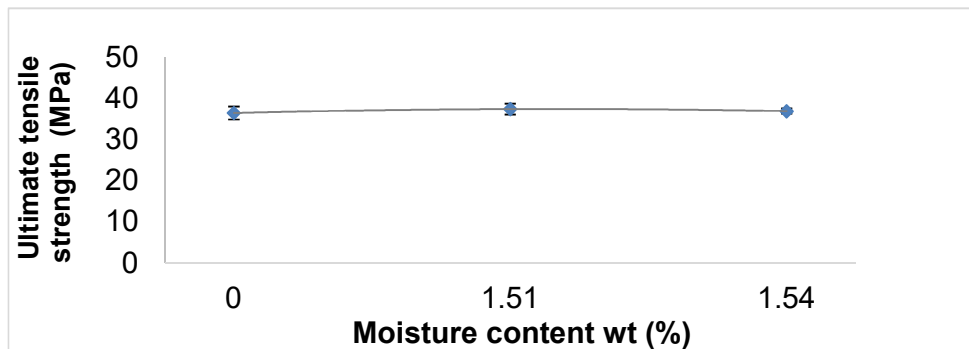


Figure 4-15 Variation ultimate tensile stress vs. moisture content wt (%)

Analysing Figure 4-15, at 1.51 % moisture content there was a small increment of the tensile strength compared with 0 % moisture (unaged state) and at 1.54 %, the stress showed a reduction compared to the unaged state. All of these changes were within the margin of error, confirming that the tensile stress remained constant after moisture absorption.

The elastic modulus (E) moisture dependence is shown in Figure 4-16. The elastic modulus average obtained for unaged specimens was about 1750 MPa with a high standard deviation equal to 117 MPa. After 84 hygrothermal cycles at 1.51 % moisture, the E modulus increased to 1900 MPa. Then, at 1.54 % moisture content (168 cycles), the E average went down by 4 %.

The E modulus of bulk adhesive didn't show a significant change after taking the maximum moisture content of 1.54 %. The experimental elastic modulus is noticeably smaller than 3000 MPa reported by Zavatta [118], but it agrees with 1750 MPa reported by Roh, H.S [117].

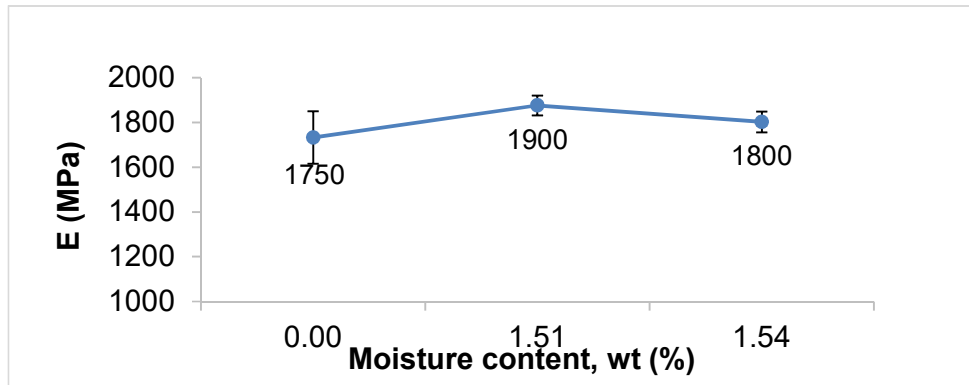


Figure 4-16 Elastic modulus as function moisture content

According to these results, moisture uptake during the hygrothermal cycles apparently does not affect the mechanical properties of the FM94. However, as mentioned in chapter 2, the moisture ingress in adhesives can cause changes in the strength, stiffness and strain [119], which will be discussed in chapter 6.

4.3 Adhesive bonded single lap joint test

Single lap joints were manufactured using laminates of CFRP Hexcel T800/M21 and film adhesive Cytec FM94K. The surface preparation used was peel ply and

the method of joining used was secondary bond following the instructions of the Cytec's data sheet. Two tip initiation cracks were included in the joints by the use of Polytetrafluoroethylene (PTFE), 0.1 mm thickness and 2mm width, laid in the free ends of the bonded joint, as described in section 3.3.

4.3.1 Mechanical testing

The results of tensile test and fatigue test are presented in this section; similarly, the fracture failure analysis is discussed. As mentioned in section 3.7.3, three to five samples were tested for each category.

4.3.1.1 Lap Shear Test

To investigate the influence of ageing on hygrothermal cycles on the joint strength, unaged and aged specimens were tested under shear lap load. The procedure was described in section 3.7.3.1.

The expected maximum load for the single lap joint was 13.7 kN; a value calculated using the FM94 tensile shear of 23.8 MPa for secondary bonding of Epoxy/Graphite substrates for 575 mm² area [103].

Load-displacement curves of unaged and aged specimens are shown in Figure 4-17, one representative curve has been chosen for each set. Load-displacement measurements do not start from zero as grip closure introduces a preload.

The load-displacement curves have shown brittle behaviour and similar loading slope. However, the unaged sample showed a largely linear trend, while the aged samples showed a moderate nonlinear behaviour before failure. Linear behaviour has been reported for CFRP bonded joints for 2 mm adherend thickness [2]. Park et al., (2010) reported a variation from linear to nonlinear response after ageing (elevated temperature and wet conditions) [120]

An apparent reduction of the stiffness with the hygrothermal cycles increase is observed. Although a variation of the stiffness behaviour can be seen as load and displacement increase, this effect on the apparent stiffness is caused by the eccentricity of the single lap joints. This rotation affects the displacement

measurement recorded by the laser extensometer, therefore the resultant data may be deemed unreliable.

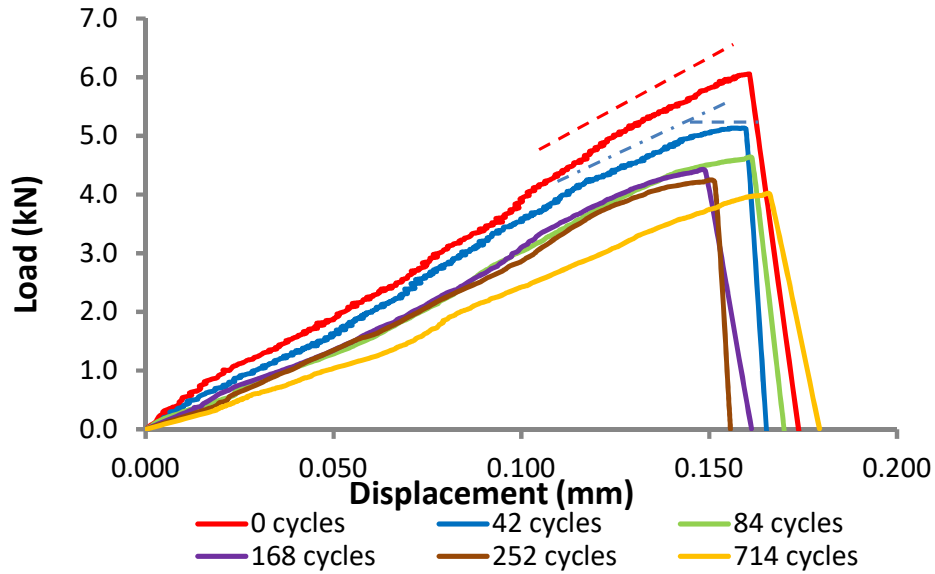


Figure 4-17 Load-displacement curve unaged and aged SLJ

The maximum failure load average was 6.58 kN for the unaged samples. It was 52 % lower than the expected maximum load, as shown in Table 9. The lower ultimate load can be attributed to the influence of multiple factors, such as moisture entrapment on the adhesive bond, surface preparation and the pre-crack tip in the joint.

Table 9 Summary of test data unaged and aged SLJ

HYGROTHERMAL CYCLES	FAILURE LOAD		DISPLACEMENT		INITIAL STIFFNESS
	kN		mm		N/mm ³
	Average	Standard deviation	Average	Standard deviation	
0	6.58	0.43	0.18	0.03	54.40
42	5.09	0.42	0.17	0.02	54.20
84	4.41	0.48	0.15	0.02	51.23
168	4.60	0.18	0.16	0.02	57.22
252	4.19	0.63	0.13	0.02	52.29
714	3.79	0.19	0.13	0.03	52.16

The failure load decreased gradually with an increasing number of hydrothermal cycles. The main reduction occurred at 42 cycles, decreasing by 23 % joint

strength compared with unaged specimens. The decreasing trend continued until 84 cycles, after that the strength reduction levelled off. After 714 cycles, the loss of joint strength achieved the figure of 42 %.

Figure 4-18 begins with a dramatic decrease in strength as the number of cycles increase. This was followed by a small strength increase to 168 cycles and from that point onwards, fell away to the figure of 6.6 MPa at 714 cycles. It must be noted that this fall is within the standard deviation.

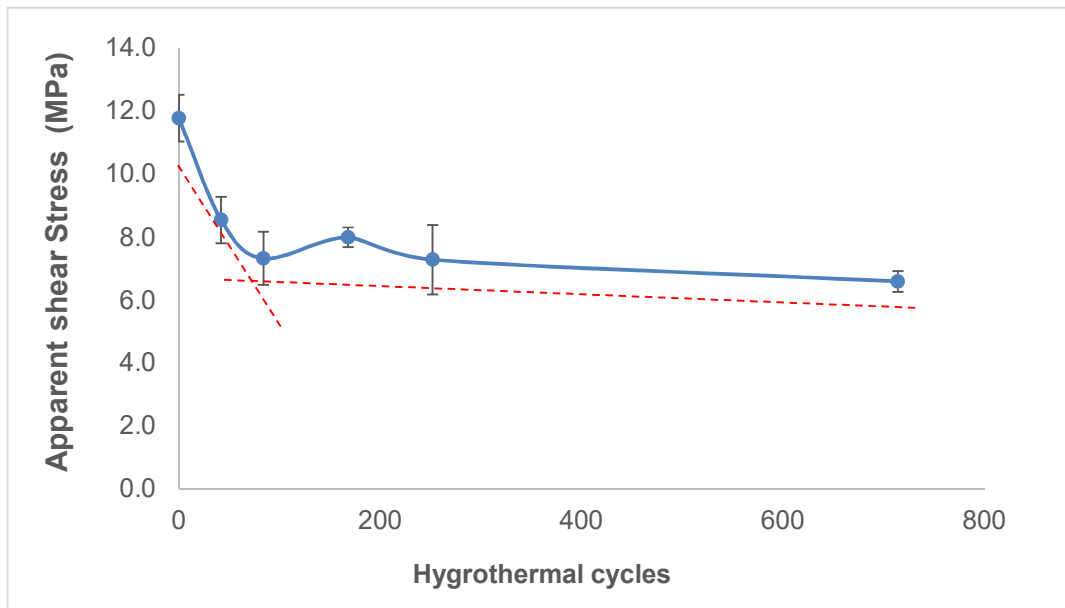


Figure 4-18 Shear strength as function of hygrothermal cycles

A similar trend was reported by Knight et al (2012), who studied the ageing of CFRP-CFRP single lap joint under hot wet conditioning over two years. The shear strength reduction after 500 days was 35 % less than the control sample, and the levelling off was attributed to the saturation.

There is a significant effect of hygrothermal cycles on joint strength, which contrasted with the findings on the bulk adhesive tensile strength, showed in section 4.2.5. This may be due to water diffusion into the interface which occurs more rapidly than in the bulk adhesive, to a low affinity of the FM94 to the water, and possibly to an unstable condition of the interface, as will be discussed later in section 6.4.1.

Figure 4-19 shows a bar graph of the maximum displacement average against the hygrothermal cycles from SLJ. Due to an apparent elastic relaxation after failure (seen in Figure 4-17), the maximum displacement value was taken at maximum failure load.

The displacement at failure fell with hygrothermal ageing, decreasing from 0.18 mm to 0.13 mm. The reduction was interrupted at 168 cycles with a displacement of 0.16mm, when an apparent increment occurred. From this point the fall continued to 0.13mm at 252 cycles and levelled off at this figure.

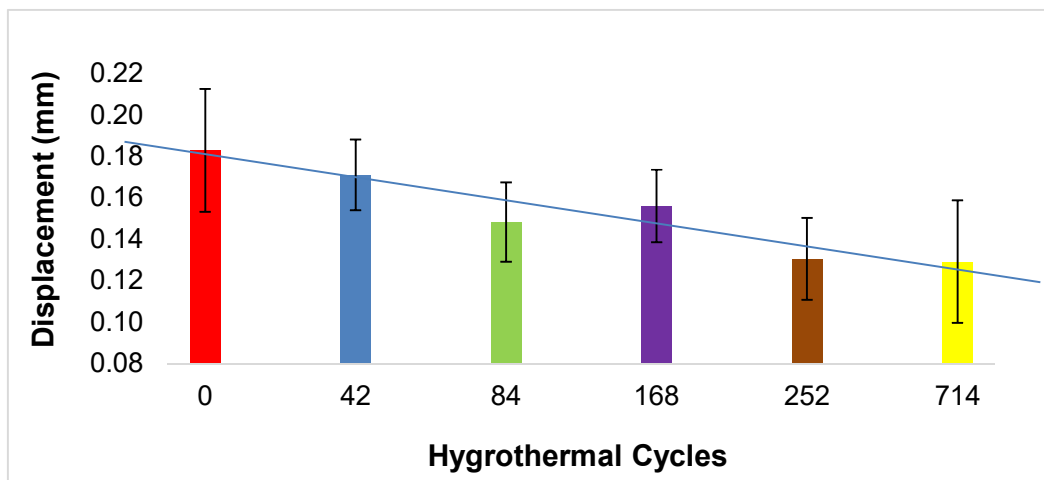


Figure 4-19 Displacement at failure of unaged and aged single lap joints

Post-failure analysis

Microscopy was used to evaluate fracture surfaces in detail. Figure 4-20 shows the typical failure surface of joints (conditioned and unconditioned). In the photograph, it can be seen that the fracture occurred along the adherend/adhesive interface. The adhesive was fractured at both substrate sides, showing two failure modes: adhesion failure, and higher proportion of the thin cohesive layer.

The morphology may indicate that the cracks have initiated from both edges (PTFE areas) and propagated through the interface toward the opposite edge. Additionally, a noticeable amount of porosity can be seen along the adhesive layer in Figure 4-20.

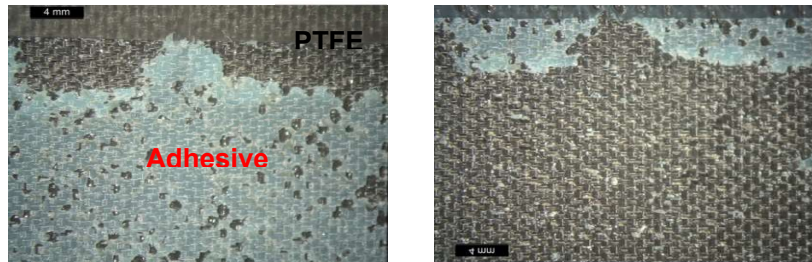


Figure 4-20 Typical surface failure

The thin-layer cohesive failure (interface failure) can be seen as a light dusting of adhesive Figure 4-21 (a). The laminate surface contours produced by peel ply preparation retained some fractured adhesive, it can be evidenced that the adhesive impregnation on the adherend (after curing) was uniform, as shown in Figure 4-21 (b).

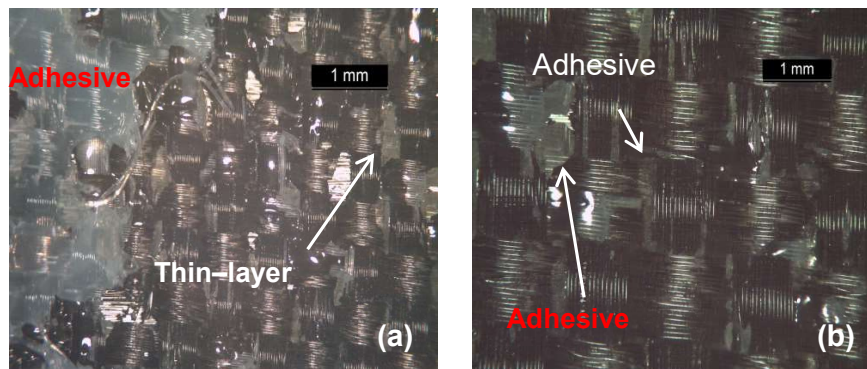


Figure 4-21 Photograph of failure surface unaged and aged (a) fracture failure, (b) adhesive contours

After 84 cycles, the joint failures showed a variation in the fracture pattern, total separation did not occur, as is shown in Figure 4-22. The adhesive layer showed a plastic behaviour that induced the adherents to remain connected.

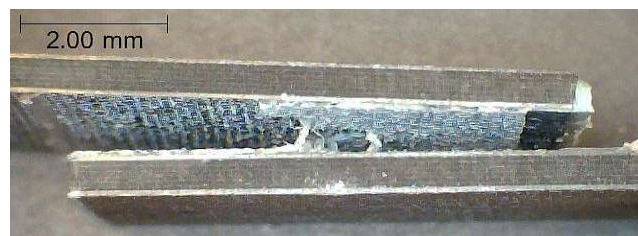


Figure 4-22 Fracture failure after 84 cycles

4.3.1.2 Fatigue Test

To determine the SLJ fatigue life (for unaged and aged specimens), fatigue tests were carried out under a constant amplitude, ratio $R=0.1$ and frequency of 5 Hz. The testing ran up to 10^6 cycles following the procedure described in section 3.7.3.2.

The fatigue life was normalised with respect to the ultimate static strength of the unaged joints. The fatigue life was studied for 0 cycles, 84 cycles and 336 cycles. The load (L) against the number of cycles to failure (N) plots of unaged and aged single lap joints are shown in Figure 4-23. The arrows plotted above some data refer to the fact that the specimen did not fail before 10^6 cycles.

In order to describe the fatigue behaviour, the fatigue cycles were grouped into three regions: low cycle fatigue below 10 000 cycles, high cycle fatigue between 10 000 and 10^6 cycles and infinite life after 10^6 cycles.

Unaged joints were tested at four different load levels (40 %, 45 %, 50 % and 55 % of ultimate strength). Unaged joints at lower load (40 % ultimate load) supported 10^6 cycles without failure. The unaged joints showed a high cycle fatigue life of around 25,000 cycles at 55 % maximum load.

Aged joints at 84 hygrothermal cycles were tested at 30 %, 40 % and 45 % of quasi-static strength (unaged). S-N curve normalised (84 cycles) showed a reduction of fatigue life although there was the high spread of data. At lower load level (30 %), the fatigue life was over 10^6 cycles. At 40 % load level, there was a high spread of fatigue life cycles; two specimens presented infinite life while three joints failed at high fatigue cycles (244 456, 478 768 and 572 448 life cycles).

That may be attributed to the difference of time after removing them from the environmental chamber. Aged joints tested at the first or second week after removal from the chamber failed; additionally, it was observed that the fatigue life increased as the amount of time out of the chamber increased. In contrast to those joints, SLJ evaluated after 3 weeks out of the environmental chamber were not broken. This could be caused by desorption of water from the joint/sample during the period outside of the environmental chamber (low %RH conditions),

which could allow the joint to ‘recover’. Similarly, Costa et, al. [63] present data demonstrating that a fully saturated SLJ sample has a lower fatigue life when compared with a similar SLJ that has been aged at 50 %RH. Work reported by Sugiman and Crocombe [121] are consistent with the work reported.

At higher load level (45 %) a significant reduction of the life cycles could be seen as compared with unaged joints.

Aged joints at 336 cycles were tested at the same load levels as aged joints at 84 cycles. At lower load, two of the joints exceeded the 10^6 life cycles without failing, but one joint failed unexpectedly at 13296 cycles. At 40 % load level, fatigue life showed high and low life cycles; two specimens failed over 10000 cycles and two joints failed around 1000 cycles. At higher load level (45 %), the fatigue life decreased by a factor of 10 compared with conditioned joints at 84 cycles.

Overall, the fatigue life decreased with increasing hygrothermal cycles. The life cycles showed a horizontal shift toward the left for each load tested. A similar trend has been reported by Katnam *et al.* [50] for metal bonded joints immersed in water at 50°C for one and two years.

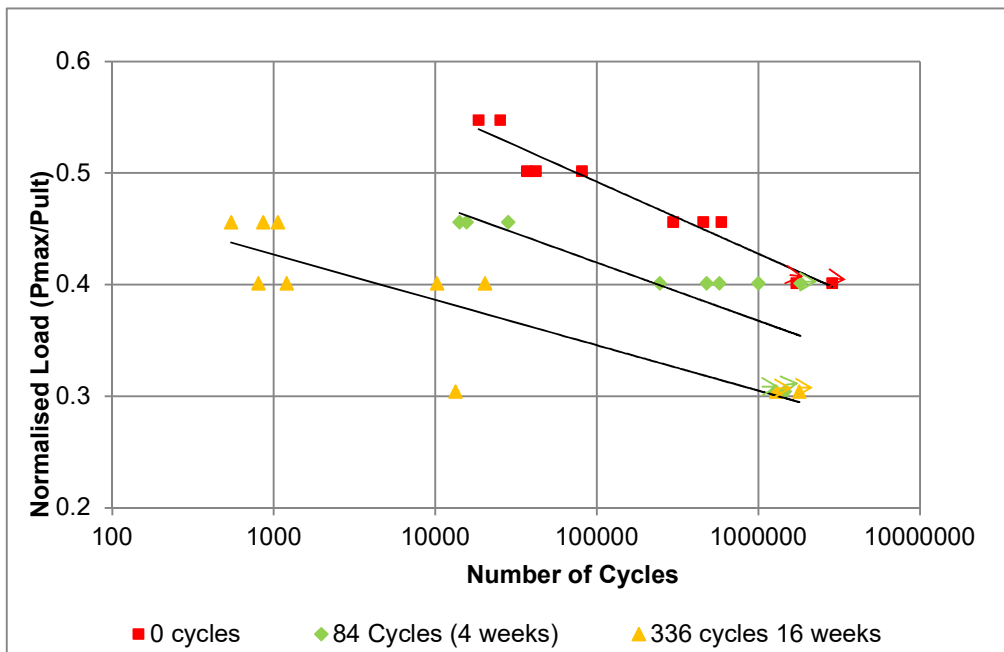


Figure 4-23 L-N normalised curves of SLJ unaged and aged (R= 0.1, f=5Hz)

Post-failure Analysis

A microscopy evaluation was performed after the fatigue test to identify the failure mode of the aged and unaged joints. A microscope with 400X of magnification was used to inspect the failure surface.

A mixed failure mode of adhesion failure and thin-layer cohesive failure can be identified on the fracture surface, as shown in Figure 4-24 (a). All joints showed failure occurred along the adherend-adhesive interface with a predominant adhesion failure type. The pattern of failure was similar in most of the specimens; two cracks initiated from the ends of the overlap and propagated towards the centre of the overlap until the final failure.

However, the joint aged at 336 cycles and tested at 30 % load level which presented a premature failure, showed a slight change of fracture pattern; only one crack propagated and the failure occurred near to one end of the overlap, as illustrated in Figure 4-24 (b).



Figure 4-24 Failure surface SLJ tested under fatigue (a) mode failure typical pattern, (b) failure pattern aged SLJ at 336 cycles

4.3.2 Non-Destructive Inspection-NDI

Visual Inspection-Microscopy evaluation

To characterise the bondline with respect to the voids or moisture effects optical microscopy was used under reflected light. A control sample was observed (previous and post ageing cycles) with a NIKON Optiphot microscope at different magnification lens (5X,10X,20X,40X).

A side view of the overlap region from the unaged specimen can be seen Figure 4-25. A great void can be seen in the bondline, and the PTFE in the free edge was highlighted with red colour. Apparently the adherends were free of defects, as shown in Figure 4-25 (a). A significant amount of voids were found along throughout the bond layer.

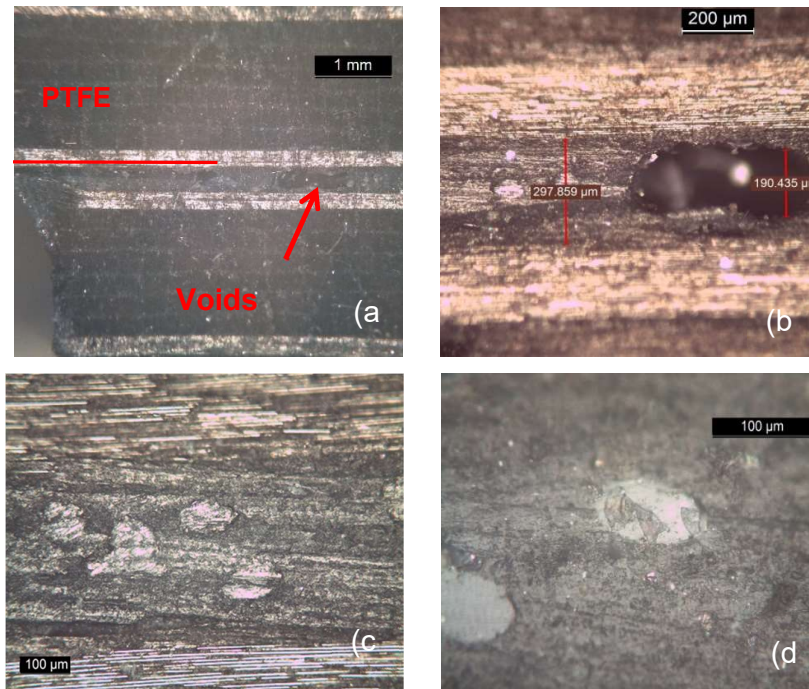


Figure 4-25 Photographs of side view of unaged SLJ (a) 5X,(b)10X,(c)20X,(d) 40X

The measurement of the bondline thickness and the void height were taken at 0.3 mm and 0.19 mm respectively. This void has occupied 64 % of the bondline height, as seen in Figure 4-25 (b). Debonding or micro-cracks haven't been identified in the bond area. There were spots with a white contour along the bond area as shown in Figure 4-25 (c-d), which seemed to trapped moisture in the bondline.

Figure 4-26 shows the microscopy images after 252 ageing cycles. Void content in the bondline is seen in Figure 4-26 (a). The bondline thickness measured was 0.3 mm. Evidence of lack of bonding, cracks or degradation were not found. The apparent moisture seen before ageing did not show changes of amount or dimensions, as shown in Figure 4-26 (c-d).

Evidence of degradation resulting from the ageing cannot be seen. There was no swelling or trapped moisture in the bondline after the ageing. The white contours cannot be assumed as trapped moisture. But, there were a high amount of voids identified along the bond edge.

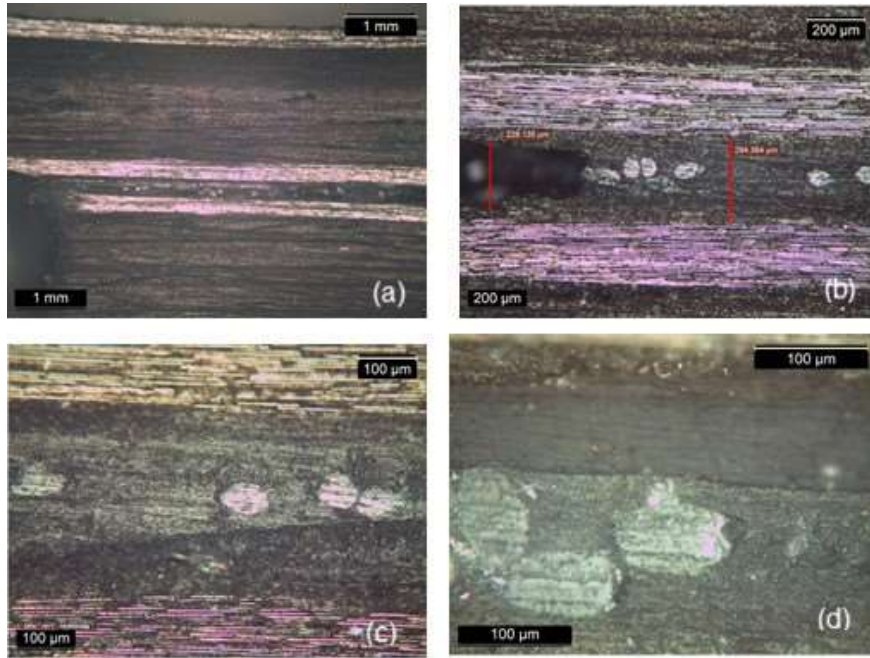


Figure 4-26 Photographs of side view of aged bondline (252 cycles) bondline (a) 5X, (b)10X, (c) 20X, (d) 40X

Ultrasonic Inspection

Ultrasonic C-scan 5 MHz with a gain of 31dB was used to evaluate the quality of the bonded joints (unconditioned and conditioned) to hygrothermal cycles in an environmental chamber. A control single lap joint was evaluated pre and post ageing process. This joint was removed from the environmental chamber at 84, 168 and 252 cycles, and inspected through the ultrasonic C-scan as described in section 3.4.2.

A high amplitude energy transmitted through the bond line is interpreted as good quality bond (100 % amplitude). The amplitude variation of the reflected signal passing through the (adherend-adhesive) interface represents attenuations associated with discontinuities in the adhesive layer. Hence, the measurement of

ultrasonic energy going through the healthy bond is greater due to less attenuation [114].

The C-scanned images of the joint (unaged and aged) and the signal amplitude are shown in Figure 4-27. Note that the good bond quality is taken as red coloured contours and the lack of bond quality is taken as blue/white coloured contours.

The unaged image shows a significant variation of the amplitude. A good bond quality is seen in the middle of the joint. A slight attenuation can be seen as a yellow coloured contour (60 % signal amplitude) which can be interpreted as differences of adhesion. Furthermore, the lowest amplitude signal can be appreciated at the end of the overlap (blue coloured contour); particularly on the right side. This lack of adherence may be associated to the PTFE crack initiators, as shown in Figure 4-27 (a).

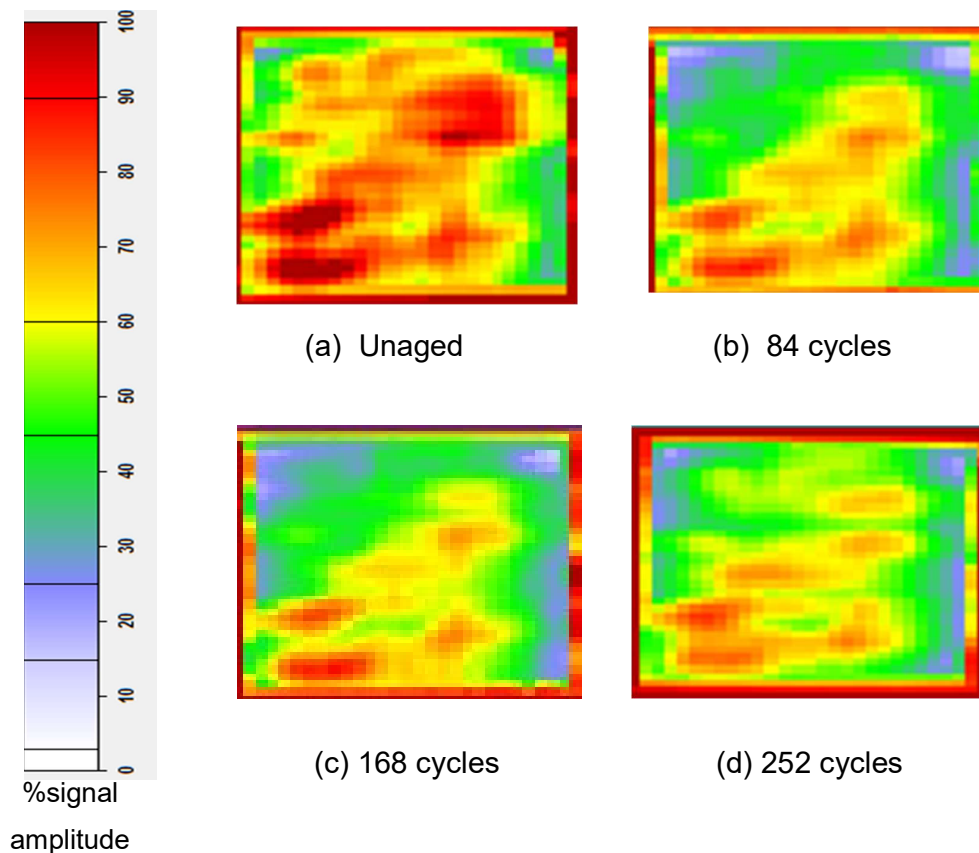


Figure 4-27 C-scan images of the bond region obtained at different ageing states

After 84 hygrothermal cycles, the C-scan image showed a reduction of the amplitude. The attenuation was greater around all of bond area (green and yellow coloured contours), which can be interpreted as bond deficiencies. At 168 cycles, the amplitude mapped did not show changes compared with that of 84 cycles, as shown in Figure 4-27 (b) (c).

And at 252 cycles, the spectra of the ultrasonic signal showed little change compared to 168 ageing cycles. There was a moderate rise of amplitude signal in some parts of the overlap, as can be seen in Figure 4-27 (d).

Overall, the signal penetrated the bond area and provided information about the condition of the bond. The joint inspected before exposure to environmental attack presented bond discontinuities along the overlap. This lack of homogeneity can be associated with bond defects, such as porosity or lack of adhesion. In conclusion, the joint was not a healthy joint before ageing.

Inspection of the joint after hygrothermal ageing showed changes in the spectrum of the ultrasonic signal. This increment of the mismatched areas may indicate degradation of the bond compared to the unaged condition.

By comparing the ageing images (84,168,252 cycles), slight changes of the ultrasonic signal were found. However, they cannot be taken as evidence of incremental mismatching of the bond, because of any presence of water being able to affect the sensitivity of the incident ultrasonic wave [122].

5 DEGRADATION MODELLING OF ADHESIVELY BONDED SINGLE LAP JOINT

To predict the environmental effects on the adhesive joints, a methodology that couples experimental data with numerical modelling approach has been proposed.

The methodology has been divided principally into three steps; in the first step theoretical model was carried out to identify the diffusion coefficient and the moisture concentration at a different number of cycles based on existing constitutive expressions, as shown previously in section 4.

The second step consisted of developing a numerical model, which was established to determine the effect of the moisture concentration on the elastic modulus of the bulk adhesive. The adhesive properties as a function of moisture content were evaluated through a thermal-displacement analysis. The moisture characterisation of the first step was used as input for performing the bulk finite element (FE) analysis.

An adhesively bonded single lap joint (SLJ) degradation was modelled in the third step based on cohesive law. It was developed to determine the progression of damage in the bondline area due to moisture absorption and mechanical loading. The degraded parameters of SLJ were determined based on the joint's experiments and analysis of the bulk adhesive.

5.1 Finite Element Analysis

Two numerical analyses were carried out using Abaqus 3D models: A bulk adhesive model, which used a moisture diffusion displacement method in order to achieve degraded properties, and a Cohesive Zone Model (CZM) of the joint to predict the damage caused by hygrothermal cycles and mechanical load. The analysis was carried out in Abaqus Standard using the implicit solver. The implicit finite element technique is used to solve linear and non-linear problems, the implicit solver requires iterate solutions with each time increment. It has been

adequate for brittle adhesive behaviour under tensile loading [84]. To achieve a greater numerical stability and accuracy a longer time step size is necessary.

5.1.1 Bulk adhesive

To determine the adhesive elasticity modulus degradation due to moisture content, a moisture displacement analysis was performed using an analogy between heat transfer law (Fourier's Law) and moisture diffusion law (Fick's Law), [123].

Heat transfer expression is presented in equation (5-1):

$$\frac{\partial T}{\partial t} = \left(\frac{k}{c\rho}\right)\nabla^2 T \quad (5-1)$$

Where,

T is temperature,

t is time,

k is thermal conductivity,

c is specific heat,

ρ is density,

$\nabla^2 T$ the temperature gradient

Moisture diffusion law is shown in equation (5-2):

$$\frac{\partial C}{\partial t} = D\nabla^2 C \quad (5-2)$$

Where,

C is moisture concentration,

D is diffusion coefficient

$\nabla^2 C$ the concentration gradient.

Using the equations, the diffusion is modelled using the material model of heat/transfer built in Abaqus, using the diffusion coefficient as thermal conductivity and concentration as temperature.

For such analysis, density and specific heat can be taken as a unit as proposed by [70]. The coefficient of moisture expansion (CME) used was 0.0016/ wt(%) [97], [54]. The diffusion coefficient was taken from the experimental results of FM94, section 4.1.1.1. The FM94 properties used to model the bulk are shown in Table 10.

Table 10 FM94 properties

PROPERTIES	UNIT	VALUE
Elastic Modulus (E)	MPa	3000
Poisson's ratio (ν)		0.35
Shear modulus (G)	MPa	1111
Diffusion Coefficient (D)	mm ² /s	1.64E-06

5.1.1.1 Geometry and boundary conditions

The bulk adhesive geometry is shown in Figure 5-1. To simulate tensile loading a full restraint (clamped) was assigned to one edge of the bulk specimen, while the other edge was subjected to displacement. The points A and B are reference points used to measure displacement variation, both experimentally using a laser extensometer, and numerically.

To perform the moisture diffusion-displacement analysis, two coupled temperature-displacement steps were implemented: In the first step, the condition before moisture diffusion was defined. A load (type body heat flux) was applied uniformly distributed with a magnitude of 0.0001 (assumed as lowest moisture concentration), this magnitude was taken as the moisture concentration at time zero. In the second step, a load (type body heat flux) with the final moisture concentration (for each number of cycles studied: 1.49, 1.51, 1.54) and a displacement (10 mm) at the edge of the specimen were applied. The magnitude of the load was given as the percentage of moisture concentration for any time interval.

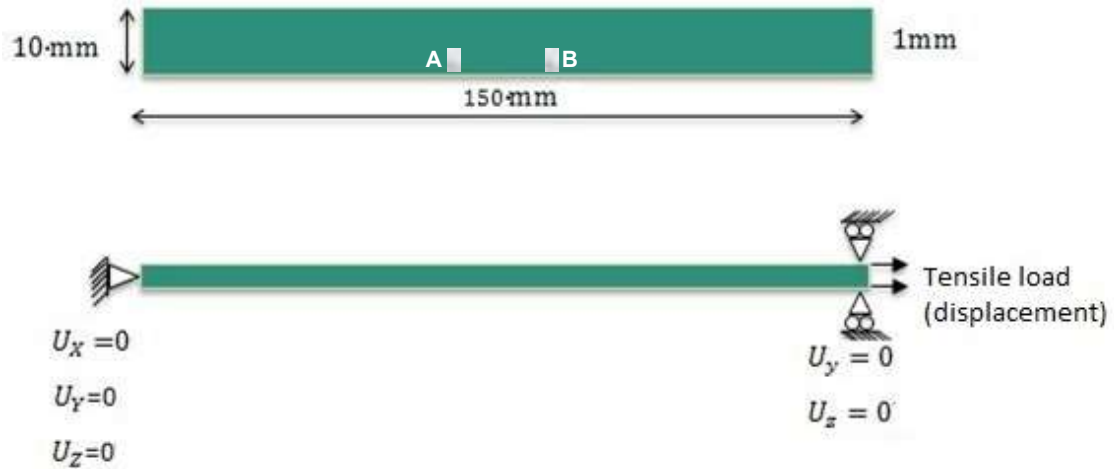


Figure 5-1 Configuration of Bulk adhesive

Moisture concentration in the bulk was assumed to be equal to the percentage of moisture concentration determined in the experiments for each time interval. The hygrothermal degradation of the adhesive was assumed to be only a function of the moisture concentration. The temperature cycles effect in the properties was considered implicit in the moisture concentration.

A mesh convergence study was performed for different mesh sizes (12 configurations) on 3D models, where the stress in the bulk adhesive was compared, as detailed in Table 11. The bulk adhesive samples were modelled and subjected to 10 mm displacement as mentioned earlier. Von Misses stresses are plotted against a number of elements as shown in Figure 5-2. It can be noted that convergence was achieved at 700 elements.

The bulk adhesive was modelled as elastic plastic continuum with 2000 quadratic hexahedral thermal-displacement-coupled elements (C3D20T). The mesh configuration can be seen in Figure 5-3.

Table 11 Details of different meshes employed in the mesh convergence analysis

MESH CONFIGURATION	NUMBER ELEMENTS	VON MISSES STRESS
Mesh 1	13	203.80
Mesh 2	15	200.60
Mesh 3	19	199.90
Mesh 4	50	197.40
Mesh 5	114	195.50
Mesh 6	375	198.69
Mesh 7	700	199.30
Mesh 8	1500	198.90
Mesh 9	1837	198.60
Mesh 10	2112	199.01
Mesh 11	2444	198.90
Mesh 12	2996	199.50

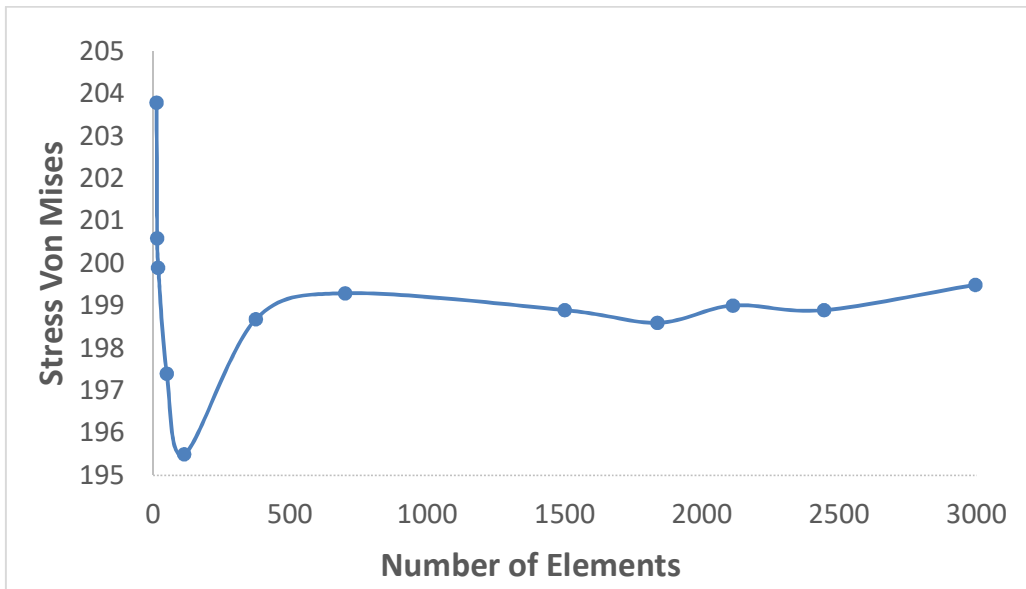


Figure 5-2 Von Misses stresses for different mesh densities

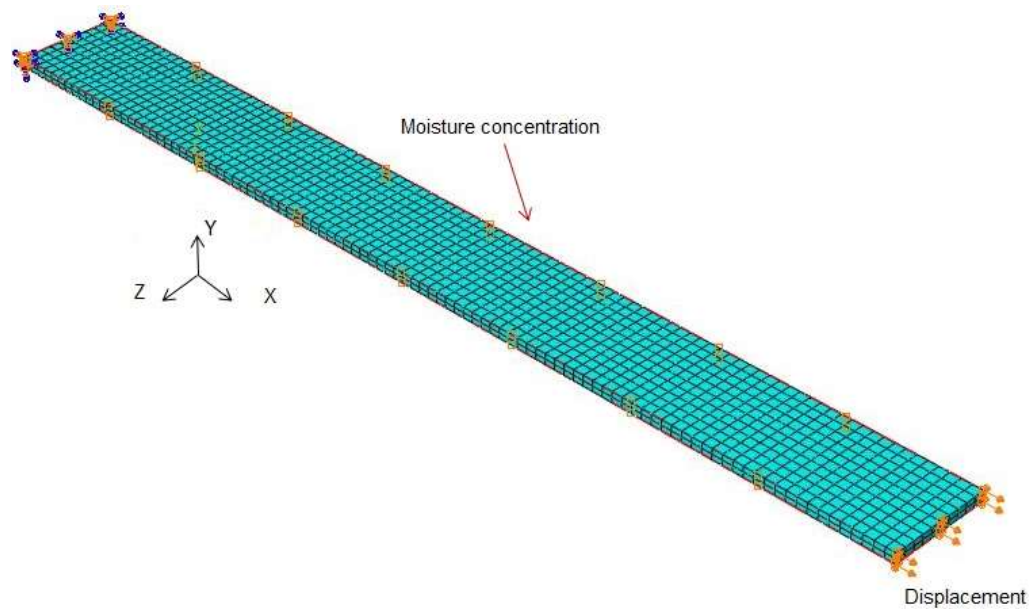


Figure 5-3 Mesh Bulk adhesive

The modulus (E) was predicted at each different moisture concentration (experimentally taken at each number of cycles), it was obtained from the curve stress-strain at different moisture concentration. Table 12 shows the E modulus predicted for the moisture concentration. A reduction in the elastic modulus can be seen along the increment of moisture. The analysis was limited to moisture concentration in saturation state (1.54 %). This concentration was defined for 168 hygrothermal cycles, based on experimental data, so for that reason the elasticity prediction was not performed beyond this time.

Table 12 Finite Elements results

NUMBER CYCLES	NUMBER OF WEEKS	Wt (%)	NUMERICAL E MODULUS (MPa)
0	0	0	3 000
42	2	1.49	2 432
84	4	1.51	2 422
168	8	1.54	2 414

The modulus (E) was predicted and experimental results and number of hygrothermal cycles were plotted in Figure 5-4. The modulus decreased linearly to 42 cycles, dropping to 19 % of the initial E modulus. Later, the reduction trend levelled off exhibiting slight changes reaching a value of 2414 MPa at the maximum moisture concentration.

The 3D numerical model results were compared with the experiment results. By contrast, in the experiments the modulus did not present variations after exposing the adhesive to hygrothermal cycles, as described in section 4.2.1.2. Nevertheless, elastic modulus degradation has been reported by other authors [95] and [97]; Sugiman, Crocombe and Aschroft [54] reported a reduction of 38 % after 1 year of immersion in water at 50 °C, and achieved a saturation of 5.5 Wt%. Additionally, Mubashar [70] studied the moisture cycling effects on adhesive properties. He found that major reduction occurred during the first absorption cycle and the trend of reduction was stabilised after 2 % wt of moisture concentration.

The elastic modulus predicted for the hygrothermal cycles was used in the degradation model of the SLJ to determine stiffness degradation of CZM.

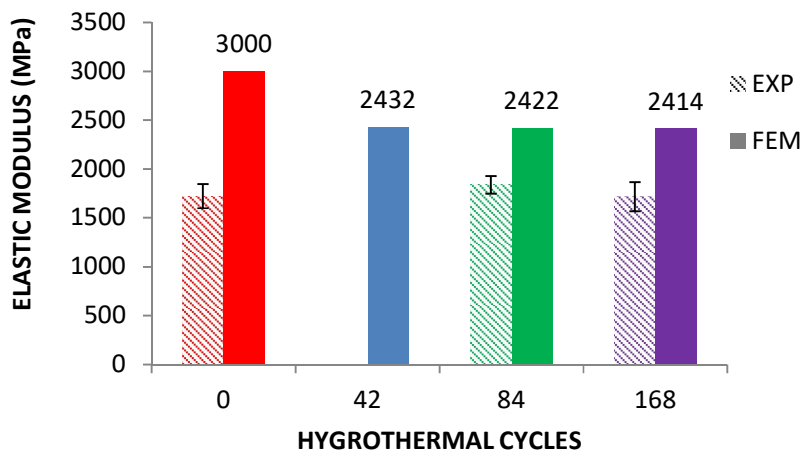


Figure 5-4 FM94 Elastic modulus experimental and numerical data, the value of 3000 MPa was set

5.1.2 Single Lap Joint model

The SLJ degradation was predicted using CZM to simulate the composite-adhesive interface mechanical response. To predict the damage in the SLJ exposed to environmental conditions the cohesive parameters were degraded based on numerical methods and experimental data. An empirical equation was defined from the lap shear experiments to calibrate the cohesive strength (tipping stress) in the model.

5.1.2.1 Geometry and boundary conditions

SLJ geometry configuration and boundary conditions are shown in Figure 5-5. To simulate the shear load test condition, one edge was fixed and the opposite edge was subjected to a tensile displacement load in X direction. The points A and B are reference points used to measure displacement variation, both experimentally using a laser extensometer, and numerically.

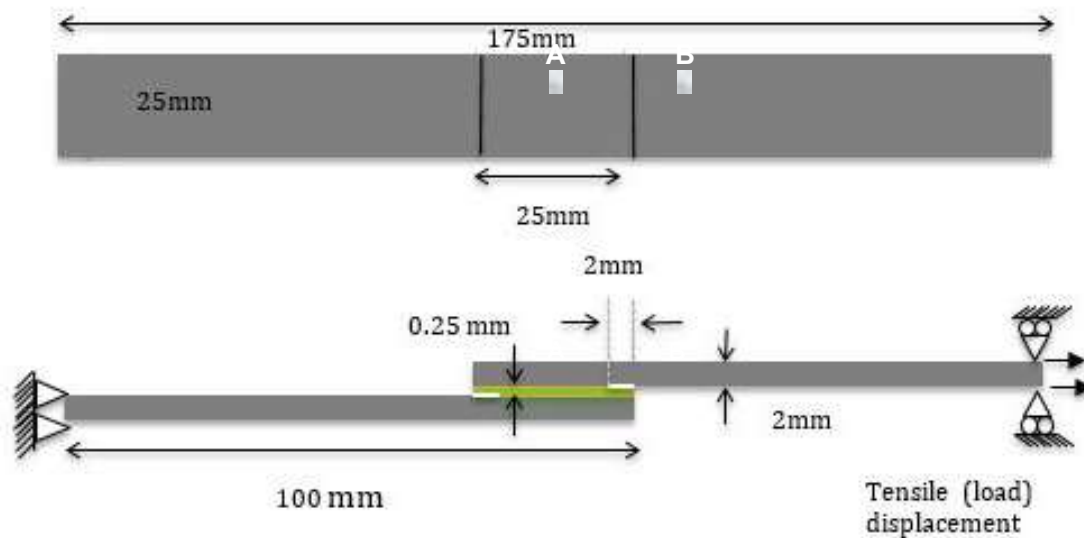


Figure 5-5 SLJ Configuration and boundary conditions

Composite adherends were simulated as an orthotropic material. Engineering constants were determined via a laminate analysis (NPL's composite design analysis CoDA) and results are shown in Table 13. Adherends were modelled using 3D continuum elements with reduced integration (C3D8R). Reduced

elements integration refers to a rule order less than the full rule used to integrate the element's internal forces and stiffness [124].

The adhesive was modelled using 3D cohesive elements layer (COH3D) to represent cohesive crack propagation path at the bond [125]. Two millimetres length were reduced at each end of bondline elements to simulate the crack initiators. A refined mesh was applied near to the overlap to achieve better accuracy with the smallest element size of 0.26 mm.

Table 13 Composite Laminate Properties T800/M21 [UD 0°/45°/90°/-45°]_s

PROPERTIES		VALUE
Elastic Modulus (MPa)	E1	50921
	E2	50921
	E3	9732
Poisson's ratio	v12	0.32
	v23=v13	0.36
Shear modulus (MPa)	G12	19326
	G13 =G23	3134

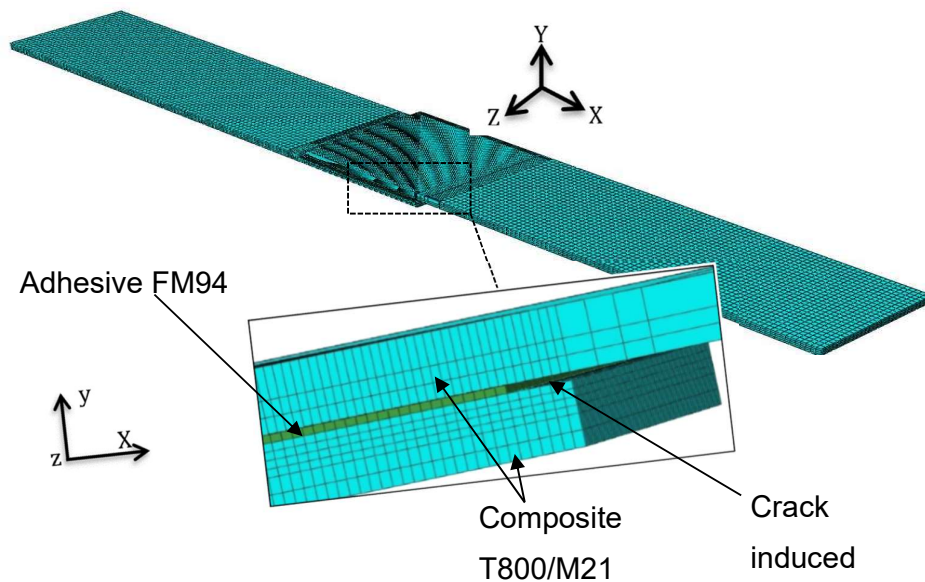


Figure 5-6 Meshing of the SLJ

The minimum number of elements were defined to satisfy the condition of a minimum of three elements in the length of cohesive zone (lc_z). The lc_z is the

value for the distance from the crack tip to the point where maximum cohesive traction occurs, refer to Figure 2-12. The values for l_{cz} for mode I and mode II were calculated following the equation (5-3), where E and G are tension and shear modulus respectively [126]. So, a maximum cohesive element size (l_e) of 0.26 mm was defined for this model.

$$l^I_{cz} = \frac{9\pi}{32} E \frac{G_{Ic}}{T_n^{0.2}} \text{ and } l^{II}_{cz} = \frac{9\pi}{32} G \frac{G_{IIc}}{T_s^{0.2}} \quad (5-3)$$

As discussed in section 2.6.3, the bi-linear law is shown to provide simplicity and adequate accuracy, being the configuration with less convergence difficulties with the SLJ modelling [84].

5.1.2.2 Damage Criterion

The CZM has three steps Figure 2-14: damage initiation criterion, a propagation governed by cohesion law and the stiffness degradation down to failure. At final failure, all elements are removed [70][127]

Damage initiation can adopt four criterions: maximum stress, maximum strain, quadratic stress, and a quadratic strain criterion. For this model, a quadratic nominal stress criterion (QUADS-in Abaqus) was adopted, as illustrated in equation(5-4) [126] [127].

$$\left\{ \frac{\langle T_n \rangle}{T_n^0} \right\}^2 + \left\{ \frac{T_s}{T_s^0} \right\}^2 + \left\{ \frac{T_t}{T_t^0} \right\}^2 = 1 \quad (5-4)$$

A QUADS criterion assumes that all stress directions are connected by a quadratic relationship. The values of T_n^0 , T_s^0 and T_t^0 traction represent the maximum permissible nominal stresses in normal, first and second shear directions respectively. T_n , T_s , and T_t are tractions in each direction and for any time increment. The McCauley bracket($\langle \dots \rangle$) affirms that the damage is not initiated by a purely normal compression stress or deformation [84], i.e if $T_n < 0$, $\langle T_n \rangle = 0$.

Fracture energy was chosen as damage evolutions criterion with a linear power behaviour as predicted by equation (5-5) [128].

$$\left(\frac{G_{IC}}{G_I}\right)^\alpha + \left(\frac{G_{IIC}}{G_{II}}\right)^\alpha = 1 \quad (5-5)$$

Where,

G_{IC} and G_{IIC} are work done by the traction in mode I and mode II respectively.

G_I and G_{II} are the critical fracture energy of the adhesive, and the empirical value of α was assumed to be one [129].

5.1.2.3 Cohesive Parameters

In this model the cohesive traction (T) and the cohesive fracture energy (Gc) are the major properties for achieving an accurate response [78]. To calibrate the parameters, the fracture energy was taken from experimental studies and the cohesive traction was calibrated via comparison of simulations and the experiment results[128].

The stiffness parameters (Kn and $Ks = Kt$) were obtained by dividing the Young's modulus (E) and Shear modulus (G) by the adhesive thickness [127][130], e.g. $Kn = \frac{E}{t}$; and $Kt = \frac{G}{t}$.

Values of $G_{IC}=1.7$ and $G_{IIC}=2.5$ N/mm have been reported by Zavatta [118]. They were adopted in this study. Some tests were carried out to identify the adequate cohesive traction for SLJ (under initial condition). The parameters used are shown in Table 14 described below.

Initially, values of $T_n^0=50$ MPa and $T_s^0=T_t^0=30$ MPa were chosen assuming that T_n^0 is equal to ultimate stress (σ_{ul}) as reported in the literature for FM94 [118]. Using that ultimate stress taken from literature a failure load of 8.4kN was predicted. The results overestimated the experimental data of 6.58 by 28 %.

Regarding the post-mortem evaluation shown in section 4.3.2, the failure mode was mainly adhesion failure, evidencing that the adhesive/adherend interface strength was less than that estimated. Consequently, the approach suggested by

Belnoue *et al.* (*adhesion failure approach*) [131], who modelled adhesion failure with CZM, was implemented and compared with the previous findings.

The approach consisted of a modification of the cohesive parameters based on the effective mode II properties when the interface is under through-thickness compressive stresses. The new strength ($T_s^{0'}$) and fracture toughness ($G_{II}'c$) for mode II were calculated using equations (5-6) and (5-7):

$$T_s^{0'} = T_s^0 + \eta(\sigma_{33}) \quad (5-6)$$

$$G_{II}'c = G_{IIc} \left(\frac{T_s^{0'}}{T_s^0} \right) \quad (5-7)$$

Where,

σ_{33} is the through-thickness stress, it is equal to the maximum traction in shear

η is an empirically derived analogous enhancement factor, with a value of 0.3 [131].

(T_s^0) mode I traction was assumed to be 50MPa and mode II traction to be 21MPa. The new fracture energy in mode II was reduced to 1.75 N/mm [131].

Table 14 CZM Calibration

CZM PARAMETERS						RESULTS			
COHESIVE						Stiffness		Failure load	
Kn	$Ks = Kt$	T_n	$T_s = T_t$	G_I	G_{cII}	FEM	Exp Avg	FEM	Exp Avg
(N/mm ³)		(MPa)		(N/mm)		(N/mm ³)		(kN)	
12000	4 444	50	30	1.7	2.5	71	56.6	8.44	6.58
		50	21	1.7	1.75	70		7.23	
		36	15	1.7	1.75	66		6.84	

The Figure 5-7 shows load-displacement curve for the SLJ unconditioned compared with the FEM results for $T_n = 50$ MPa with $T_s = 30$ MPa and $T_s = 21$ MPa

(adhesion failure approach). The change of displacement was measured in the overlap area, as evaluated in the lap shear test.

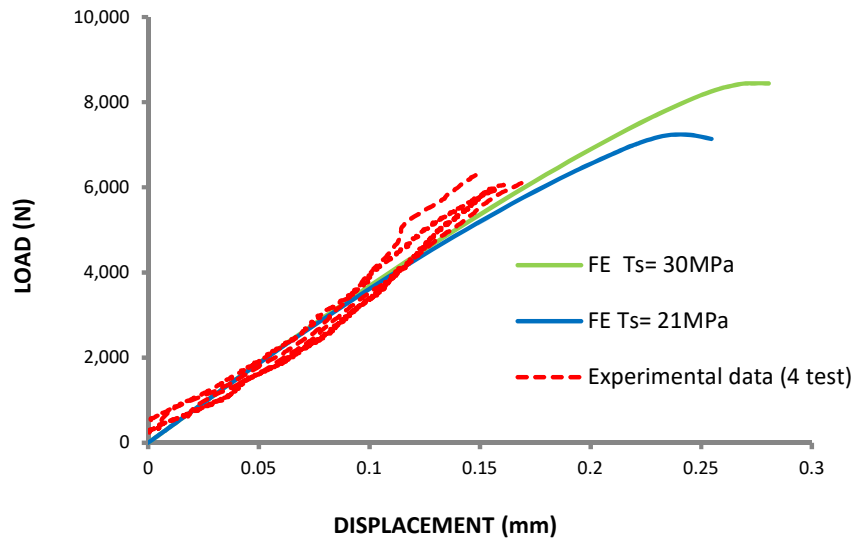


Figure 5-7 Comparative load-displacement SLJ behaviour using experimental and numerical data

Using the reduction proposed for adhesion failure ($T_s = 21$ MPa); the peak failure predicted was 7.2kN, hence a significant reduction of peak load was found by applying the reduction in shear strength and fracture energy. The failure load predicted was 9 % higher than the average experimental data. The maximum displacement did not show noticeable changes. Results are shown in Table 14.

Calibration of CZM parameters based on unaged bulk experiments were conducted for modelling adhesive bonded joints [130] [95]. Hence based on experimental data, the adhesive tensile strength of 36MPa (section 4.2.2) was used as T_n^0 . Maximum traction in mode II (T_s^0) was calculated considering the ratio of (50/30) taken from theoretical data. The traction mode II ($T_s^{0'}$) -adhesion failure approach- was obtained from the (T_s^0), as described earlier.

Figure 5-8 shows load-displacement experimental and numerical curves for unconditioned joints. The model predicted a failure load of 6.8kN for unconditioned joints, in full agreement with the actual data i.e. 3.8 % greater than the average experimental peak load.

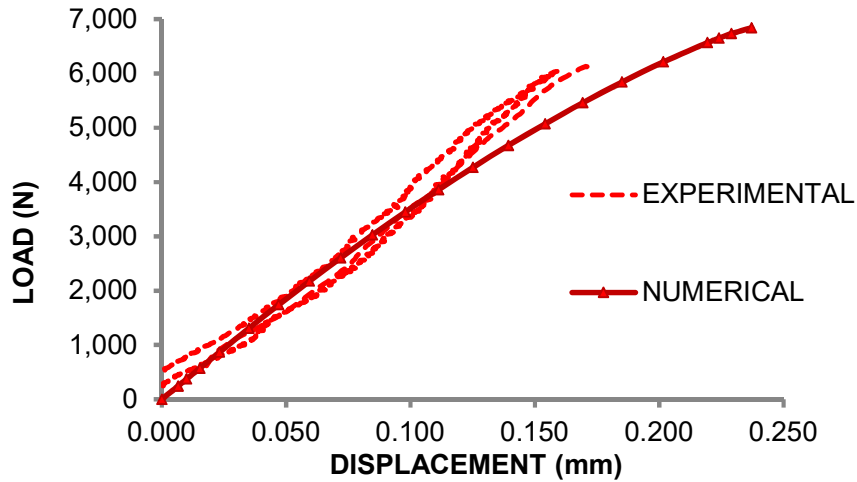


Figure 5-8 Load-displacement behaviour of unconditioned SLJ

The initial stiffness predicted was also in close agreement, only marginally higher than the stiffness in the experiments. The maximum displacement achieved was 0.24 mm, larger than the experimental displacement average (0.16 mm). Results can be seen in Table 15.

Table 15 Load-displacement results validation unaged SLJ

CONDITION	STIFFNESS		FAILURE LOAD		DISPLACEMENT	
	FEM	Exp	FEM	Exp Avg.	FEM	Exp Avg
Hygrothermal Cycles	(N/mm ³)		(kN)		(mm)	
0	68.71	54.40	6.84	6.58	0.24	0.16

Figure 5-9 illustrates the damage evolution in different stages of the deformation process during tensile loading. The legend shows the damage variable (SDEG-Abaqus) contours. The material point (element) is considered undamaged when SDEG is equal to 0, and fully damaged when the value is equal to 1. The adhesive layer prior to damage is shown in Figure 5-9 (a), the damage initiated in the middle of one end of the overlap and the growth progressed in $\pm Z$ direction until reaching the edges, as shown in Figure 5-9 (b). Later, a second crack initiated at the opposite end and both cracks propagated in direction X, as seen in Figure 5-9(c). The failure occurred when both cracks met in the middle of the overlap, as shown in Figure 5-9 (d).

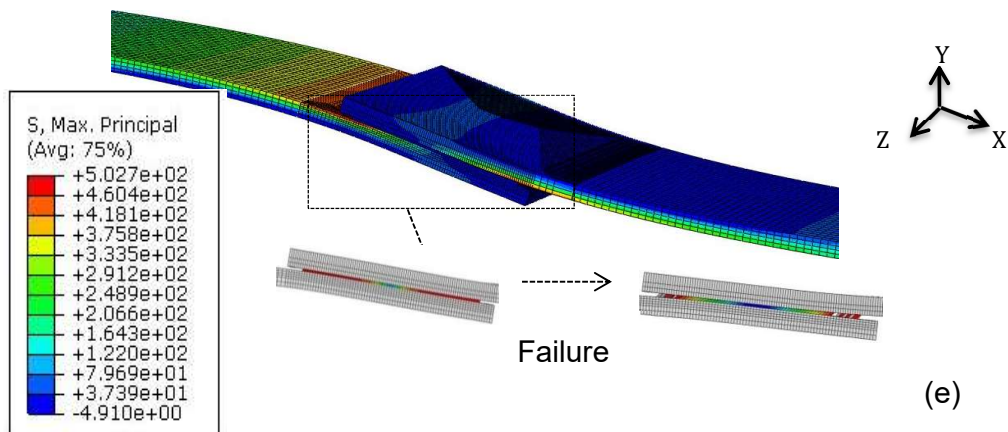
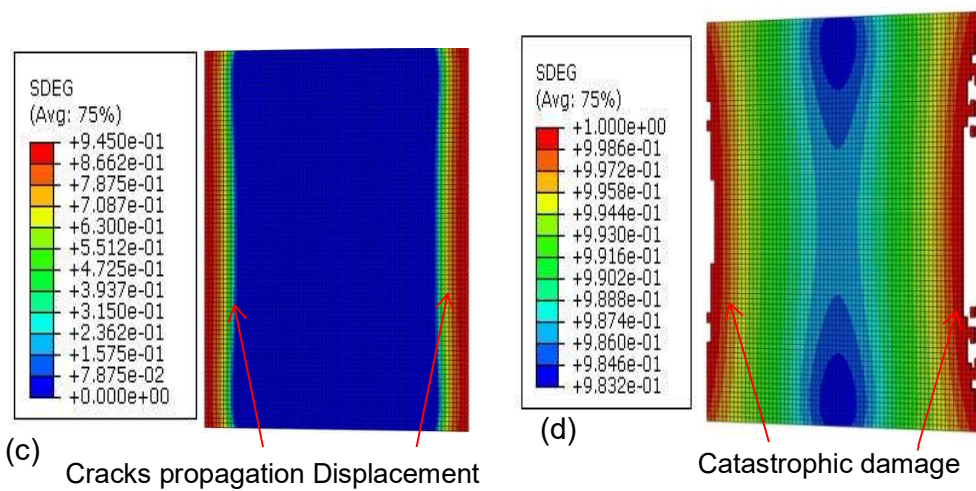
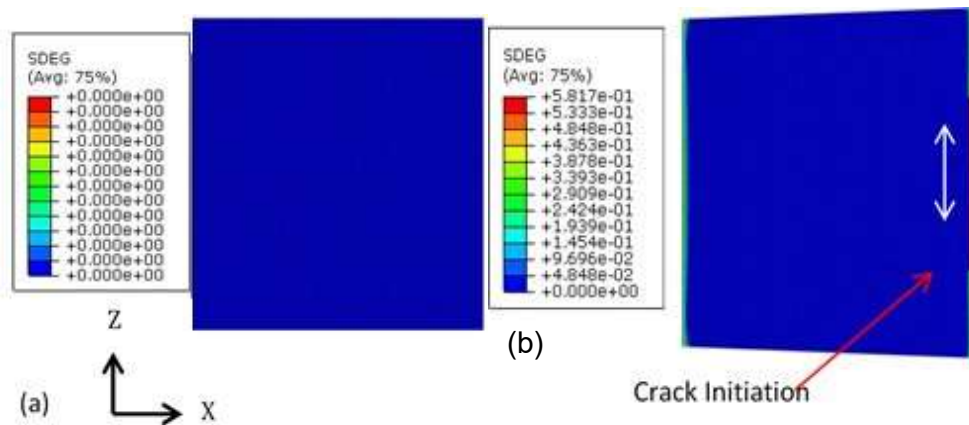


Figure 5-9 Failure process in SLJ (a) before damage,(b)crack initiation,(c) crack propagation, (d)Full damage

The maximum stress principal distribution in the SLJ is shown in Figure 5-9 (e). The highest stress concentrations occurred in the substrates near to overlap edge. Peel and shear stresses achieved their maximum value. Additionally, damage variation before and after failure are highlighted.

5.1.2.4 Degradation parameters

Single lap joint ageing under hygrothermal cycles and load were modelled using CZM to predict damage caused by the degradation. The numerical model of the bulk adhesive was carried out to predict the elastic modulus degraded as a function of the moisture cycles. Based on the SLJ test results, an empirical equation was defined to identify the cohesive traction degradation in mode I.

The bilinear traction-separation law is illustrated in Figure 5-10. The tipping traction (T°) is the maximum traction before damage initiates. The critical value of displacement δ° refers to the damage initiation and δ_f refers to the displacement at ultimate failure. The stiffness before damage in the elastic regime is K , the slope of the curve. The area under the curve gives the fracture energy (G_c).

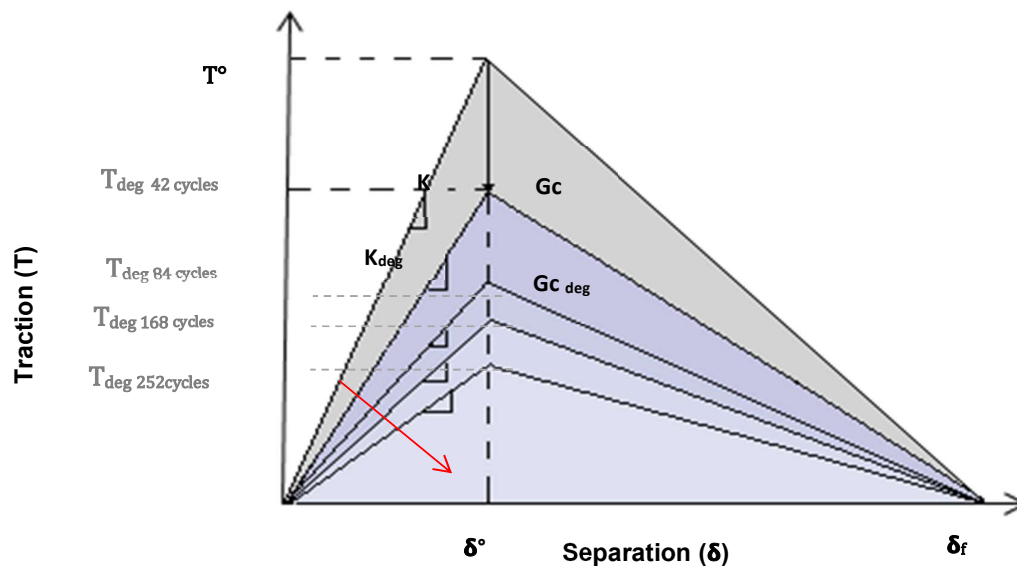


Figure 5-10 schematic degradation process for bilinear traction-separation curve

The degraded stiffness, K_{deg} for each number of cycles was obtained by dividing the E numerical modulus of adhesive bulk results by the adhesive thicknesses, e.g. $K_{deg} = \frac{E_{deg}}{t}$.

To determine the degraded traction as a function of the hygrothermal cycles, the gradient of reduction (from the lap shear strength results) was used as a factor of degradation. Hence, the empirical equation (5-8) was defined to predict the traction in tension (T_n^{Deg}) as function of number of cycles (h).

$$T_n^{Deg} = T_n^0 (2e^{-6} h^2 - 0.0018h + 0.8626) \quad (5-8)$$

As fracture energies were reduced proportionally to the cohesive strength reduction, then the fracture energy mode I was obtained using the equation (5-9), where the δ^f calculated for unconditioned state remained constant for all ageing conditions.

$$G_{Ic}^{deg} = \frac{T_n^{deg}}{\delta^f} \quad (5-9)$$

As was defined earlier, a cohesive strength of 36MPa was identified as tipping traction in mode I for non-conditioned state. The procedure to calculate the parameters in case of adhesion failure was followed. Table 16 summarises the CZM parameters for ageing SLJ.

Table 16 Properties of aged adhesive and cohesive used in the CZM of SLJ

Hygrothermal Cycles	ADHESIVE		COHESIVE				G_{Ic}	G_{II}
	E (MPa)	Kn (N/mm ³)	Ks=Kt (N/mm ³)	T_n (MPa)	$T_s = T_t$ (MPa)	(N/mm)		
0	3000	12000	4444	36	15	1.7	1.75	
42	2432	9728	3602	28	12	1.32	1.36	
84	2422	9688	3588	26	11	1.23	1.26	
168	2414	9656	3576	22	9	1.04	1.07	
252	2414	9656	3576	19	8	0.9	0.92	
714	2414	9656	3576	21	8.8	0.99	1.02	

5.1.2.5 Model validation

The calibrated parameters were applied to predict the SLJ exposed to hygrothermal cycles. The 3D model was validated with the experimental results. The predicted and experimental failure load for SLJ ageing under hygrothermal cycles are shown in Figure 5-11. The error bars refer to the standard deviation calculated for each data of cycles.

The variation of the static strength of SLJ, exposed to hygrothermal conditions, demonstrated strength degradation with the increase in the number of cycles. The strength decreased noticeably in the first 42 cycles. Then a gradual reduction continued until 252 cycles reaching a failure load of 4.02 kN. Later, the joint strength rose marginally at 714 cycles. Table 17 summarises the experimental and numerical results.

The failure load for zero cycles was slightly over predicted, being within the standard deviation of the experimental results (4 %). The numerical stiffness was found to be around 20 % higher than the experimental joint stiffness. Likewise, the displacement predicted was about 50 % greater than the measured failure displacement average.

Additionally, displacement was measured between the points A and B, refer to section 5.1.2.1, as measured during experimental testing. This analysis provides a comparison of variation in displacement over the bonded area. Each adherend has a single point attached and the initial distance between pints is 12 mm.

At 42 cycles the maximum predicted load was 5.59kN, an over-prediction of almost 13 %. The displacement predicted was 0.19 mm, 21 % greater than the experiments. The numerical stiffness was 23 % higher than the experiments.

At 84 cycles, the overprediction of the failure load was at its highest: 5.27kN. Likewise, the stiffness was 29 % above the experimental results. While the displacement was well predicted with a value of 0.18 mm.

At 168 and 252 cycles, the model closely predicted the failure load and the displacement with 1 % being the difference between the experiments and the

numerical value. Nevertheless, the predicted stiffness maintained a difference of 20 % with the results of the test. Finally, the prediction for 714 cycles was greater by 13 % for both the maximum load and displacement.

Figure 5-12 shows the load against displacement curves for numerical and experimental results. It is noted that the model is capable of predicting the degradation of the joint strength. In summarizing, the prediction showed closer alignment with the results as the cycles increased. However, the observed experimental strength reduction at 714 cycles was not predicted by the model. The empirical equation, defined to predict the normal degraded traction was influenced by the errors within the experimental results.

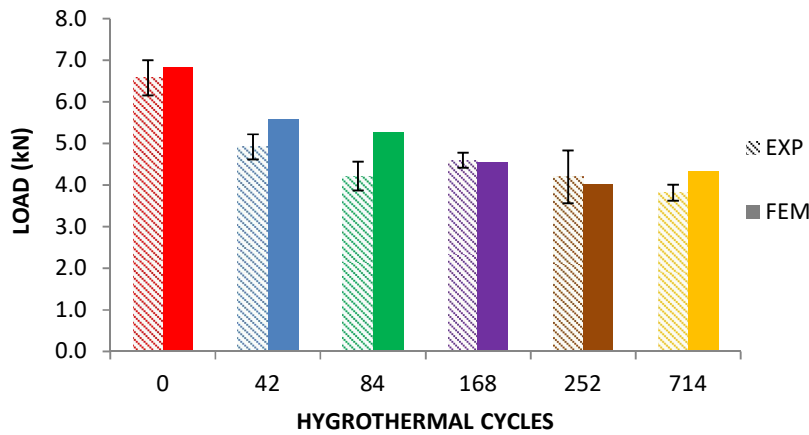


Figure 5-11 Variation Strength of SLJ

Table 17 Comparison static response SLJ under hygrothermal ageing conditions

CONDITION	STIFFNESS		FAILURE LOAD		DISPLACEMENT	
	FEM	Exp	FEM	Exp Avg.	FEM	Exp Avg
Hygrothermal Cycles	(N/mm ³)		(kN)		(mm)	
0	68.71	54.40	6.84	6.58	0.24	0.16
42	67.05	54.20	5.59	4.92	0.19	0.15
84	66.46	51.23	5.27	4.22	0.18	0.16
168	65.47	57.22	4.56	4.60	0.16	1.14
252	64.44	52.29	4.02	4.20	0.15	0.15
714	64.5	52.16	4.34	3.82	0.15	0.13

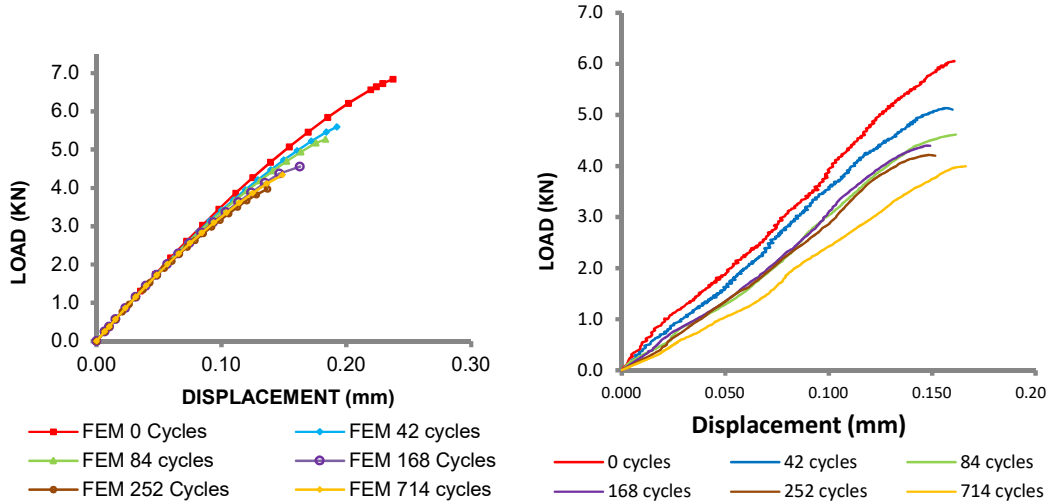


Figure 5-12 Numerical and experimental load-displacement curves FM94

5.2 Summary

A coupled analysis (experimental-numerical) was implemented to model the mechanical behaviour and to predict the failure load of the adhesive SLJ aged (under hygrothermal cycles). Firstly, the adhesive degraded E modulus was determined using a moisture-diffusion displacement analysis, and after a cohesive zone model (set with the degraded parameters) was carried out to predict the damage for each number of hygrothermal cycles.

In the case of the moisture diffusion-displacement analysis, the moisture concentration value (wt %) for each hygrothermal cycle, taken from the experimental data (section 4.2.1), was assumed as the maximum moisture concentration and homogeneously distributed in the adhesive. The degraded modulus was used to calculate the degraded stiffness.

The degradation of the traction separation parameters i.e, traction and fracture energy were calibrated based on an empirical equation defined from the lap shear experimental results.

The degradation modelling focused on the degraded properties of the adhesive/adherend interface, the cohesive parameters (traction and fracture energy) were reduced as the degradation rate showed in the joints after the

hygrothermal cycles. Hence, the cohesive traction (for each one of hygrothermal cycles) was calculated using an empirical equation and these values then became the parameter in the CZM. The predicted static strength showed a very good correlation with the experimental data.

6 DISCUSSION

6.1 Introduction

The aim of this work was to evaluate the structural strength of the bonded joints exposed to temperature and moisture cycles and load. Mechanical tests were performed to determine the static response of bulk adhesive and the static and fatigue response of single lap joints after the hygrothermal cycles (ageing). The mechanical test results that were presented in chapter 4 are discussed in this section. A novel approach for prediction of the strength degradation was presented in chapter 5.

6.2 Moisture absorption

Moisture diffusion in both FM94 bulk and composite T800/M21 exposed to the hygrothermal cycles have been fitted to a Fick's second Law behaviour equation. Table 18 summarises moisture diffusion properties found in the literature and the experiments taken from this study.

Fick's Law is the main model used to describe the moisture absorption in adhesives, as seen in Table 18. Principally, alternative studies have focused on the absorption properties under static conditions (humidity and temperature).

Nevertheless, Fick's behaviour has not always been reported for epoxy adhesives as mentioned in section 2.6.2. A Dual Fick model predicted the absorption diffusion of FM73 bulk adhesive exposed to absorption-desorption cycles at two different temperatures (immersed in water at 50 °C and 70 °C), demonstrating a closer alignment than Fick's second Law for absorption [70].

As previously mentioned in section 3.3.1, both FM73 and FM94 are manufactured by Cytec; FM94 shows better performance at high temperature than FM73 [103].

Comparing the experimental results of the FM94 with the absorption at dynamic conditions as reported by Mubashar (absorption-desorption cycles at 50 °C)[70], the rate of diffusion of the FM94 (under the hygrothermal cycles) was higher than that of FM73, but the maximum moisture content of FM94 was 13 % smaller than FM73. These differences of diffusion and saturation agree with [116], who affirms

that the amount of time necessary to reach the saturation depends on the temperature, but the moisture saturation is only driven by the surrounding humidity.

Table 18 Comparison of moisture diffusion properties found for FM94 with other results reported

AUTHORS	MATERIAL	EXPOSE CONDITION	Dh (m²/s)	Mm (%)	MODEL
Aschcroft et al. (2003)	Film Adhesive	Humid environment 90°C/97 % RH	7.20E-12	1.50	Fick's
Wahab et al. (2002)	FM73	Immersion water at 60°C	1.5-2E-13		Fick's
Crocombe et al. (2006)	AV119	Humid environment 50°C/ 81.2 %RH	3.85E-13	3.06	Fick's
Liljedahl (2006)	FM73	Humid environment 70°C/79.5 % RH	7.90E-12	1.20	Fick's
Mubashar (2010)[70]	FM73	Immersion water at 50°C (cycles absorption and desorption)	9.72E-13 4.75E-14	1.78 1.78	Dual
Liu (2016)	SY14	Immersion water (60 h) at 90°C	6.28E-12	6.77	Fick's
Experimental results	FM94	Hygrothermal cycles (70°C 85 %RH and -20°C/0 %RH), gravimetric test after removing at hot wet conditions	1.52E-12	1.54	Fick's

On the other hand, comparing FM94 results of absorption with the results reported by Liljedahl (FM73 exposed to 70°C/79.5 % RH) [48], it was noted that the diffusion coefficient was five times slower, and the maximum moisture content achieved was slightly higher than FM73.

This indicated that the diffusion into FM94 was affected by the dynamic conditions which can reduce the rate of diffusion [76]; and therefore cooling after saturation can lead to more water absorption [60].

The analysis is confirmation that under the hygrothermal cycles studied, either temperature or surrounding relative humidity influences the maximum moisture

content in the adhesive FM94. This coincides with the results presented by Mubashar [70] who found that the temperature increased the diffusivity and the saturated moisture content.

In the case of CFRP, some moisture diffusion properties reported for CFRP laminated are summarised in Table 19. The diffusion coefficient obtained for T800/M21UD was in agreement with results for CFRP found in the literature. The moisture absorption in CFRP may also be studied considering the anisotropy of the material. With this approach, the diffusion in the direction of the fibre and transverse to the fibre, as presented by Liu et al and Liljedahl, was determined [132][48].

Table 19 Comparison of moisture diffusion properties found for CFRP T800/M21, together with other results reported

AUTHORS	MATERIAL	EXPOSE CONDITION	Dh (m ² /s)	Mm (%)	MODEL
Aschcroft et al (2003) [94]	CFRP UD	Humid environment 90°C and 97 %RH	7.90E-12	0.8	Fick's
Liljedahl (2006) [48]	IM7/8552	Humid environment 70°C and 79.5 %RH	1.40E-12 5.00E-13	PF TF	0.8 Fick's
Liu et al (2016) [97]	CFRP T800/5228E	Immersion water (60 h) 90°C	5.60E-13 2.90E-13	PF TF	1.5 Fick's
Guermazi et al (2015)[45]	CF G814	Immersion water 70°C	4.85E-13	1.55	Fick's
Experimental results	CFRP T800/M21 UD	Hygrothermal cycles (70°C and 85 %RH / - 20°C) Removed at hot wet condition (70°C and 85 %RH) for gravimetric test	4.69E-13	0.68	Fick's

PF Parallel to Fibre
TF Transverse to Fibre

The highest diffusion was identified by Ashcroft, Wahab and Crocombe [94] for CFRP UD at 90°C and 97 % RH of 7.20 E-12 m²/s; as discussed earlier the temperature leads directly to the rate of diffusion. Nevertheless, the difference of maximum moisture content compared with T800/M21 (subject to hygrothermal cycles) was only 0.12 %.

The moisture content found for T800/5228E [97] and for CF G814 [45] is significantly higher, and may be caused by the greater thickness (3.2 mm and 4 mm) because the maximum content increases proportional to laminate thickness [46].

In general, the fibre reinforced composites are capable of absorbing relatively small amounts of water, the maximum content of the majority of CFRP (2 mm thickness) does not exceed 1 %.

A study of T300 graphite/epoxy composite immersed in water at 25°C, 60°C and 80°C, demonstrated that at 25°C and 60°C, moisture absorption showed a Fick's diffusion behaviour. However, at 80°C diffusion occurred with non-Fick's behaviour. This being attributed to the high temperature, since it increases the molecular chain relaxation decreasing the T_g and bonding strength, so the water flows into the space more easily [46].

The moisture absorption found for T800/M21 (2mm thickness) under hygrothermal cycles was compared with the moisture absorption of carbon-epoxy G814 (4 mm thickness) exposed to water at 24 °C, 70 °C and 90 °C as reported by Guerhazi *et al.*, (2015), seen in Figure 6-1. Analysing Figure 6-1, it can be stated that the maximum moisture content and the diffusion rate of the CFRP G814 increases with temperature. Second, the absorption diffusion and moisture content determined for T800/M21 (under hygrothermal cycles) is lower compared with the diffusion of G814 (immersed in water at 70°C), the reduction can be attributed to the differences in thickness and the effect of cyclic conditions (temperature/moisture) suffered by T800/M21.

In conclusion, the lower diffusivity shown by T800/M21 compared with the G814 & IM7/8552 can be due to the polymer relaxation caused by the changes in humidity and moisture concentration [47].

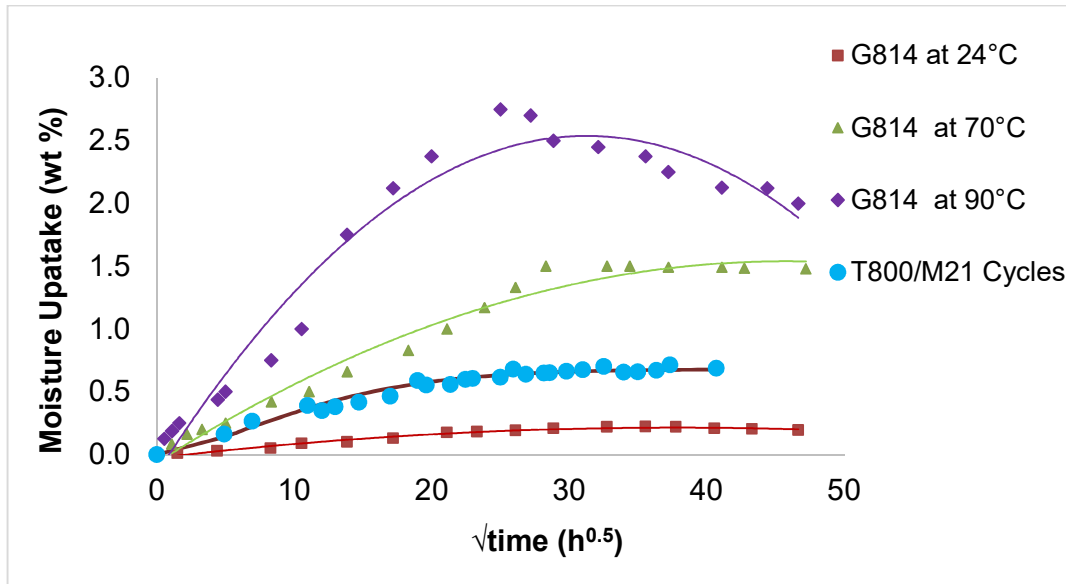


Figure 6-1 Moisture absorption CFRP G814 (4 mm thickness) exposed to water at different temperatures reported by [45] and T800/M21 (2mm thickness) exposed to hygrothermal cycles

Faced with the analysis of swelling and desorption results, it can be stated that the FM94 or the T800/M21 exposed to hygrothermal cycles did not show a molecular chemical interaction and the main absorption occurred through diffusion into the free volume. This is supported by the statement that any gain of volume in the adhesive depends on the chemical structure of the polymer, the amount of water within it and the interaction between both [32].

Modes of water ingress into the joint occur in the following ways: travel through the adhesive, travel along the adhesive/adherend interface, or by capillary action through crack and crazes in the adhesive, or by diffusing into the adherend [76]. The moisture permeability of the CFRP allows a shorter moisture path through the interface adhesive/adherend [133]. Hence, the moisture diffusion is faster through the interface adhesive/adherend than through the adhesive.

6.3 Moisture effect adhesive mechanical properties

According to these results (section 4.2.5, p85-87), moisture uptake during the hygrothermal cycles apparently does not affect the mechanical properties of the

FM94. However, as was discussed in section 2.4.1 the moisture ingress in the bulk adhesive may cause changes of the strength, stiffness and strain [119].

The results are different from the results reported for FM73 bulk adhesive samples by Sugiman, Crocombe and Aschroft, [54] who reported a degradation of 38 % of tensile strength and 24 % of E modulus, after immersion in water at 50°C over two years with 5.5 wt% moisture absorption. Mubashar [70] reported for the same adhesive a reduction by 39 % tensile stress and 37 % E modulus, after moisture cycles at 70°C and a moisture uptake of 2.5 wt%. Han et al., [95] found a reduction of E modulus by 15 % for FM73, after immersion in water at 50°C, showing a moisture content of 3.75 %.

According to Cytec, FM94 offers high moisture resistance and a better performance at high temperatures than FM73 [103]. Hence, the lack of strength degradation of the FM94 exposed to hygrothermal cycles may be influenced by low affinity of this polymer with the water [47].

However, the moisture content reached by FM94 after the hygrothermal cycles (1.54 wt%) should cause an effect in the plasticity due to the hygrothermal history [134]. Hence, other factors could affect the results, such as the high amount of voids in the bulk adhesive samples (as mentioned in section 3.3.1) and the freezing cycles. The voids could attract a significant amount of water and avoid the interaction between moisture with the polymer molecules.

The effect of freeze-thaw cycles was studied in two adhesive epoxies (Sikadur 330 and Sikadur 30 [58]. After exposure at 38°C and 100 %RH for 8h followed by freezing at -18°C for 16h, there was evidence of differences in the mechanical responses. Sikadur 330 and Sikadur 30 showed a reduction of elastic modulus by 19 % and 14 % respectively. But, in the case of tensile strength Sikadur 30 did not show any important changes.

Therefore, the effect of cycles at low temperature on the mechanical properties of the FM94 should be more vigorously studied in the future.

6.4 Mechanical test results

6.4.1 Lap Shear Test

As was mentioned in section 4.3.1, the maximum strength expected for unconditioned joint was 13.8 KN, but the joint only had a strength of 6.58 KN. The reduced strength can be accounted for by the inclusion of tip crack initiator and voids in the bondline.

The crack initiators of PTFE films were included in the bond area to try and provide consistent failure results. However, they avoided the effect of the fillet, causing an increment of the peel stress and reducing the joint strength [135].

Compared to the work by Bhanushali, Ayre and Nezhad [136], who evaluated SLJ of T800/M21 bonded with FM94, peel ply surface preparation and 25mm X 25 mm overlap, the joints with tip crack were 61 % weaker than joints without crack initiators.

The visual inspection showed a high number of voids in the bondline previous to the ageing, refer to section 4.3.2.1. Pre-bond trapped moisture in the adhesive combined with a vacuum bag curing can lead to void formation and cause an important effect on the bond strength [137]. According to MIL-HDBK-17 [19] a level of 0.2 % pre-bond moisture in the material can lead to a strength reduction by as much as 80 %.

The pre-bond moisture can be caused by first the hygroscopic nature of the adhesive films, as the moisture can be absorbed before use (condensation during thaw when removed from the freezer) and second the moisture can be absorbed by the T800/M21 laminate before bonding [138]. Although the laminates were dried before bonding, the drying may not have been sufficient to remove the trapped moisture.

Other causes of low failure strength of the joints can be the surface preparation mode, the literature indicates that the surface preparation treatment affects the bond strength. The use of peel ply has shown in preliminary studies to offer a

smaller bond strength compared with grit blasting and plasma treatment in bonded joints without ageing [34], [35].

The cycles of moisture and temperature in the adhesive joints, employed in this study, resulted in a degradation of the mechanical properties. The bond strength decreased with the number of exposed cycles. The main strength degradation was achieved during the first 42 cycles of ageing (2 weeks), then the gradient of reduction tended to level off. This polynomial behaviour has also been observed by other authors and attributed to saturation of moisture in the adhesive [95], [26], [54].

A long-term exposure is needed to reduce strength under hygrothermal static ageing; composite SLJ joints exposed to 82°C and 85 %RH over 2 years were mechanically degraded by 30 % and changed the failure mode [26]. Aluminium single lap joints bonded with FM73 and immersed in water at 50°C were degraded by 22.1 % strength after one year of exposure [54].

The hygrothermal cycles caused higher impact in the joint strength (about 40 % reduction at 8 weeks) than ageing under static hot-wet conditions as expected and mentioned in section 2.4.2. Thermal cycling of the sample containing 'trapped' water molecules acts to accelerate any degradation process. However, the mechanism for this observed degradation is not yet fully understood.

Additionally, studies have shown that under cold conditions, the bond degradation does not always act in the same form [51]; Agarwal et al., [58] tested steel-CFRP joints bonded with two different epoxy adhesives (Sikadur 330 and Sikadur 30), reporting strength reduction of 27.5 % and 18 % respectively, after 40 freeze-thaw cycles (6 weeks of cycles); in the case of Sikadur 30 the degradation didn't level off. Hu et al., [27] reported 5.61 % strength degradation of a CFRP-steel SLJ, conditioned under temperature cycles (maximum 80°C and minimum temperature -40°C) and 20 %RH for 28 days. Whereas, Kim in [58] reported an increase of 36 % after freeze-thaw cycles, attributed to additional curing of the epoxy adhesive in moisture conditioning and contrasted with the stiffness degradation.

Regarding the non-affected FM94 bulk adhesive properties after the hygrothermal cycles, discussed before; the lap joint results indicate that the main degradation occurred in the adhesive/adherend interface rather than the adhesive. Moreover, the interfacial failure mode (evidenced by broken joints) confirms the weakness of the composite/ adhesive interface. As stated by Parker [53] for bonded joints, with a tendency towards interfacial failure mode, that the composite/adhesive interface may be weakened by the exposure to moisture.

These findings are contrary to the findings of Baena and da Silva [44], who argue that in epoxy/FRP composite interface the thermodynamic work of adhesion remains positive after ageing in water, reducing the probability of interfacial failure.

Under the hygrothermal cycle, the adhesive/adherend interface degradation could have been affected by the expansion of any water present (at low temperature stage) inside the bondline, this in turn can cause cracks and voids that lead to more moisture absorption and which then causes plasticization and debonding, as suggested by [59]. As illustrated in Figure 4-22 the plasticity increased with the number of cycles.

Although the plasticity behaviour was observed (see Figure 4-22), the effect of hygrothermal cycles in the strain was not clearly evidenced as expected [63], probably because the strain monitoring was not accurate enough. Moreover, the low strain effect might be due to the stress concentration caused by the voids that reduce the resistance to the crack propagation and also the presence of the crack initiators.

6.4.2 Fatigue test

The static strength and the fatigue life of the composite bonded joint were reduced as hygrothermal cycles increased. But, the static strength remained nearly constant after 168 hygrothermal ageing cycles, whereas the fatigue life continues its deterioration.

The hygrothermal cycling effect increases with the load level, as can be seen at 45 % quasi-static strength, the joint life time is reduced by a factor of roughly 1000

compared with unaged joint, reference Figure 4-23 . Also, the ‘safe-life’ can be identified at 30 % static strength load and no further than one million fatigue cycles.

The results coincide with the reduction of fatigue reported by [50], who tested adhesive joints aged under static hygrothermal conditions. In the same way, Ferreira et al. evaluated the fatigue life of glass fibre reinforced bonded joints, after exposure to static hygrothermal conditions (immersed water at 20°C, 40 °C and 70 °C), finding that the reduction of the number of cycles is greater and faster at higher temperature, as seen Figure 6-2 [139].

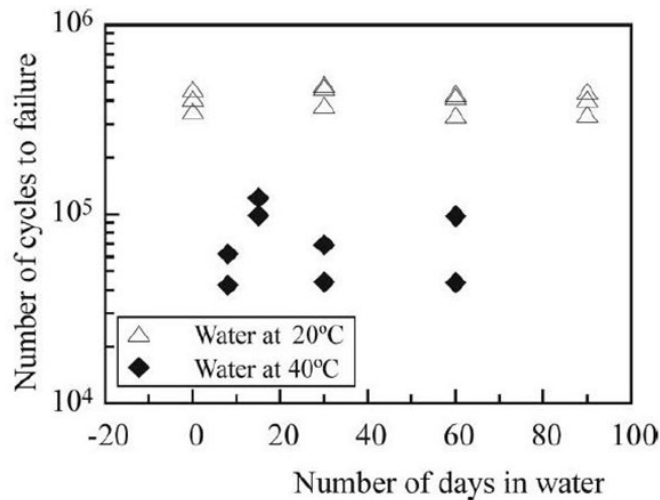


Figure 6-2 Influence of water and Temperature on fatigue life for a fixed stress range of 4.7 MPa [139]

Similarly, Abdo and Aglan [64] reported a reduction of 47 % of the joint lifetime after 6 weeks of hygrothermal cycles condition. As with the present study, joints subjected to temperature and humidity cyclic conditions were similarly affected by the combined effect of temperature/humidity, as well as a hygrothermal expansion phenomenon that aggravated the harsh conditions.

The fatigue cycles suffered by a joint of any aircraft must be obtained by data collection or through computer algorithms. However, assuming that the joint is part of the lower wing root panel of a transport aircraft [140], one hour flight in average is equivalent to 100 load cycles. Hence, the SLJ life was reduced from

10.000 flight hours to 10 flight hours, after 336 hygrothermal cycles at 40 % quasi-static strength, refer to Figure 4-23.

Not many studies have shown fatigue studies of composite bonded joints, and the effect on fatigue life. Although, findings have revealed that the durability of the joint has decreased with the hygrothermal cyclic attack, further evaluation of crack growth and strain variation caused by the thermal cycle is needed.

6.5 Non-destructive Inspection of adhesive bonded joints

A high amount of voids were identified in the bondline of the joints. These voids in the adhesive bond can result from the evolution of gases during the heat curing. The gases have three main sources: volatiles presents in the bond process, water absorbed by the adhesive and water absorbed by the adhered [137]. Also, FM94 has been found to have a tendency to produce more voids than FM73 [117].

Using vacuum bag curing could have increased the size and number of voids because the lower pressure achieved (compared to autoclave) was unable to dissolve the bubbles and the volatiles, which remained trapped in the adhesive [137], [141]. However, voids have also been shown in the bondline of composite bonded joints cured in an autoclave [26].

The joint manufacture in the autoclave is not always possible, especially when the repairs are made in-situ; as such the quality of bond needs to be monitored as processes are developed to minimise defects and voids in the joint [6].

Ultrasonic inspection showed indications of the bond quality, some zones with lack of adhesion were detected pre-ageing. After the hygrothermal cycles, the defects were greater; however, these results need therefore to be interpreted with caution because the inspection is dependent on the competence and skill of the technician, and the difficulties in calibration for each specimen (thickness variations causing uncertainty).

6.6 Degradation Modelling

As mentioned in the literature review, moisture-diffusion analysis has been performed by other authors to identify the moisture ingress process along the

bondline [96] [142]. Therefore, using the moisture concentration distribution, a simultaneous stress-diffusion analysis is performed for each element to define the moisture-stress dependence on each one.

The present study differs from previous research in that a moisture concentration value was assumed as homogeneous distribution throughout the adhesive layer, at each hygrothermal cycle. The maximum moisture found experimentally was assumed as the maximum concentration for each hygrothermal cycle which means the moisture may be higher than the real condition. In such a way the degraded E modulus could be over predicted.

The results of the bulk adhesive moisture-diffusion displacement analysis showed a reduction on the E modulus by 20 % after 42 hygrothermal cycles (1.49 % moisture content), and with the increment of moisture the elasticity remained nearly constant until saturation (1.54 % moisture content). These findings, contrary to the FM94 tensile experimental results are consistent with other researchers [143], [70] and with the plasticity variation observed in the joints post failure evaluation. For that reason, the E degraded values were used to calculate the joint stiffness degraded as a parameter in the CZM.

To calibrate the SLJ model, an unaged joint CZM was performed in order to simulate the progressive interfacial failure. The cohesive parameters were modified on mode II to promote the adherend/adhesive interface strength reduction. Additionally, a mechanical damage in the form of induced crack initiators was included in the cohesive elements to simulate the SLJ test conditions. The outcomes showed good correlation with the experiments predicting the unaged joint strength with an error of 4%, and damage propagation as shown in Figure 5-8 and Figure 5-9.

However, the predicted unaged joint stiffness had an error of 20% compared with the experiments, this may occur due to the fact that the E modulus employed was reported in the literature and was found to be higher than that viewed in the experiments, as mentioned in section 4.2.5.

The prediction of the degraded strength was accurate and kept within the margin of standard deviation up to 252 cycles. Nonetheless, at 714 hygrothermal cycles the model over predicted the strength by an error of 13 %. This unexpected increment in the predicted failure could be attributed to a deviation offered by the empirical equation used to calibrate the parameters.

Some studies have also focused on the hygrothermal expansion of both adherend and adhesive which introduced residual stress and strain in the joint [54][143][97]. Thermal strain and swelling residual strain have been included in the FEM by means of subroutines to make more realistic simulations. However, Liljedahl et, al. [143] observed that the non-inclusion of residual strain in analysis does not necessarily affect the accuracy of the numerical models of mixed mode flexure (MMF) and notched coating adhesion (NCA) specimens.

The most interesting and notable finding was that the model developed can be used as a tool to rapidly predict the degradation of single lap joints subjected to hygrothermal cycles and mechanical damage.

7 CONCLUSIONS AND CONTRIBUTION

The E modulus and the tensile strength of the adhesive FM94 did not evidence changes after the exposure to hygrothermal cycles. On the other hand, the shear strength of the SLJ showed reductions of about 42 % after 714 hygrothermal cycles compared with the control specimen. The hygrothermal environment is most likely to affect the adhesive/adherend interface of the SLJ specimen and 'saturation' was achieved after 84 hygrothermal cycles.

The results obtained in this study show moisture absorption of both FM94 adhesive and T800/M21 laminated exposed to hygrothermal cycles (flight operations) in line with Fick's second Law, with a dynamic behaviour that showed the highest absorption rate during hot-wet stages (on the ground or non-flight). FM94 reached the moisture saturation of 1.54 % wt at 120 hours of exposure while T800/M21 achieved moisture saturation at 0.68 % wt at 672 hours. As T800/M21 is approximate 60 % fibre weight fraction, the moisture uptake in resin in composite was 1.7 % wt, so too epoxy resin in composite and epoxy resin film adhesive (FM94) absorbed moisture to similar saturation levels.

The SLJ fatigue life was reduced with the increase of the ageing cycles, with percentages greater than 45 % (quasi-static strength), the life cycles diminished from 500 000 cycles to 1 000 cycles.

The static and fatigue failure obtained from unaged and aged joints was predominantly by adhesion failure (adhesive/adherend interface); although some thin cohesive failure mode was observed in unaged joints. To improve the joint strength and stability of the interface could be used coupling agents or suitable surface pre-treatment, such as primer based on silane molecules [144] could be used.

The numerical diffusion moisture-displacement analysis results are consistent with experimental observations reported by others (Sugiman, Crocombe and Aschroft [54], Han et al., [95] and Liu *et al.* [97]) but do not agree with the experimental findings of this work - the elasticity dropped by 20 % after 1.4 %

moisture uptake (42 hygrothermal cycles) -. Therefore, a different degradation analysis treatment should be determined to reflect the observed experimental results.

A combined experimental-numerical approach was employed to predict the strength and crack propagation in aged joints. The model includes harsh and realistic conditions, such as mechanical damage (induced crack initiator) and exposition to humidity and temperature cycles. This conservative CZM model allows a prediction of the behaviour of SLJ to be made with an accuracy of 4 % for zero hygrothermal cycles, 1 % for 252 hygrothermal cycles, and 13 % for 714 hygrothermal cycles.

This model can predict the reduction of the resistance of composite SLJ exposed to up to 714 hygrothermal cycles.

The use of ultrasonic inspection to evaluate the joints at pre and post-exposure, helped to identify manufacture defects and detect changes in the bond quality. The inspection with C-scan at 5 MHz, 31dB and normal incidence technique, revealed changes of amplitude interpreted as bond quality issues in unaged joints, and in a similar way the integrity of the aged joint changed due to hygrothermal cycles.

The results of this investigation showed the extent of damage, strength reduction and fatigue life of the composite SLJ, providing valuable data to validate the predicted cohesive zone modelling. Under static load the reduction reached a stabilized condition after 84 hygrothermal cycles whereas the fatigue life showed a continuous reduction as hygrothermal cycles increased.

FURTHER WORK

Discrepancies between numerical analysis results and experimental results indicate a different numerical treatment might better reflect experimental observations. Localised diffusion at the adhesive/adherend interface is one such area for consideration (including capillary phenomenon). This model should include the strain conditions caused by the thermal and hygrothermal expansions within the joint.

Other areas for further work are:

- To extend the model for the joint fatigue life prediction, which includes conditions caused by hygrothermal expansion within the joint and identify the crack propagation under these conditions.
- To implement this study using other surface preparation methods, with coating over surface different to the overlap.
- To study the effect of using other type of joints (realistic applications in aerospace repairs) in the joint strength.
- To incorporate the computational tomography with application of NDE methods to determine the mechanical properties after hygrothermal ageing.
- To evaluate the effect of hygrothermal cycles in joints subjected to fatigue by impact and variable amplitude.

REFERENCES

- [1] I. A. Ashcroft, M. M. A. Wahab, A. D. Crocombe, D. J. Hughes, and S. J. Shaw, "The effect of environment on the fatigue of bonded composite joints. Part 1: testing and fractography," *Compos. Part A Appl. Sci. Manuf.*, vol. 32, no. 1, pp. 45–58, 2001.
- [2] J. Li, Y. Yan, T. Zhang, and Z. Liang, "Experimental study of adhesively bonded CFRP joints subjected to tensile loads," *Int. J. Adhes. Adhes.*, vol. 57, pp. 95–104, 2015.
- [3] K. B. Katnam, L. F. M. Da Silva, and T. M. Young, "Progress in Aerospace Sciences Bonded repair of composite aircraft structures : A review of scientific challenges and opportunities," vol. 61, pp. 26–42, 2013.
- [4] D. Gay and S. V Hoa, *Composite Materials: Design and Applications*, Second. USA: CRC Press, 2007.
- [5] A. Escarpita, H. Elizalde, and R. A. Ramirez, "Caracterizacion de mecanismos de falla y propagacion de daño en materiales compuestos Parte I-Revision del Estado del Arte," 2007.
- [6] Federal Aviation Administration FAA, "DOT/FAA/TC-14/39 Literature Review of Weak Adhesive Bond Fabrication and Nondestructive Inspection for Strength Measurement," 2015.
- [7] S. Sugiman, A. D. Crocombe, and I. A. Ashcroft, "The fatigue response of environmentally degraded adhesively bonded aluminium structures," *Int. J. Adhes. Adhes.*, vol. 41, pp. 80–91, 2013.
- [8] I. A. Ashcroft and S. J. Shaw, "Mode I fracture of epoxy bonded composite joints 2. Fatigue loading," *Int. J. Adhes. Adhes.*, vol. 22, no. 2, pp. 151–167, 2002.
- [9] J. Ekh, *Multi-Fastener Single-lap Joints in Composite Structures*. 2006.
- [10] I. A. Ashcroft, D. J. Hughes, and S. J. Shaw, "Mode I fracture of epoxy bonded composite joints 2. Fatigue loading," *Int. J. Adhes. Adhes.*, vol. 22, no. 2,

pp. 151–167, 2002.

- [11] J. Bardis and K. Kedward, “Effects of Surface Preparation on Long-Term Durability of Composite Adhesive Bonds. Report No. DOT/FAA/AR-01/08,” no. April, p. 23, 2001.
- [12] A. Amelia, S. Azari, M. Papini, and J. K. Spelt, “Characterization and prediction of fracture properties in hygrothermally degraded adhesive joints : an open-faced approach,” *J. Adhes. Sci. Technol.*, vol. 27, no. 10, pp. 1080–1103, 2012.
- [13] NPL National Physical Laboratory Materials Centre, “NPL Manual Design and Testing of Bonded and Bolted Joints,” 2007.
- [14] F. . Matthews and T. . Tester, “The influence of stacking sequence on the strength of bonded CFRP single lap joints,” *Int. J. Adhes. Adhes.*, vol. 5, no. 1, pp. 13–18, 1985.
- [15] L. J. Hart Smith, “Adhesive bonded single lap joints,” 1973.
- [16] J. Custódio, J. Broughton, and H. Cruz, “A review of factors influencing the durability of structural bonded timber joints,” *Int. J. Adhes. Adhes.*, vol. 29, no. 2, pp. 173–185, 2009.
- [17] R. . Adams and W. C. Wake, *Structural adhesive joints in engineering*. Essex: ELSEVIER APPLIED SCIENCE, 1984.
- [18] M. S. Kafkalidis and M. D. Thouless, “The effects of geometry and material properties on the fracture of single lap-shear joints,” *Int. J. Solids Struct.*, vol. 39, no. 17, pp. 4367–4383, 2002.
- [19] Department of Defense from United States of America, *Composite Materials Handbook; Volume 3: Polymer Matrix Composites Materiales Usage, Design and Analysis*, vol. 3. 2002.
- [20] A. A. Taib, R. Boukhili, S. Achiou, S. Gordon, and H. Boukehili, “Bonded joints with composite adherends. Part I. Effect of specimen configuration, adhesive thickness, spew fillet and adherend stiffness on fracture,” *Int. J.*

Adhes. Adhes., vol. 26, no. 4, pp. 226–236, 2006.

- [21] M. G. Song *et al.*, “Effect of manufacturing methods on the shear strength of composite single-lap bonded joints,” *Compos. Struct.*, vol. 92, no. 9, pp. 2194–2202, 2010.
- [22] M. Y. Tsai, J. Morton, and F. L. Matthews, “Experimental and Numerical Studies of a Laminated Composite Single-Lap Adhesive Joint,” *J. Compos. Mater.*, vol. 29, pp. 1254–1275, 1995.
- [23] M. Saleem, R. Zitoune, I. El Sawi, and H. Bougherara, “Role of the surface quality on the mechanical behavior of CFRP bolted composite joints,” *Int. J. Fatigue*, vol. 80, pp. 246–256, 2015.
- [24] Y. Zhai, D. Li, X. Li, L. Wang, and Y. Yin, “An experimental study on the effect of bolt-hole clearance and bolt torque on single-lap, countersunk composite joints,” *Compos. Struct.*, vol. 127, pp. 411–419, 2015.
- [25] A. Ataş and C. Soutis, “Application of cohesive zone elements in damage analysis of composites: Strength prediction of a single-bolted joint in CFRP laminates,” *Int. J. Non. Linear. Mech.*, vol. 66, pp. 96–104, 2014.
- [26] G. a. Knight, T. H. Hou, M. a. Belcher, F. L. Palmieri, C. J. Wohl, and J. W. Connell, “Hygrothermal Aging of Composite Single Lap Shear Specimens Comprised of AF-555M Adhesive and T800H/3900-2 Adherends,” *Int. J. Adhes. Adhes.*, vol. 39, pp. 1–7, 2012.
- [27] P. Hu, Z. W. Shi, X. X. Wang, W. D. Li, S. G. Zhou, and X. Han, “Strength Degradation of Adhesively Bonded Single-Lap Joints in a Cyclic-Temperature Environment Using a Cohesive Zone Model,” *J. Adhes.*, vol. 91, no. April 2015, pp. 587–603, 2014.
- [28] J.-H. Hong, M.-G. Han, and S.-H. Chang, “The Effects of Environmental Temperature and Additional Pressure on the Bonding Characteristics of Co-cured Carbon/Epoxy-Aluminum Single Lap Joints,” *J. Adhes.*, vol. 91, no. 3, pp. 197–213, 2015.

- [29] K. Bodjona, K. Raju, G.-H. Lim, and L. Lessard, "Load sharing in single-lap bonded/bolted composite joints. Part I: Model development and validation," *Compos. Struct.*, vol. 129, pp. 268–275, 2015.
- [30] M. M. Abdel Wahab and M. M. Abdel Wahab, "Fatigue in Adhesively Bonded Joints: A Review," *ISRN Mater. Sci.*, vol. 2012, no. c, pp. 1–25, 2012.
- [31] T. A. Schmid Fuertes, T. Kruse, T. Körwien, and M. Geistbeck, "Bonding of CFRP primary aerospace structures – discussion of the certification boundary conditions and related technology fields addressing the needs for development," *Compos. Interfaces*, vol. 22, no. 8, pp. 795–808, 2015.
- [32] ASM International Handbook, *Adhesives and Sealants. Engineered Materials Handbook Volume 3*. ASM International Handbook Committee, 1990.
- [33] R. Delmdahl and F. Gabler, "Excimer lasers clean CFRPs for optimised adhesive bonding," *The laser User*, no. 72. www.coherent.com, p. 2013, 2013.
- [34] R. Kumar Singh, "Identification and evaluation of QA tools for composite surface for adhesive bonding," 2015.
- [35] M. R. Gude, S. G. Prolongo, and a. Ureña, "Hygrothermal ageing of adhesive joints with nanoreinforced adhesives and different surface treatments of carbon fibre/epoxy substrates," *Int. J. Adhes. Adhes.*, vol. 40, pp. 179–187, 2013.
- [36] R. Vaananen, P. Heikkila, M. Tuominen, J. Kuusipalo, and A. Harlin, "Fast and Efficient Surface Treatment for Nonwoven Materials By Atmospheric pressure plasma," *AUTEX Res. journal*, vol. 10, no. March, pp. 8–13, 2010.
- [37] J. S. Serrano, A. Urena, S. Lazcano Urena, and T. Blanco Verala, "New approach to surface preparation for adhesive bonding of aeronautical composites: atmospheric pressure plasma. Studies on the pretreatment lifetime and durability of the bondline," *Compos. Interfaces*, vol. 6440, no.

July, pp. 22–26, 2015.

- [38] L. J. Hart-Smith, G. Redmon, and M. . Davis, “The curse of the nylon peel ply,” Anaheim, California, 1996.
- [39] M. Madge, E. Brousseau, M. Eaton, C. Fetherston, and E. Williams, “Materia prima,” in *Adhesive Bonding of Laser Processed CFRP Panels*, 2014, vol. 21, no. 1, p. DOI: 10.13140/2.1.2566.9126 .
- [40] R. R. Gomatam and E. Sancaktar, “Effects of various adherend surface treatments on fatigue behavior of joints bonded with a silver-filled electronically conductive adhesive,” *J. Adhes. Sci. Technol.*, vol. 19, no. 8, pp. 659–678, 2005.
- [41] N. Encinas *et al.*, “International Journal of Adhesion & Adhesives Surface modification of aircraft used composites for adhesive bonding,” vol. 50, pp. 157–163, 2014.
- [42] B. G. Kumar, R. P. Singh, and T. Nakamura, “Degradation of Carbon Fiber-reinforced,” *J. Compos. Mater.*, vol. 36, no. 24, pp. 2713–2733, 2002.
- [43] S. Pantelakis and K. I. Tserpes, “Adhesive bonding of composite aircraft structures: Challenges and recent developments,” *Sci. China Physics, Mech. Astron.*, vol. 57, no. 1, pp. 2–11, 2014.
- [44] M. D. Banea and L. F. M. da Silva, “Adhesively bonded joints in composite materials: an overview,” *Proc. Inst. Mech. Eng. Part L J. Mater. Des. Appl.*, vol. 223, no. 1, pp. 1–18, 2009.
- [45] N. Guermazi, A. Ben Tarjem, I. Ksouri, and H. F. Ayedi, “On the durability of FRP composites for aircraft structures in hygrothermal conditioning,” *Compos. Part B Eng.*, vol. 85, pp. 294–304, 2015.
- [46] Wong, “Moisture absorption characteristics and effects on mechanical behaviour of carbon/epoxy composite : application to bonded patch repairs of composite structures,” 2013.
- [47] M. R. Vanlandingham, R. F. Eduljee, and J. W. Gillespie, “Moisture

- Diffusion in Epoxy Systems," *J. Appl. Polym. Sci.*, vol. 71, no. July, pp. 787–798, 1998.
- [48] C. D. M. Liljedahl, "Modelling the interfacial degradation in adhesively bonded joints," 2006.
- [49] a. S. Maxwell, W. R. Broughton, G. Dean, and G. D. Sims, "Review of accelerated ageing methods," *Report*, p. 84, 2005.
- [50] K. B. Katnam, A. D. Crocombe, H. Sugiman, H. Khoramishad, and I. A. Ashcroft, "Static and Fatigue Failures of Adhesively Bonded Laminate Joints in Moist Environments," *Int. J. Damage Mech.*, vol. 20, no. 8, pp. 1217–1242, 2011.
- [51] M. Heshmati, R. Haghani, and M. Al-emrani, "Environmental durability of adhesively bonded FRP / steel joints in civil engineering applications : State of the art," vol. 81, 2015.
- [52] M. P. Zanni-Deffarges and M. E. R. Shanahan, "Diffusion of water into an epoxy adhesive: comparison between bulk behaviour and adhesive joints," *Int. J. Adhes. Adhes.*, vol. 15, no. 3, pp. 137–142, 1995.
- [53] B. M. Parker, "Some effects of moisture on adhesive-bonded CFRP-CFRP joints," *Compos. Struct.*, vol. 6, no. 1–3, pp. 123–139, 1986.
- [54] S. Sugiman, A. D. Crocombe, and I. A. Aschroft, "Experimental and numerical investigation of the static response of environmentally aged adhesively bonded joints," *Int. J. Adhes. Adhes.*, vol. 40, pp. 224–237, 2013.
- [55] J. Korta, A. Mlyniec, and T. Uhl, "Experimental and numerical study on the effect of humidity-temperature cycling on structural multi-material adhesive joints," *Compos. Part B Eng.*, vol. 79, pp. 621–630, 2015.
- [56] K. L. DeVries, "Environmental effects," in *Engineered Materials Handbook. Volume 3 Adhesives and Sealants*, C. Dostal, Ed. United States of America: ASM International Handbook Committee, 1990, pp. 613–615.

- [57] J. Jedidi, F. Jacquemin, and A. Vautrin, "Design of accelerated hygrothermal cycles on polymer matrix composites in the case of a supersonic aircraft," *Compos. Struct.*, vol. 68, no. 4, pp. 429–437, 2005.
- [58] A. Agarwal, S. J. Foster, E. Hamed, and T. S. Ng, "Influence of freeze-thaw cycling on the bond strength of steel-FRP lap joints," *Compos. Part B Eng.*, vol. 60, pp. 178–185, 2014.
- [59] J. Wang, H. GangaRao, R. Liang, and W. Liu, "Durability and prediction models of fiber-reinforced polymer composites under various environmental conditions: A critical review," *J. Reinf. Plast. Compos.*, vol. 35, no. 3, pp. 179–211, 2016.
- [60] D. Powers, "Interaction of Water with Epoxy," 2009.
- [61] M. M. Abdel Wahab, "Fatigue in Adhesively Bonded Joints: A Review," *ISRN Mater. Sci.*, vol. 2012, no. c, pp. 1–25, 2012.
- [62] R. D. Broughton, W R and Mera, "Report No. 12 Cyclic Fatigue Testing of Adhesive Joints Environmental Effects," 1999.
- [63] M. Costa, G. Viana, L. F. M. da Silva, and R. D. S. G. Campilho, "Environmental effect on the fatigue degradation of adhesive joints: A review," *J. Adhes.*, vol. 93, no. 1–2, pp. 127–146, 2017.
- [64] Z. Abdo and H. Aglan, "Analysis of aircraft adhesive joints under combined thermal and mechanical cyclic loadings," *J. Adhes. Sci. Technol.*, vol. 11, no. 7, pp. 941–956, 1997.
- [65] Federal Aviation Administration FAA, "Bonded Joints and structures techniques issues and certification considerations;PS-ACE100-2005-1003," 2005.
- [66] A. Kapadia, "Best Practice Guide Non-Destructive Testing of Composite Materials," 2006.
- [67] B. Ehrhart, B. Valeske, C.-E. Muller, and C. Bockenheimer, "Methods for the Quality Assessment of Adhesive Bonded CFRP Structures - A

- Resumé," *Proc. Int.*, pp. 1–9, 2010.
- [68] R. (Australian D. F. A. Heslehurst, "Optical NDT of adhesively bonded joints," *Mater. Eval.*, vol. 67, no. 7, pp. 837–842, 2009.
- [69] J. M. Allin, "Disbond detection in adhesive joints using low-frequency ultrasound," 2002.
- [70] A. Mubashar, "Modelling degradation in adhesive joints subjected to fluctuating service conditions," 2010.
- [71] B. Broughton, "Measurement good practice guide no.28 Durability performance of Adhesive Joints," Teddington Middlesex Uk, 2000.
- [72] L. C. Bank, T. R. Gentry, and A. Barkatt, "Accelerated test methods to determine the long-term behavior of FRP composite structures: environmental effects," *J. Reinf. Plast. Compos.*, vol. 14, no. JANUARY, pp. 559–587, 1995.
- [73] M. M. A. Wahab, I. a. Ashcroft, a. D. Crocombe, and S. J. Shaw, "Diffusion of Moisture in Adhesively Bonded Joints," *J. Adhes.*, vol. 77, no. 1, pp. 43–80, 2001.
- [74] J. Crank, *The mathematics of diffusion*. 1975.
- [75] A. Ameli, N. V. Datla, M. Papini, and J. K. Spelt, "Hygrothermal Properties of Highly Toughened Epoxy Adhesives," *J. Adhes.*, vol. 86, no. 7, pp. 698–725, 2010.
- [76] A. J. Kinloch, *Durability of structural adhesives*. London: Applied Science Publishers Ltd, 1983.
- [77] A. Mubashar, I. A. Ashcroft, G. W. Critchlow, and A. D. Crocombe, "Strength prediction of adhesive joints after cyclic moisture conditioning using a cohesive zone model," vol. 78, pp. 2746–2760, 2011.
- [78] K. B. Katnam *et al.*, "The Static Failure of Adhesively Bonded Metal Laminate Structures : A Cohesive Zone Approach," pp. 1–41.

- [79] J. L. Högberg, "Mixed mode cohesive law," *Int. J. Fract.*, vol. 141, no. 3–4, pp. 549–559, 2006.
- [80] S. R. Hallett and P. W. Harper, "Modelling delamination with cohesive interface elements," *Numer. Model. Fail. Adv. Compos. Mater.*, pp. 55–72, 2015.
- [81] K. N. Roshdestwensky, J. L. Mroginski, C. A. Morel, R. J. B. D'Ambra, and Juan M. Podestá, "Modelado Numérico Del Comportamiento De La Interfase En Materiales Compuestos," *Asoc. Argentina Mec. Comput.*, vol. XXXII, pp. 1653–1670, 2013.
- [82] R. Kregting, "Cohesive zone models," no. February, 2005, pp. 1–31.
- [83] J. L. Högberg and K. Salomonsson, "Simulation of an adhesive layer using a novel mixed mode cohesive law," vol. 46, no. 0, 2005.
- [84] L. F. M. da Silva and R. D. S. G. Campilho, *Advances in numerical modeling of adhesive joints*. 2012.
- [85] S. Eliasson and A. Lundberg, "Investigation and Comparison of Cohesive Zone Models for Simulation of Crack Propagation," pp. 1–5, 2015.
- [86] M. J. van den Bosch, P. J. G. Schreurs, and M. G. D. Geers, "An improved description of the exponential Xu and Needleman cohesive zone law for mixed-mode decohesion," *Eng. Fract. Mech.*, vol. 73, no. 9, pp. 1220–1234, 2006.
- [87] A. Needleman, "A continuum model for void nucleation by inclusion debonding," *J. Appl. Mech.*, vol. 54, no. 3, p. 525, 1987.
- [88] V. Tvergaard, "Effect of fiber debonding in a whisker-reinforced metal," *Mater. Sci. Eng. A*, vol. 125, no. 2, pp. 203–213, 1990.
- [89] V. Tvergaard and J. W. Hutchinson, "The relation between crack growth resistance and fracture process parameters in elastic-plastic solids," *J. Mech. Phys. Solids*, vol. 40, no. 6, pp. 1377–1397, 1992.
- [90] X.-P. Xu and A. Needleman, "Void nucleation by inclusion debonding in a

- crystal matrix," *Model. Simul. Mater. Sci. Eng. Mater. Sci. Fmg*, vol. 1, no. 1, pp. 111–132, 1993.
- [91] I. Scheider and W. Brocks, "Simulation of cup–cone fracture using the cohesive model," *Eng. Fract. Mech.*, vol. 70, no. 14, pp. 1943–1961, 2003.
- [92] G. T. Camacho and M. Ortiz, "Computational modelling of impact damage in brittle materials," *Int. J. Solids Struct.*, vol. 33, no. 20, pp. 2899–2938, 1996.
- [93] A. M. G. Pinto, A. G. Magalhães, R. D. S. G. Campilho, M. F. S. F. de Moura, and A. P. M. Baptista, "Single-Lap Joints of Similar and Dissimilar Adherends Bonded with an Acrylic Adhesive," *J. Adhes.*, vol. 85, no. 6, pp. 351–376, 2009.
- [94] I. a. Ashcroft, M. M. A. Wahab, and a. D. Crocombe, "Predicting Degradation in Bonded Composite Joints Using a Semi-Coupled Finite-Element Method," *Mech. Adv. Mater. Struct.*, vol. 10, no. 3, pp. 227–248, 2003.
- [95] X. Han, A. D. Crocombe, S. N. R. Anwar, and P. Hu, "The strength prediction of adhesive single lap joints exposed to long term loading in a hostile environment," *Int. J. Adhes. Adhes.*, vol. 55, pp. 1–11, 2014.
- [96] X. Han, a. D. Crocombe, S. N. R. Anwar, P. Hu, and W. D. Li, "The Effect of a Hot–Wet Environment on Adhesively Bonded Joints Under a Sustained Load," *J. Adhes.*, vol. 90, no. 5–6, pp. 420–436, 2014.
- [97] S. Liu, X. Cheng, Q. Zhang, J. Zhang, J. Bao, and X. Guo, "An investigation of hygrothermal effects on adhesive materials and double lap shear joints of CFRP composite laminates," *Compos. Part B Eng.*, vol. 91, pp. 431–440, 2016.
- [98] Astm D 5868-01, "Standard Test Method for Lap Shear Adhesion for Fiber Reinforced Plastic (FRP) Bonding," *Standards*, vol. 1, no. Reapproved 2014, pp. 1–2, 2001.

- [99] B. Broughton and M. Gower, "Measurement Good Practice Guide No. 47 Preparation and Testing of Adhesive Joints," 2001.
- [100] W. R. Broughton, L. E. Crocker, and M. R. L. Gower, "Design Requirements for Bonded and Bolted Composite Structures," no. January, p. 46, 2002.
- [101] P. D. Soden, M. J. Hinton, and A. S. Kaddour, "Lamina Properties , Lay-Up Configurations and Loading Conditions for a Range of Fibre-Reinforced Composite Laminates," vol. 58, 1998.
- [102] Hexcel, "Hexply M21 Product Data," *Product Data*. pp. 1–6, 2010.
- [103] Cytec Industries, "AEROSPACE MATERIALS FM ® 94 Adhesive Film." pp. 1–9, 2015.
- [104] ASTM standard, "ASTM D 5229– 14 – Standard Test Method for Moisture Absorption Properties and Equilibrium Conditioning of Polymer Matrix Composite Materials," *Annu. B. ASTM Stand.*, vol. 92, no. Reapproved, pp. 1–13, 2014.
- [105] British Standards Institution, "BS EN ISO 62:2008 Plastics-Determination of water absorption," vol. 3, no. 1. British Standards, London, 2008.
- [106] S. J. Christian, "Mechanical Characterization and Structural Assessment of Biocomposites for Construction," Stanford University, 2009.
- [107] L. Marin, D. Trias, P. Badallo, G. Rus, and J. A. Mayugo, "Optimization of composite stiffened panels under mechanical and hygrothermal loads using neural networks and genetic algorithms," *Compos. Struct.*, vol. 94, no. 11, pp. 3321–3326, 2012.
- [108] British Standards Institutions, "BS EN ISO 527:2012 Plastics— Determination of tensile properties. Part 2: Test conditions for moulding and extrusion plastics," vol. 44, no. 0, 2012.
- [109] British Standards Institution, "BS EN ISO 527-3Plastics — Determination of tensile properties- Part 3: Test conditions for films and sheets," *Part*, vol. 1, pp. 527–1, 2004.

- [110] W. R. Broughton and G. D. Dean, "Measurement Good Practice Guide No. 104: Fatigue and Creep Testing of Adhesives and Thermoplastic Joined Systems," no. 104, 2007.
- [111] Y. Feng, C. Gao, Y. He, T. An, C. Fan, and H. Zhang, "Investigation on tension – tension fatigue performances and reliability fatigue life of T700 / MTM46 composite laminates," *Compos. Struct.*, vol. 136, pp. 64–74, 2016.
- [112] M. D. Banea and L. F. M. Da Silva, "Static and fatigue behaviour of room temperature vulcanising silicone adhesives for high temperature aerospace applications," *Materwiss. Werksttech.*, vol. 41, no. 5, pp. 325–335, 2010.
- [113] D. Palumbo, R. Tamborrino, U. Galietti, P. Aversa, A. Tat??, and V. A. M. Luprano, "Ultrasonic analysis and lock-in thermography for debonding evaluation of composite adhesive joints," *NDT E Int.*, vol. 78, pp. 1–9, 2016.
- [114] R. L. Vijayakumar, M. R. Bhat, and C. R. L. Murthy, "Non destructive evaluation of adhesively bonded carbon fiber reinforced composite lap joints with varied bond quality," *AIP Conf. Proc.*, vol. 1430, no. 31, pp. 1276–1283, 2012.
- [115] ASTM standard, "ASTM D 5229– 92 – Standard Test Method for Moisture Absorption Properties and Equilibrium Conditioning of Polymer Matrix Composite Materials," *Annu. B. ASTM Stand.*, vol. 92, no. Reapproved, pp. 1–13, 2010.
- [116] W. Seneviratne, J. Tomblin, and M. Kittur, *Fatigue and Fracture of Adhesively-Bonded Composite Joints*. Elsevier, 2015.
- [117] and C. T. S. Roh, H. S., "The strength of double strap joint with brittle and ductile adhesives.," in *Failure in Composites 4*, 2013, pp. 231–239.
- [118] N. Zavatta, "Influence of adhesive thickness on adhesively bonded joints under fatigue loading," Universita di Bologna, 2015.
- [119] G. Viana, M. Costa, M. Banea, and L. da Silva, "A review on the temperature and moisture degradation of adhesive joints," *Proc. Inst.*

Mech. Eng. Part L J. Mater. Des. Appl., vol. 0, no. 0, pp. 1–14, 2016.

- [120] Y. Bin Park, M. G. Song, J. J. Kim, J. H. Kweon, and J. H. Choi, “Strength of carbon/epoxy composite single-lap bonded joints in various environmental conditions,” *Compos. Struct.*, vol. 92, no. 9, pp. 2173–2180, 2010.
- [121] S. Sugiman and A. D. Crocombe, “The static and fatigue responses of aged metal laminate doublers joints under tension loading,” *J. Adhes. Sci. Technol.*, vol. 30, no. 3, pp. 313–327, 2015. DOI 10.1080/01694243.2015.1104079
- [122] R. L. Vijaya Kumar, M. R. Bhat, and C. R. L. Murthy, “Some studies on evaluation of degradation in composite adhesive joints using ultrasonic techniques,” *Ultrasonics*, vol. 53, no. 6, pp. 1150–1162, 2013.
- [123] A. Szekeres, “Analogy between heat and moisture,” *Comput. Struct.*, vol. 76, no. 1–3, pp. 145–152, Jun. 2000.
- [124] Dassault Systèmes Simulia, A. . Fallis, and D. Techniques, “ABAQUS documentation,” *Abaqus 6.12*, vol. 53, no. 9, pp. 1689–1699, 2013.
- [125] D. C. O’Mahoney, K. B. Katnam, N. P. O’Dowd, C. T. McCarthy, and T. M. Young, “Taguchi analysis of bonded composite single-lap joints using a combined interface-adhesive damage model,” *International Journal of Adhesion and Adhesives*, vol. 40, pp. 168–178, 2013.
- [126] K. Song, C. Davila, and C. Rose, “Guidelines and parameter selection for the simulation of progressive delamination,” *2008 ABAQUS User’s Conf.*, pp. 1–15, 2008.
- [127] L. M. Fernández-Cañadas, I. Iváñez, and S. Sanchez-Saez, “Influence of the cohesive law shape on the composite adhesively-bonded patch repair behaviour,” *Compos. Part B Eng.*, vol. 91, pp. 414–421, 2016.
- [128] S. Jimenez and R. Duddu, “On the parametric sensitivity of cohesive zone models for high-cycle fatigue delamination of composites,” *Int. J. Solids*

- Struct.*, vol. 82, pp. 111–124, 2015.
- [129] W. Xu and Y. Wei, “Strength and interface failure mechanism of adhesive joints,” *Int. J. Adhes. Adhes.*, vol. 34, pp. 80–92, 2012.
- [130] R. D. S. G. Campilho, M. F. S. F. De Moura, and J. J. M. . Domingues, “Using a cohesive damage model to predict the tensile behaviour of CFRP single-strap repairs,” *Int. J. solid Struct.*, vol. 45, pp. 1497–1512, 2008.
- [131] J. P. Belnoue, S. Giannis, M. Dawson, and S. R. Hallett, “Cohesive / adhesive failure interaction in ductile adhesive joints Part II : Quasi-static and fatigue analysis of double lap-joint specimens subjected to through-thickness compressive loading,” *Int. J. Adhes. Adhes.*, vol. 68, pp. 369–378, 2016.
- [132] M. Li, H. Liu, Y. Gu, Y. Li, and Z. Zhang, “Effects of carbon fiber surface characteristics on interfacial bonding of epoxy resin composite subjected to hygrothermal treatments,” *Appl. Surf. Sci.*, vol. 288, pp. 666–672, 2014.
- [133] M. Heshmati, R. Haghani, and M. Al-Emrani, “Environmental durability of adhesively bonded FRP/steel joints in civil engineering applications: State of the art,” *Compos. Part B Eng.*, vol. 81, pp. 259–275, 2015.
- [134] X. Chen, Y. C. Lin, and X. Chen, “Moisture sorption-desorption-resorption characteristics and its effect on the mechanical behavior of the epoxy ...,” no. October 2014, 2005.
- [135] K. S. Kim, J. S. Yoo, Y. M. Yi, and C. G. Kim, “Failure mode and strength of uni-directional composite single lap bonded joints with different bonding methods,” *Compos. Struct.*, vol. 72, no. 4, pp. 477–485, 2006.
- [136] R. Bhanushali, D. Ayre, and H. Y. Nezhad, “Tensile Response of Adhesively Bonded Composite-to-composite Single-lap Joints in the Presence of Bond Deficiency,” *Procedia CIRP*, vol. 59, no. November, pp. 139–143, 2017.
- [137] P. J. Pearce, D. R. Arnott, a Camilleri, M. R. Kindermann, G. I. Mathys,

- and a R. Wilson, "Cause and effect of void formation during vacuum bag curing of epoxy film adhesives," *J. Adhes. Sci. Technol.*, vol. 12, no. 6, pp. 567–584, 1998.
- [138] B. M. Parker, "The effect of composite prebond moisture on adhesive-bonded CFRP-CFRP joints," vol. 14, no. 3, pp. 226–232, 1983.
- [139] J. A. . Ferreira, P. . Reis, J. D. . Costa, and M. O. . Richardson, "Fatigue behaviour of composite adhesive lap joints," *Compos. Sci. Technol.*, vol. 62, no. 10, pp. 1373–1379, 2002.
- [140] D. Lowak, H. · De Jonge, J.B. · Franz, J. · Schutz, "The Transport Wing Standard programme (TWIST)," 1979.
- [141] L. F. M. da Silva, R. . Adams, and M. Gibbs, "Manufacture of adhesive joints and bulk specimens with high-temperature adhesives," *Int. J. Adhes. Adhes.*, vol. 7496, no. August 2016, pp. 69–83, 2004.
- [142] K. B. Katnam, J. P. Sargent, A. D. Crocombe, H. Khoramishad, and I. A. Ashcroft, "Characterisation of moisture-dependent cohesive zone properties for adhesively bonded joints," *Eng. Fract. Mech.*, vol. 77, no. 16, pp. 3105–3119, 2010.
- [143] C. D. M. Liljedahl, A. D. Crocombe, M. A. Wahab, and I. A. Ashcroft, "The effect of residual strains on the progressive damage modelling of environmentally degraded adhesive joints," *J. Adhes. Sci. Technol.*, vol. 19, no. 7, pp. 525–547, 2005.
- [144] A. Baldan, "Adhesion phenomena in bonded joints," *Int. J. Adhes. Adhes.*, vol. 38, pp. 95–116, 2012.